Field Trip and Workshop on the Martian Highlands and Mojave Desert Analogs

October 20–27, 2001

Program and Abstract Volume

LPI Contribution No. 1101

Field Trip and Workshop on the Martian Highlands and Mojave Desert Analogs

Las Vegas, Nevada, and Barstow, California

October 20–27, 2001

Conveners
Alan Howard, University of Virginia
Jeffrey Moore, NASA Ames Research Center
James Rice, Arizona State University

Sponsored by
Lunar and Planetary Institute
National Aeronautics and Space Administration

Lunar and Planetary Institute 3600 Bay Area Boulevard Houston TX 77058-1113

LPI Contribution No. 1101

Compiled in 2001 by
LUNAR AND PLANETARY INSTITUTE

The Institute is operated by the Universities Space Research Association under Contract No. NASW-4574 with the National Aeronautics and Space Administration.

This volume may be cited as

Author A. B. (2001) Title of abstract. In *Field Trip and Workshop on the Martian Highlands and Mojave Desert Analogs*, p. xx. LPI Contribution No. 1101, Lunar and Planetary Institute, Houston.

This report is distributed by

ORDER DEPARTMENT
Lunar and Planetary Institute
3600 Bay Area Boulevard
Houston TX 77058-1113, USA
Phone: 281-486-2172
Fax: 281-486-2186
E-mail: order@lpi.usra.edu

Please contact the Order Department for ordering information.

Preface

This volume contains the program and abstracts that have been accepted for presentation at the Field Trip and Workshop on the Martian Highlands and Mojave Desert Analogs, October 20–27, 2001. The Scientific Organizing Committee consisted of conveners Alan Howard (*University of Virginia*), Jeffrey Moore (*NASA Ames Research Center*), and James Rice (*Arizona State University*). Other members were Raymond Arvidson (*Washington University*), Robert Craddock (*Smithsonian Center for Earth and Planetary Sciences*), William E. Dietrich (*University of California, Berkeley*), Ronald Greeley (*Arizona State University*), Leslie McFadden (*University of New Mexico*), David Des Marais (*NASA Ames Research Center*), Stephen G. Wells (*Desert Research Institute*), Kelin Whipple (*Massachusetts Institute of Technology*), and James Zimbleman (*Smithsonian Center for Earth and Planetary Sciences*).

Logistics, administrative, and publications support were provided by the Publications and Program Services Departments of the Lunar and Planetary Institute.

Contents

Program

Saturday, October 20, Las Vegas

7:30–9:30 p.m. Registration and icebreaker social

Sunday, October 21

8:30 a.m. Introduction, logistics, and late registration

10:00 a.m. Bus departure from Las Vegas

Field Activities:

- Onboard Bus
  - Introduction to Basin and Range/Mojave Desert geology and structure (Anderson)
  - Introduction to desert surface water and subsurface hydrology (Howard)
  - Lunch

- Tecopa Hot Springs Area
  - Lake bed and tephra deposits (Howard and Moore)
  - Erosional History (Howard)

- Death Valley
  - Zabriskie Point and vicinity
    - Deformed alluvial fan, lakebed, and shoreline facies (Whipple)
    - Rainfall-sculpted vertical slopes (Howard)
  - Lake Manly shoreline on Beatty Cutoff Road (Moore and Parker)
  - Death Valley dune field (Howard)

- Overnight at Stovepipe Wells

Monday, October 22, Field Trip

Field Activities:

- Death Valley
  - Ventifacts at "Mars Hill" (Laity)
  - Playa deposits (Devil's Golf Course): Origin, chemistry, remote sensing (Farmer)
  - Fan deposits: Fluvial and debris flow processes, tectonic deformation (Whipple)
  - Salt weathering (Moore)
  - Shorelines (Howard and Parker)

- Silver Lake Playa (Howard, Wells, McFadden)
- Arrive at Barstow

Tuesday, October 23, Workshop in Barstow

Session I: Craters and Crater Degradation, Tectonics

Barlow: *Impact Cratering on Mars During the Noachian Period*

Kereszturi: *Double Craters and Crater Modification*

Forsythe and Blackwelder: *Perspectives on the Geologic Evolution of Early Martian Crater Basins*

Parker and Grant: *Accessing Martian Fluvial and Lacustrine Sediments by Landing in Holden Crater, Margaritifer Sinus*

Howard: *Degraded Crater Morphology: Fans, Playas and Lakes*

Group Discussion: *Craters, craters everywhere: How can we decipher what they tell us?*

Session II: Fluvial Processes on the Martian Highlands

Carr: *Channels on the Highlands: Recent Research on Their Morphology and Distribution* [Invited]

Irwin and Craddock: *Drainage Basin Integration in the Martian Highlands*

Aharonson, Zuber, Rothman, Whipple, and Schorghofer: *Topography of Drainage Basins and Channels: Mars and Terrestrial Analogs*

Burke: *Mojave Desert Stream Beds Resembling Martian Channels*

Craddock, Irwin, and Howard: *Martian Drainage Densities: Analyses from MOLA Digital Elevation Models*

Group Discussion: *Sources of water, extent of fluvial erosion and deposition, and climatic implications of valley networks: Have MOC high-resolution images and MOLA topography brought us any closer to a consensus?*

Session III: Regional Studies in the Highlands

Hynek and Phillips: *The Enigmatic Arabia Terra, Mars*

Mest and Crown: *Fluvial Degradation of the Circum-Hellas Highlands of Mars*

Anderson and Dohn: *Noachian Faulting: What do Faults Tell Us About the Early Tectonic History of Tharsis?*

Moore, Howard, and Schenk: *Geomorphic History of the Southern Isidis Rim: Extensive Fluvial Erosion and Possible Deep Oceans*

Group Discussion: *The role of regional studies in deciphering the geologic history and environment of early Mars*

Session IV: Terrestrial Analogs to the Martian Highlands

Informal discussion and short presentations about possible terrestrial analogs to martian highlands landforms other than the Mojave Desert/Basin and Range.

Wednesday, October 24, Sessions at Barstow, Continued

Session V: Rocks, Minerals, and Soils

Catling: *Geochemistry of Sediments on Early Mars* [Invited]

Kirkland, Herr, Salisbury, Keim, Adams, and Hackwell: *Detecting Minerals on Mars Using TES, THEMIS, and Mini-TES*

Kochemasov: *The Composition of the Martian Highlands as a Factor of Their Effective Uplifting, Destruction and Production of Voluminous Debris*

Harvey: *The Ferrar Dolerite: An Antarctic Analog for Martian Basaltic Lithologies and Weathering Processes*

Noreen, Chapman, and Tanaka: *Possible Formation Processes for Martian Crystalline Hematite*

Group Discussion: *What weathering processes and products would have been produced on Mars under wet and warm versus cold and dry conditions? Where are the carbonates, anyway?*

Session VI: Exploration Techniques and Strategies

Kuhlman et al: *SNOOPY: Student Nanoexperiments for Outreach and Observational Planetary Inquiry*

Nishiizumi: *Surficial Studies of Mars Using Cosmogenic Nuclides*

Grant, Schultz, and Campbell: *Exploring the Martian Highlands using a Rover-deployed Ground-penetrating Radar*

Farr: *Imaging Radar in the Mojave Desert — Death Valley Region* [invited]

Group Discussion: *Geomorphic perspectives on desirable instrumentation on space-borne or in-situ Mars exploration.*

Session VII: Eolian Processes

Greeley: *Mojave Desert Eolian Processes: Similarities and Differences with Martian Highlands Eolian Features* [Invited]

Kuhlman, Marshall, Evans, and Luttge: *Australian Red Dune Sand: A Potential Martian Regolith Analog*

Laity, Bridges, and Boyle: *Ventifact Formation in the Mojave Desert: Field Analogs for Martian Processes*

Bridges and Laity: *Rock Abrasion and Ventifact Formation on Mars from Field Analog, Theoretical, and Experimental Studies*

Zimbelman: *Aeolian and Pluvial Features in the Eastern Mojave Desert as Potential Analogs for Features on Mars*

Group Discussion: *Important issues in the role of eolian processes in the highlands: Abrasion, deflation, deposition, bedforms, sediment budgets, and rates.*

Session VIII: Mojave Desert as an (Imperfect?) Martian Analog

Obviously Mars and the Mojave Desert have many differences today. The modern martian surface is intensely cold and extremely dry, whereas the Mojave Desert can be very hot and sporadically very wet. However, during the time in early Mars history when much of the landscape of the ancient highlands was being shaped, Mars was warmer and wetter, perhaps something like the current conditions in the high Arctic, such as at Devon Island. Thus it is worth asking whether we are seeing alluvial fans, runoff gullies, and even playas and shore traces in the martian highlands, and what components of our terrestrial experience informs us about these ancient martian features. Equally important, how is our terrestrial experience potentially a source of deception in our assessment of the ancient landscapes of Mars?

Open discussion moderated by Bill Dietrich (for terrestrial side) and Alan Howard (for planetary community).

Thursday, October 25, Field Trip

Field Activities:

- Afton Canyon: Lake Manix, shorelines, lakebeds, Mojave River history, and hydrology (Wells)
- Soda Lake
- Pediments along Kelbaker Road (Wells)
- Cima Volcanic field: Weathering and erosional processes on lava flows (McFadden, Wells)
- Kelso Dunes: Transport pathways and sand deposits in the eastern Mojave (Zimbelman)
- Soldier Mountain Sand Ramp and Ventifacts (if time permits) (Zimbelman and Laity)
- Return to Barstow

Friday, October 26, Field Trip

Field Activities:

- Yardangs at Rogers Dry Lake, Edwards Air Force Base (Ward, Laity)
- Searles Lake: Lakebed deposits, shorelines, Trona tufa towers, and Apes (Moore, Howard)
- Return to Barstow

Saturday, October 27

8:00 a.m. Board bus to return to Las Vegas airport

TOPOGRAPHY OF DRAINAGE BASINS AND CHANNELS: MARS AND TERRESTRIAL ANALOGS. O. Aharonson, M. T. Zuber, D. H. Rothman, K. X. Whipple, N. Schorghofer, *Dept. of Earth, Atmospheric and Planetary Science, Massachusetts Institute of Technology, Cambridge, MA 02139, USA, (oded@mit.edu).*

Introduction: Valley networks and channels on Mars were discovered during the Mariner 9 mission [1]. Alternatives for their origin have been suggested, but the most widely accepted formation hypothesis is by erosion, and the most likely erosive agent is water [2,3]. Morphometric criteria have been developed to detect incision by groundwater sapping and surface runoff [4–6]. A distinction can be made by the change of valley widths, which increases downstream for runoff features but remains essentially constant for sapping features; by the shape of valley heads, which are tapered in rivers but theater-formed for sapping features; and by dendritic networks that are indicative of surface runoff. Such criteria require only planimetric images. Knowledge of the topography permits extension of such analyses using additional quantitative criteria. Longitudinal stream profiles, locations of channels relative to surface topography, and transverse cross-sections of valleys [7] may now be used to constrain the genesis and evolution of Martian valleys. The analysis here proceeds by watershed computation of the of drainage systems, has been developed and tested extensively in terrestrial landscapes [8], and is also applied on Mars in [9].

Methods: The implemented watershed analysis requires knowledge of the surface topography sampled on a regular grid. For each grid-cell, flow direction is defined by the steepest downhill slope S, where undefined flow directions are resolved iteratively [8] such that "pits" are artificially filled, allowing the computation to proceed through them. The level of the filling is selected such that the flow is continuous in the relevant channels. The total area draining into each cell is referred to as the contributing area A. In order to consider the dependence of S on A, the slope data is sorted in logarithmically spaced bins in A, and the logarithms of the slopes are averaged within each bin. Recent measurements made by the Mars Orbiter Laser Altimeter (MOLA) [10] on board the Mars Global Surveyor (MGS) [11] allow construction of a digital elevation model (DEM) from topographic profiles of typical vertical accuracy $\sim$ 1 m, interpolated on a grid with spatial resolution 1 km $\times$ 1 km (undersampled in the latitudinal direction and typically oversampled in the longitudinal direction).

Results: On Earth, the lower Escalante River, located on the Colorado Plateau, provides a useful analog for some channels on Mars [4]. Analysis indicates that tributaries west of the Escalante river evolved primarily by surface runoff erosion. East of the river, channel incision appears to have progressed via head-ward erosion of the cliff-face by seepage of groundwater at its base. The topography of runoff channels west of the Escalante river is almost without exception concave upwards, longitudinal profiles are usually smooth, and slope and contributing area are strongly correlated. In contrast, east of the river the canyon floors are linear or only slightly concave, and individual sections are separated by knickpoints. The lowest floor segment follows an impermeable lithologic layer

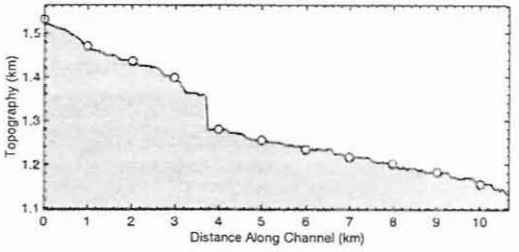

Figure 1: Topography of Bown's Canyon, Utah. 1 km intervals along the stream are indicated by circles.

identified as the Kayenta Formation. The topography along Bown's Canyon is shown in Figure 1.

On Mars, the nature of Ma'adim Vallis has been the subject of a number of investigations. Incision by runoff erosion has been inferred [3, 12–14] based on interpretation of features in Viking images. Sapping processes were later suggested [15] to play a role in carving the valley, with multiple episodes of flow. In Figure 2 the topography of Maadim Vallis is shown. Long, linear segments are seen along the main stream profile, and even occasional short convex segments exist. These are particularly prone to erosion and hence attest to the juvenile fluvial character of the system. The unevolved nature of the surface with respect to runoff erosion is also evident in the large number of local minima [16], and in the low density of tributaries and high order streams [17, 18], absent also in high resolution images [19]. Figure 3 shows a contributing area map of the region.

Many studies in terrestrial drainage environments (e.g. [20–22]) and numerical simulations [23,24] find general characteristics of drainage topography. Among these are smooth valley profiles with distinctive upwards-concave shape. This observation is often quantified in terms of a power law relationship such that $S \sim A^{-\theta}$, where θ is the concavity exponent. For terrestrial fluvial systems, the exponent θ is typically in the range $0.3 - 0.7$ [20, 22, 25]. The concavity absent from longitudinal profiles on Mars is also weak in basin averaged quantities (Figure 4). Over $\sim$3 orders of magnitude in A, where $A > 30$ km^2, θ is small. Also shown for reference are lines corresponding to $\theta = 0.3$, a value that is comparatively low but still appropriate for some terrestrial runoff environments [22, 26]. In the range of high drainage areas, fits to the averaged slope data yield values for θ indistinguishable from those expected for random topography [27]. Hence, at large A, the slope-area relation shows no evidence for extensive fluvial sculpting of the terrain in an environment where flow discharge increases steadily downstream, as would be expected for sustained, runoff-driven erosion.

The longitudinally flat floor segments may provide a direct indication of lithologic layers in the bedrock and pressure gradients in the ground water hydrological systems would be

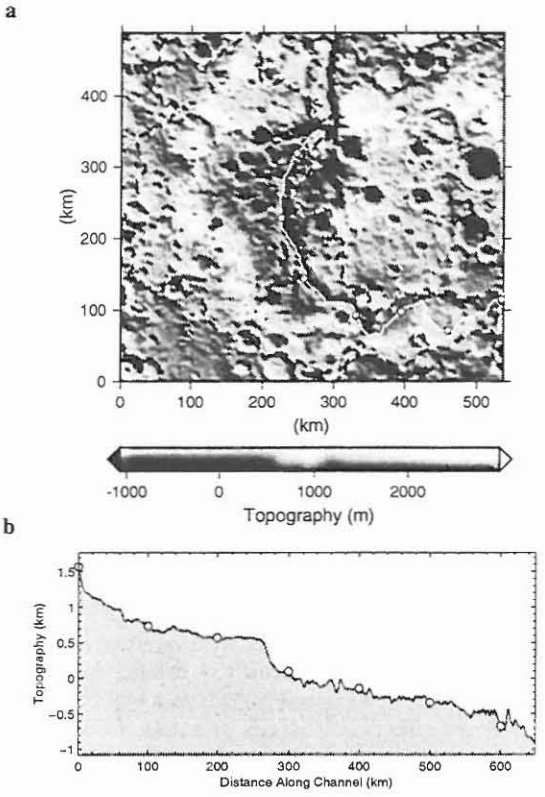

Figure 2: Topography of Ma'adim Vallis, Mars (a) map view, and (b) longitudinal profile. Circles indicate 100 km invervals along the stream. Drainage basin boundaries are shown by the dashed line.

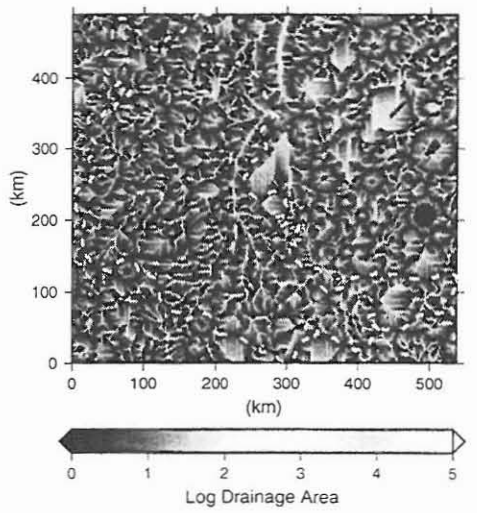

Figure 3: Drainage area map, Ma'adim Vallis.

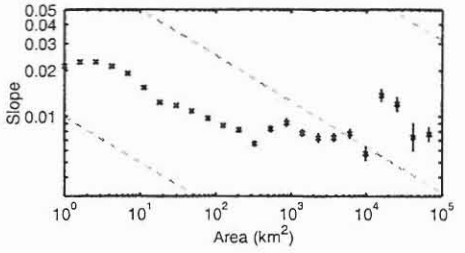

Figure 4: Slope-area relations for Ma'adim Vallis. Vertical bars indicate the standard errors in the mean slope. Also shown are reference lines (dashed green) with concavity exponent $\theta = 0.3$.

controlled by any such impermeable structures, although the indication of layers can be viewed as independent of the precise nature of the erosion process. Lacking rainfall, the problem of recharging the large aquifers necessary for voluminous seepage remains. Morphologic evidence for surface-runoff certainly exists [28], but the results here indicate that there has not been a significant amount of landscape evolution by fluvial erosion in areas where runoff incision has been previously interpreted. The emerging picture is that the large volumes of incision were controlled by lithologic structures with seepage likely occurring at their interfaces, while fluvially unevolved runoff networks incise the surface superficially. Quantitative analysis of fluvial topography together with further study of terrestrial analogs hold the promise of evaluating the extent to which lithologic heterogeneity, intensity of erosion, and erosion process have influenced morphology of river channels and hence the ancient hydrology of Mars.

References: [1] McCauley J.F. et al. (1972) *Icarus 17*, 289–327. [2] Carr M.H. (1981) *The Surface of Mars* Yale University Press, New Haven. [3] Baker V.R. (1982) *The Channels of Mars* University of Texas Press, Austin. [4] Laity J.E. and Malin M.C. (1985) *Geol. Soc. Am. Bull. 96*, 203–217. [5] Kochel R.C. and Piper J.F. (1986) *J. Geophys. Res. 91*, E175. [6] Gulick V.C. and Baker V.R. (1990) *J. Geophys. Res. 95*, 14,325–14,344. [7] Goldspiel J.M. and Squyres S.W. (2000) *Icarus 148*, 176–192. [8] Tarboton D.G. (1997) *Water Resour. Res. 33*(2), 309–319. [9] Aharonson O. et al. (2001) *Lunar and Planet. Sci. Conf. XXXII*, # 2153. [10] Smith D.E. et al. (in press) *J. Geophys. Res.*. [11] Albee A.L. et al. (in press) *J. Geophys. Res.*. [12] Sharp R.P. and Malin M.C. (1975) *Geol. Soc. Am. Bull. 86*, 593–609. [13] Masursky H. et al. (1980) *NASA Tech. Memo. 82385* 184–187. [14] Carr M.H. and Clow G.D. (1981) *Icarus 48*, 91–117. [15] Cabrol N.A. et al. (1998) *Icarus 132*(2), 362–377. [16] Banerdt W.B. and Vidal A. (2001) *Lunar Planet. Sci. XXXII*, #1488. [17] Carr M.H. (1995) *J. Geophys. Res. 100*, 7479–7507. [18] Carr M.H. and Chuang F.C. (1997) *J. Geophys. Res. 102*, 9145–9152. [19] Malin M.C. and Carr M.H. (1999) *Nature 397*, 589–591. [20] Flint J.J. (1974) *Wat. Resour. Res. 10*, 969–973. [21] Howard A.D. and Kerby C. (1983) *Geol. Soc. Am. Bull. 94*, 739. [22] Whipple K.X. and Tucker G.E. (1999) *J. Geophys. Res. 104*, 17661–17674. [23] Willgoose G. et al. (1991) *Wat. Resour. Res. 27*, 1697–1702. [24] Howard A.D. (1994) *Wat. Resour. Res. 30*, 2261–2285. [25] Tarboton D.G. et al. (1989) *Water Resour. Res. 25*(9), 2037–2051. [26] Howard A.D. et al. (1994) *J. Geophys. Res. 99*(B7), 13,971–13,986. [27] Schorghofer N. and Rothman D.H. (2001) *Phys. Rev. E 63*, 026112. [28] Craddock R.A. and Howard A.D. (submitted) *J. Geophys. Res.*.

Noachian Faulting: What Do Faults Tell Us About The Early Tectonic History of Tharsis?

R. C. Anderson[1], and J. M. Dohm[2], [1]Jet Propulsion Laboratory, Pasadena, CA 91109, [2]University of Arizona. robert.anderson@jpl.nasa.gov.

Introduction and Background: The western hemisphere of Mars is dominated by the formation of Tharsis, which is an enormous high-standing region (roughly 25% of the surface area of the planet) capped by volcanics, including the solar system's largest shield volcanoes. Tharsis is surrounded by an enormous radiating system of grabens and a circumferential system of wrinkle ridges that extends over the entire western hemisphere of Mars [*1,2,3,4,5,6*]. This region is perhaps the largest and most long-lived tectonic and volcanic province of any of the terrestrial planets with a well-preserved history of magmatic-driven activity that began in the Noachian and has lasted throughout Martian geologic time [*7,8*].

Tharsis and the surrounding regions comprise numerous components, including volcanic constructs of varying sizes and extensive lava flow fields, large igneous plateaus, fault and ridge systems of varying extent and relative age of formation, gigantic outflow channel systems, vast system of canyons, and local and regional centers of tectonic activity. Many of these centers [*7*] are interpreted to be the result of magmatic-related activity, including uplift, faulting, dike emplacement, volcanism, and local hydrothermal activity. Below we present a summary of our work for Tharsis focusing primarily on the earliest stage of development, the Noachian period. Here we hone in on the early centers and how they relate to the early development of the Tharsis Magmatic Complex (TMC) [*9*].

***Methodology*:** The tectonic history of Tharsis is recorded in the spatial and temporal distribution of tectonic features that can be mapped on its surface (e.g., grabens and wrinkle ridges). This is best exemplified in the Tharsis and surrounding regions where 24,452 tectonic features of the western hemisphere of Mars were mapped, digitized, and characterized using Viking data [*10*]. Stratigraphic and crosscutting relations among stratigraphic/morphologic units permitted us to construct a map of the faults and grabens as they formed during five successive stages based largely on the age classification scheme of *Dohm and Tanaka* [*11*]. In this study, we have concentrated on the initial development of the Tharsis Rise during the Noachian and have identified possible secondary centers that were not recognized in our previous research.

Noachian: The Noachian period consists primarily of ancient crustal rocks formed during the period of late bombardment. This is the first time for the western hemisphere of Mars that we observe evidence for the presence of the Tharsis Rise. Of the 24,452 tectonic structures mapped for the western hemisphere during this time [*7*], 81% were mapped as extensional features and 19% were mapped as compressional features. From our previous research, simple grabens were by far the dominant structure found within the Tharsis region and more than half of these grabens were classified as Noachian in age (Stage 1) [*7*].

For the Noachian period, grabens were found primarily in the Syria Planum, Thaumasia, and Tempe Terra regions (Figure 1a). Many of these features are radial to Claritas; a large elongated topographic high region, which contains numerous simple and complex grabens (Figure 1b). It is believed that this center represents the earliest evidence of tectonic activity for Tharsis and corresponds to the early phase of Thaumasia

faulting discussed by *Plescia and Saunders* [*3*] and *Frey* [*12*].

In addition to the Stage 1 Claritas center, additional tectonic activity has been identified at Tempe and Uranius (predating the relatively young shield volcano and associated lava flows). The two secondary concentrations in the Tempe Terra region may be related to previously identified deep-seated intrusives in this area [*13*].

Our work has further unfolded the intricate complexity of the Tharsis and surrounding regions, including some of the major contributors to Noachian resurfacing in and around the Tharsis magmatic complex. The next stage of our research will be to investigate the impact that the early Tharsis magmatic complex had on the Noachian global environmental and climatalogical conditions, as well as pre-Tharsis conditions.

Reference: [*1*] Carr, M.H., *J. Geophys. Res.,* 79, 26, 3943-3949, 1974. [2] Wise, D.U., Golombek, M.P., and G.E. McGill, *Icarus*, 38, 456-472, 1979. [*3*] Plescia, J.B., and R.S. Saunders, *J. Geophys. Res.,* 87, 9775-9791, 1982. [*4*] Scott, D.H., and J.M. Dohm, *in Proc. of the 20th Lunar Planet. Sci. Conf.,* 487-501, 1990. [*5*] Tanaka, K.L., et al., *J. Geophys. Res.*, 96, 15,617-15,633, 1991. [*6*] Banerdt, W.B., et al., Chpt. 8, p. 249-297, *in* MARS, 1992. [*7*] Anderson, R.C. et al., *in press J. Geophys. Res.*, 2001. [*8*] Phillips, R.J., *Science*, v. 291, 2587-2591, 2001. [*9*] Dohm, J.M., et al., *in press J. Geophys. Res.*, 2001. [*10*] Anderson et al., *Lunar Planet. Sci. Conf.,* 24, 1881-1882, 1998. [*11*] Dohm, J.M., and K.L. Tanaka, *Planet. & Space Sci.*, 47, 411-431, 1999. [*12*] Frey, H., *J. Geophys. Res.*, 84, 83, 1009-1023, 1979. [13] Scott, D.H., and Dohm, J.M., *in Proc. of the 20th Lunar Planet. Sci. Conf., 503-513,* 1990.

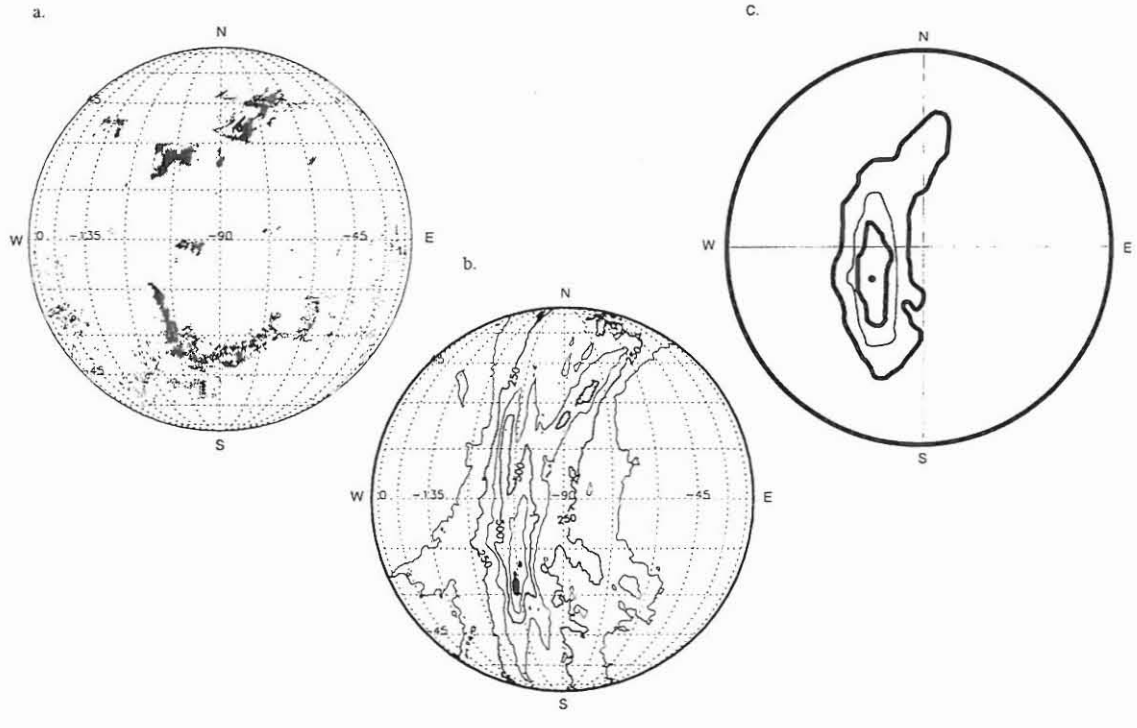

Figure 1. (a) Stage 1 features mapped for the western hemisphere of Mars. (b) Contour plot of stage 1 features obtained from the vector analysis technique (contour interval is 125 fault intersections; center is 803 radial features or 9.6%). Black areas represent primary centers of tectonic activity; shaded areas represent secondary concentrations. (c) Contour plot of the stage 1 features from the beta analysis technique (contour interval represents density of intersections of 2%).

IMPACT CRATERING ON MARS DURING THE NOACHIAN PERIOD. N. G. Barlow, Dept. Physics, Univ. Central Florida, Orlando, FL 32816 ngb@physics.ucf.edu.

Introduction: The Martian highlands have been affected by numerous geologic processes, many of localized extent, but impact cratering was of major importance throughout the entire highlands. The Noachian-aged highlands materials formed during the period of late heavy bombardment when impact crater rates were substantially higher than during recent times. The craters in the highlands extend over a wider range of crater diameters than is seen for craters on post heavy bombardment aged terrains. In addition craters in the highlands display a wider range of degradation, suggesting that erosional and depositional processes were heightened during this time. Impact craters in the Martian highlands thus allow us to study (1) the population of impacting objects dominating at Mars during this early time, and (2) the degradational environment affecting the planet throughout its history.

Impact Population and the Late Heavy Bombardment Period: Crater size-frequency distribution analysis allows us to determine the relative ages of geologic units and investigate possible temporal variations in the population of impacting objects. MOC imagery has revealed very small craters distributed across the Martian surface. Analysis of these small craters has led to the discovery that volcanism may have been occurring more recently than previously thought [1], that turnover of the Martian soil by small crater "gardening" is very likely [2], and that ancient terrains may have been covered and recently exhumed [3]. However, small crater analyses are fraught with problems. For example, small craters are more readily affected by degradation processes than larger craters and thus typically are not retained as long by a surface. Many non-impact features (endogenic volcanic craters, thermokarst pits, etc.) resemble small impact craters—inclusion of such features as impact structures will lead to incorrect interpretations of ages. Secondary impact craters also begin to affect crater size-frequency distribution analyses in the small diameter range, which affects the resulting age determinations for terrain units.

Analysis of larger craters, particularly for the heavily cratered highlands of Mars, can provide important information about the early history of the planet with little effect from the problems plaguing the smaller crater population. Our studies have focused on analysis of craters larger than about 5 km in diameter. Our studies have found that this larger crater population clearly shows a different size-frequency distribution function depending on the age of the terrain. Ancient terrains such as the Martian highlands display a complicated size-frequency distribution curve which cannot be approximated by a single-sloped distribution function at all crater diameters [4, 5]. This type of crater curve is seen on both the highlands and the younger ridged plains regions. The northern plains display a crater size-frequency distribution curve which can be represented by a power law function of incremental slope –2 (-3 differential slope).

Some have argued that the multi-sloped distribution function seen in the highlands is due entirely to the erosion of smaller craters from a single-slope distribution function. We agree that some loss of small craters occurs due to erosion, but have argued that at least part of the downturn is the result of a different size-frequency distribution of impacting objects during the heavy bombardment period [6]. Our arguments include (1) the similarity of the crater size-frequency distribution curves for the lunar highlands, Mercurian surface, and Martian highlands in spite of substantially different erosional environments, and (2) the fact that the ridged plains, which display much lower degrees of degradation than the Martian highlands, show the same crater curve shape (at lower crater density). We maintain that surfaces which formed during the period of late heavy bombardment throughout the inner solar system record the size-frequency distribution of a population of impacting objects distinct from the asteroids and comets which have dominated the recent (post heavy bombardment) cratering record. This population is likely left-over material from the accretion of the planets.

The timing of the end of heavy bombardment at Mars has also been the subject of discussion. There has been a general belief that the end of the Noachian period coincides with the end of the heavy bombardment period. Analysis of the crater size-frequency distribution curves argues against this. Ridged plains mapped as Lower Hesperian in age consistently display the same multi-sloped size-frequency distribution curve structure as that seen for the Noachian-aged highlands units [6]. A Chi-squared test shows that these curves are statistically identical in shape at the 99% confidence interval. We argue that the end of the late heavy bombardment period is more likely coincident with the transition between the Upper and Lower Hesperian periods

Crater Degradation. Craters superposed on the Martian highlands display a range of degradation states, from extremely fresh to almost completely destroyed ("ghost craters"). The majority of the craters

found on highlands terrain are between these two end states. Craters on younger terrains do not typically display the range of crater degradation seen in the highlands. Studies of the morphometric properties of craters in various stages of degradation suggest a variety of responsible geologic processes, including aeolian, fluvial (including rainfall), and volcanic [7, 8, 9].

The crater size-frequency distribution curves of degraded versus non-degraded (i.e., craters with intact ejecta blankets and relatively sharp crater rims) can provide constraints on when the period of high degradation rates ceased. Size-frequency distribution curves of non-degraded craters consistently show a maximum age near the Upper Noachian-Lower Hesperian transition [6], just prior to the end of the late heavy bombardment period. This is approximately coincident with the formation of the last large impact basins, such as Argyre. Impact erosion of the Martian atmosphere was likely occurring throughout the late heavy bombardment period—calculations by Melosh and Vickery [10] show that this would be a very efficient mechanism by which a thicker Martian atmosphere could be rapidly degraded to its current thin state. According to the impact erosion model, larger meteors more effectively erode the atmosphere than smaller meteors, so this process would be most efficient during the late heavy bombardment when the large impact basins were forming. Interestingly, this also coincides with the general time period when most of the valley network systems ceased forming, except for those found around localized thermal anomalies such as the volcanoes.

We believe these observations strongly argue for a period of enhanced degradation existing for much if not all of the Noachian period. The end of this period of high degradation rates is coincident with the end of the Noachian period, but is ***not*** coincident with the end of the late heavy bombardment period. Geologic processes in addition to impact cratering were likely more pronounced at this time, particularly volcanism, tectonism, and fluvial processes (perhaps accompanied by rainfall). The combination of these geologic processes, not one process alone, was responsible for the enhanced degradation rates seen during the Noachian period. Subsequent periods of climatic change, such as those suggested to accompany the formation of a young ocean in the northern plains of Mars [11], must have been short-lived so as to not strongly affect the preservational state of craters formed on the post-Noachian aged terrain units.

Summary: Impact cratering was a major geologic process occurring during the time when the Martian highlands were forming. The Noachian ages of most of the highlands material coincides with the period of late heavy bombardment. Analysis of the crater record in the highlands (for craters ≥5 km in diameter) suggests that (1) the population of impacting objects during the late heavy bombardment period was different than the asteroids and comets which have dominated the record since that time; (2) the end of the late heavy bombardment period is not coincident with the end of the Noachian period but rather seems to have occurred at the transition between Lower and Upper Hesperian; and (3) there was a period of high degradation rates coincident with the Noachian period, the end of which is not directly related to the cessation of high impact rates from the late heavy bombardment period.

References: [1] Hartmann W. K. (1999) *Meteoritics & Planet. Sci., 34*, 167-177. [2] Hartmann W. K. et al. (2001) *Icarus, 149*, 37-53. [3] Lane M. D. et al. (2001), *LPS XXXII*, abstract #1984. [4] Barlow N. G. (1988) *Icarus, 75*, 285-305. [5] Strom R. G. et al. (1992) *Mars* (Univ. AZ Press), 383-423. [6] Barlow N. G. (1990) *JGR, 95*, 14191-14201. [7] Craddock R. A. and Maxwell T. A. (1993) *JGR, 98*, 3453-3468. [8] Grant J. A. and Schultz P. H. (1993) *JGR, 98*, 11025-11042. [9] Barlow N. G. (1995) *JGR, 100*, 23307-23316. [10] Melosh H. J. and Vickery A. M. (1989) *Nature, 338*, 487-489. [11] Baker V. R. (2000) *LPS XXXI*, abstract #1863.

ROCK ABRASION AND VENTIFACT FORMATION ON MARS FROM FIELD ANALOG, THEORETICAL, AND EXPERIMENTAL STUDIES N.T. Bridges[1] and J.E. Laity[2], [1]Jet Propulsion Laboratory, MS 183-501, 4800 Oak Grove Dr., Pasadena, CA 91109; nathan.bridges@jpl.nasa.gov, [2]Department of Geography, California State University, Northridge, CA 91330; julie.laity@csun.edu

Rocks observed by the Viking Landers and Pathfinder Lander/Sojourner rover exhibit a suite of perplexing rock textures [1-2]. Among these are pits, spongy textures, penetrative flutes, lineaments, crusts, and knobs. Fluvial, impact, chemical alteration, and aeolian mechanisms have been proposed for many of these. In an effort to better understand the origin and characteristics of Martian rock textures, abraded rocks in the Mojave Desert and other regions have been studied. We find that most Martian rock textures, as opposed to just a few, bear close resemblance to terrestrial aeolian textures and can most easily be explained by wind, not other, processes.

Flutes, grooves, and some pits on Mars are consistent with abrasion by saltating particles, as described previously. However, many other rock textures probably also have an aeolian origin. Sills at the base of rocks that generally lie at high elevations, such as Half Dome, are consistent with such features on Earth that are related to moats or soil ramps that shield the basal part of the rock from erosion. Crusts consisting of fluted fabrics, such as those on Stimpy and Chimp, are similar to fluted crusts on Earth that spall off over time. Knobby and lineated rocks are similar to terrestrial examples of heterogeneous rocks that differentially erode.

The location of specific rock textures on Mars also gives insight into their origin. Many of the most diagnostic ventifacts found at the Pathfinder site are located on rocks that lie near the crests or the upper slopes of ridges. On Earth, the most active ventifact formation occurs on sloped or elevated topography, where windflow is accelerated and particle kinetic energy and flux are increased. Integrated together, these observations point to significant aeolian modification of rocks on Mars and cast doubt on whether many primary textures resulting from other processes are preserved.

Experimental simulations of abrasion in the presence of abundant sand indicate that rocks on Mars should erode at a rate of 7.7 to 210 $\mu m\ yr^{-1}$ [3]. These rates cannot have operated over the entire history of the Pathfinder site or elsewhere on Mars, because craters, knobs, and other obstacles would be quickly worn away. More likely, rock abrasion occurs over short time periods when sand supplies are sufficient and saltation friction speeds are frequently reached [4]. Depletion or exhaustion of sand and a decline in wind fluxes at speeds greater than that of saltation friction will then act to reduce the rate of further abrasion. We are currently engaged in a new set of wind tunnel experiments coupled with theoretical models and field studies that address rock abrasion and ventifact formation on Mars and Earth [5].

These studies have implications for the Noachian, when sand supplies were probably more plentiful and the threshold friction speed was possibly lower because of a more dense atmosphere. Under these conditions, erosion rates from the wind could have been much greater than today, contributing, along with probable fluvial erosion, to the Noachian landscape that is in limited preservation today.

References:

[1] McCauley, J.F., et al (1979) *JGR, 84,* 8222-8232. [2] Bridges, N.T. et al. (1999) *JGR, 104,* 8595-8615. [3] Greeley, R. et al. (1982) *JGR, 87,* 10,009-10,024. [4] Golombek, M.P. and Bridges, N.T. (2000) *JGR, 105,* 1841-1853. [5] Bridges, N.T. et al. (2001), *Lun. Plan. Sci. XXXII*, 1873.

MOJAVE DESERT STREAM BEDS RESEMBLING MARTIAN CHANNELS. J.D. Burke, The Planetary Society, 65 N. Catalina Ave., Pasadena, CA 91106, 626-355-0732, jdburke@its.caltech.edu

Introduction: In 1970, while investigating lunar robotic roving missions, members of the JPL rover team flew over parts of the Mojave desert looking for test sites. We observed some sinuous channels quite unlike the braided arroyos normally found on alluvial fans. Investigating these channels on the ground, we found that they occur only where a stream emerges from a canyon into a region of deep windblown sand.

Stream bed character: The peculiar stream beds have steep sides, may contain inner meandering channels, taper away to nothing at their lower ends with no evidence of a delta or debris deposit , and are thus clearly the result of erosion and deposition processes different from those acting on normal Mojave Desert alluvium. In many respects they resemble lunar sinuous rilles, except that the lunar rilles (e.g., Schroeter's Valley) extend to much larger sizes. Now that similar features have been seen on Mars, it is worthwhile to re-examine the Mojave rilles as a martian analog.

Locations: The best examples of these channels are found on the Twenty-nine Palms US Marine Corps Base, northwest of the main base area. Others can be seen southeast of Interstate Highway 15 between Barstow and Baker.

Reference: Burke, J.D., Brereton, R.G., and Muller, P.M., Desert Stream Channels Resembling Lunar Sinuous Rilles. Nature 225, 5239, 1234-1236, 28 March 1970

MARTIAN DRAINAGE DENSITIES: ANALYSES FROM MOLA DIGITAL ELEVATION MODELS. Robert A. Craddock[1], Rossman P. Irwin[1], and Alan D. Howard[2], [1]Center for Earth and Planetary Studies, National Air and Space Museum, Smithsonian Institution, Washington, DC 20560-0315; craddock@nasm.si.edu, [2]Department of Environmental Sciences, University of Virginia, Charlottesville, VA 22903.

Introduction: Martian valley networks indicate that at least geologic conditions were different in the past, if not the climate. It is commonly believed that valley networks must be the result of groundwater sapping because their apparent drainage densities are lower than terrestrial runoff channels [1, 2, 3] (Figure 1a). It has also been suggested that valley networks are not uniformly distributed on topography, which would also argue in favor of groundwater sapping [4]. When coupled to the belief that early Mars was cold and dry such observations have led many investigators to suggest that valley networks were fed by geothermal heating of ground ice [4, 5, 6]. This interpretation has become so entrenched in the planetary community that geothermal heating has essentially become a panacea. Valley networks are no longer seen as some of the best evidence for past surface water. Rather, they are automatically equated to a cold, dry climate. Unfortunately, however, plotting the densities of valley networks from imagery data is easily influenced by observational bias and image interpretation. Using topographic data from Mars Global Surveyor, we are in the process of making a more impartial analysis of valley network drainage densities and morphometric characteristics.

Objective: A number of algorithms have been written to allow investigators to extract terrestrial drainage basin information from DEM's (e.g., [7]). Using the commercial software package RiverTools 2.4, we are in the process of analyzing valley network characteristics from DEM's generated from MOLA data. These results will be compared to terrestrial drainage basins located in a variety of environments.

Approach. Mars Orbiter Laser Altimeter data collected from ±30° latitude and released through May 2001, were gridded to ~1.8 km resolution (Figure 1b). The resulting digital elevation models were then subjected to the D8 algorithm. Flow direction is represented by a single angle taken as the steepest downward slope on the eight triangular facets center at each surrounding pixel. Upslope area is then calculated by proportioning flow between two downslope pixels according to how close this flow direction is to the downslope pixel. This algorithm is the same used to determine the location of the largest drainage basins on Mars [Banerdt and Vidal, 2001].

Martian DEM's differ from terrestrial DEM's in that there is a great deal of topographic expression from impact craters. Complicating this is the fact that craters were forming as valley networks developed. It appears that craters often changed the characteristics of the drainage basin completely [8]. Craters >20-km-diameter were treated as closed basins (i.e., "lakes"). Craters <20-km diameter was "filled in" to the surrounding base level so that they were essentially ignored by the algorithm. Gradients in flat areas were resolved using the imposed gradient method [9] so that flow direction remained self-consistent across these features. The resulting flow grid file was used to trace the location of valley networks (Figure 1c).

Preliminary Results. The algorithm does a poor job of predicting the location of streams with Strahler orders of ≤3 due to the resolution of the DEM and, in part, because of the irregular positions of the MOLA tracks. The algorithm also does a poor job of dealing with flat areas. Both of these are common problems when dealing with terrestrial DEM's. However, the results for streams with Strahler orders >3 are promising (Figure 1d). They are consistent with valley networks identified from Viking images, yet the bias from this method alone becomes clear. Valley networks are much more complicated, integrated systems than have been previously reported from image analyses [2, 3, 4]. Conservatively, drainage densities are a factor of 20 times higher in Figure 1 than previous estimates (~0.193 km^{-1} versus 0.01 km^{-1} [3]), and are similar to densities for terrestrial runoff channels.

References: [1] Pieri D. (1976) *Icarus, 27,* 25-50. [2] Pieri D., (1980)*Science, 210,* 895-897. [3] Carr M.H. and Chuang F.C. (1997) *J. Geophys. Res., 102,* 9145-9152. [4] Gulick V.C. (1998)*J. Geophys. Res., 103,* 19,365-19,387. [5] Brakenridge G.R. et al. (1985) *Geology, 13,* 859-862. [6] Squyres S.W. and Kasting J.F. (1994) *Science, 265,* 744-749. [7] Tarboton D.G. (1997) *Water Resourc. Res., 33,* 309-319. [8] Irwin R.P. and Craddock R.A., this volume [9] Garbrecht J. and Martz L.W. (1997) *J. Hydrol., 193,* 204-213.

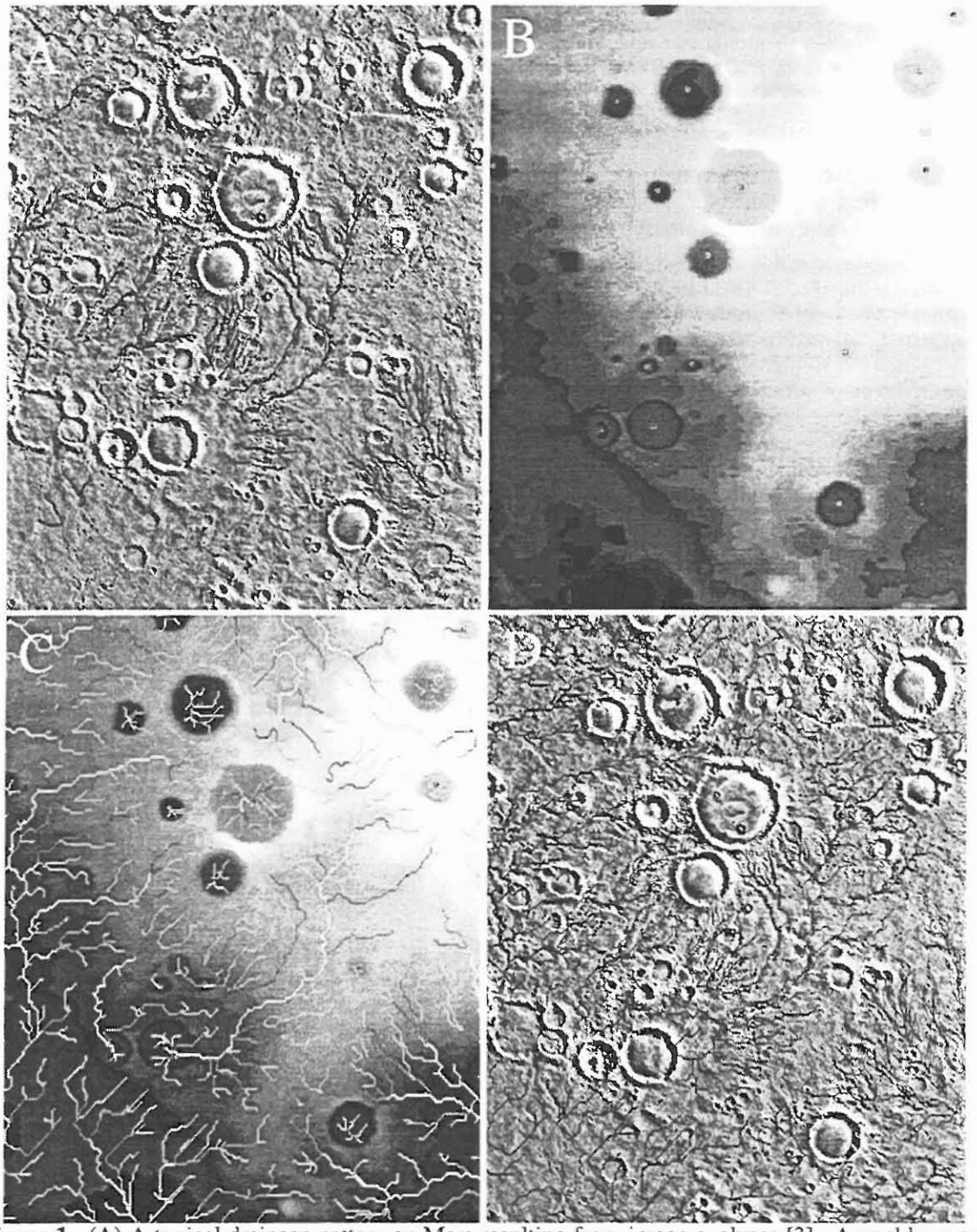

Figure 1. (A) A typical drainage pattern on Mars resulting from image analyses [3]. Arguably, many more valley networks are visible than have been plotted. (B) A MOLA DEM gridded at ~1.8 km resolution. Even at this reduced resolution, large stream channels and drainage basins can be seen. (C) A plot of streams with Strahler orders ≥4 extracted from the D8 algorithm. Note that program does a poor job of resolving streams in flat areas. (D) Results from flat areas are removed and plotted on a photomosaic base map. Compare these results with (A). Valley networks are part of much larger integrated networks. Often there development was affected by impact cratering [8].

IMAGING RADAR IN THE MOJAVE DESERT – DEATH VALLEY REGION. Tom G Farr, Jet Propulsion Laboratory, California Institute of Technology, Pasadena, CA 91109, tom.farr@jpl.nasa.gov.

The Mojave Desert – Death Valley region has had a long history as a test bed for remote sensing techniques. Along with visible-near infrared and thermal IR sensors, imaging radars have flown and orbited over the area since the 1970's, yielding new insights into the geologic applications of these technologies. More recently, radar interferometry has been used to derive digital topographic maps of the area, supplementing the USGS 7.5' digital quadrangles currently available for nearly the entire area.

As for their shorter-wavelength brethren, imaging radars were tested early in their civilian history in the Mojave Desert - Death Valley region because it contains a variety of surface types in a small area without the confounding effects of vegetation. The earliest imaging radars to be flown over the region included military tests of short-wavelength (3 cm) X-band sensors [1]. Later, the Jet Propulsion Laboratory began its development of imaging radars with an airborne sensor, followed by the Seasat orbital radar in 1978. These systems were L-band (25 cm). Following Seasat, JPL embarked upon a series of Space Shuttle Imaging Radars: SIR-A (1981), SIR-B (1984), and SIR-C (1994). The most recent in the series was the most capable radar sensor flown in space and acquired large numbers of data swaths in a variety of test areas around the world. The Mojave Desert – Death Valley region was one of those test areas, and was covered very well with 3 wavelengths, multiple polarizations, and at multiple angles.

At the same time, the JPL aircraft radar program continued improving and collecting data over the Mojave Desert – Death Valley region. Now called AIRSAR, the system includes 3 bands (P-band, 67 cm; L-band, 25 cm; C-band, 5 cm). Each band can collect all possible polarizations in a mode called polarimetry. In addition, AIRSAR can be operated in the TOPSAR mode wherein 2 antennas collect data interferometrically, yielding a digital elevation model (DEM). Both L-band and C-band can be operated in this way, with horizontal resolution of about 5 m and vertical errors less than 2 m.

In arid regions, it has been recognized that the weathering habit of a rock outcrop will determine its appearance in a radar image. Resistant, jointed rocks tend to appear bright, while fissile easily comminuted rock types appear dark. In one of the classic early radar studies, Schaber et al. [1] explained in a semi-quantitative way the response of an imaging radar to surface roughness near the radar wavelength. This laid the groundwork for applications of airborne and spaceborne radars to geologic problems in arid regions. Thus radars produce images of the physical nature of the surface, complementary to the compositional information produced by optical sensors. A secondary characteristic of the surface, its dielectric constant, which is strongly affected by moisture content plays a much smaller part, but can sometimes be seen to affect image tone around springs and after a rainfall.

When the wavelength is long and the dielectric constant is low (e.g. very dry soil) surface penetration may occur and subsurface horizons may be imaged. This was surprisingly demonstrated by SIR-A in 1981 over the Sahara Desert [2]. Bedrock and alluvial gravels covered by several meters of well-sorted, dry sand were clearly imaged at L-band (25 cm). A few sites in the Mojave Desert – Death Valley region have also demonstrated penetration at L-band and P-band (67 cm) [3, 4, 5].

Another useful application for imaging radar is mapping of surficial deposits and processes. Many surficial geomorphic processes act to change the roughness of a surface. In the southwest US, the most common processes are salt weathering (near salty playas), aeolian deposition, and desert pavement formation. Daily et al. [6] found that combining Landsat optical images with airborne radar images were useful for mapping several alluvial fan units, based on desert varnish formation in the optical wavelengths and desert pavement formation in the radar images. Taking this further afield, Farr and Chadwick [7] applied a similar approach to map fan units in a high valley in western China. These results make a case for the possibility that different surficial processes leave diagnostic signatures in multi-sensor remote sensing data, a possibility that will require much more extensive tests for uniqueness in different environments.

A more quantitative attempt at connecting radar images with surficial processes was undertaken by Farr [8]. Building on the work of Dohrenwend et al. [9] and Wells et al. [10], roughness changes with age at Cima Volcanic Field were quantified using close-range stereo photography from a helicopter. The results were then compared with radar images inverted to become maps of surface roughness [11]. The helicopter stereo photographs where reduced to profiles for the study. Profiles ranged from 10-30 m long and the points were spaced 1 cm apart. Typically about 15-20 profiles for each stereo-pair were produced. Sites for which helicopter-derived roughness profiles exist include lava flows (Pisgah Lava Flow, Amboy Lava Flow, Cima Volcanic Field, Lunar Crater Volcanic Field), alluvial fans (Death Valley, Silver Lake, Owens Valley), playas (Death Valley, Lavic Lake), and sand dunes (Death Valley). These data form a unique resource for those studying the effects of surficial processes on microtopography and remote sensing response to surface roughness.

References:

[1] Schaber, G.G., G.L. Berlin, W.E. Brown, Jr., 1976, Variations in surface roughness within Mojave Desert - Death Valley region, California: Geologic evaluation of 25-cm-wavelength radar images, Geol. Soc. Amer. Bull., v. 87,

29-41.

[2] McCauley, J.F., G.G. Schaber, C.S. Breed, M.J. Grolier, C.V. Haynes, B. Issawi, C. Elachi, R. Blom, 1982, Subsurface valleys and geoarchaeology of the eastern Sahara revealed by Shuttle Radar, Science, v. 218, p. 1004-1020.

[3] Blom, R., R.E. Crippen, C. Elachi, 1984, Detection of subsurface features in Seasat radar images of Means Valley, Mojave Desert, California, Geology, v. 12, p. 346-349.

[4] Schaber, G.G., J.F. McCauley, C.S. Breed, G.R. Olhoeft, 1986, Shuttle imaging radar: Physical controls on signal penetration and subsurface scattering in the eastern Sahara, IEEE Trans. Geosci. Rem. Sens., v. GE-24, 603-623.

[5] Schaber, G.G., 1999, SAR studies in the Yuma Desert, Arizona: Sand penetration, geology, and the detection of military ordnance debris, Rem. Sens. Env., v. 67, p. 320-347.

[6] Daily, M., T. Farr, C. Elachi, and G. Schaber, 1979, Geologic interpretation from composited radar and Landsat imagery, Photogram. Engr. Rem. Sens., v. 45, p. 1109-1116.

[7] Farr, T.G., O.A. Chadwick, 1996, Geomorphic processes and remote sensing signatures of alluvial fans in the Kun Lun Mountains, China, J. Geophys. Research, v. 101, p. 23,091-23,100.

[8] Farr, T.G., 1992, Microtopographic evolution of lava flows at Cima volcanic field, Mojave Desert, California, J. Geophys. Res., v. 97, p. 15171-15179.

[9] Dohrenwend, J.C., L.D. McFadden, B.D. Turrin, S.G. Wells, 1984, K-Ar dating of the Cima volcanic field, eastern Mojave Desert, California: Late Cenozoic volcanic history and landscape evolution, Geology, v. 12, p. 163-167.

[10] Wells, S.G., J.C. Dohrenwend, L.D. McFadden, B.D. Turrin, K.D. Mahrer, 1985, Late Cenozoic landscape evolution on lava flow surfaces of the Cima volcanic field, Mojave Desert, California, Geol. Soc. Amer. Bull., v. 96, p. 1518-1529.

[11] Evans, D.L, T.G. Farr, J.J. van Zyl, 1992, Estimates of surface roughness derived from synthetic aperture radar (SAR) data, IEEE Trans. Geosci. Rem. Sens., v. 30, p. 382-389.

Acknowledgments: Work performed under contract to NASA.

EVOLVING PERSPECTIVES ON THE GEOLOGIC EVOLUTION OF EARLY MARTIAN CRATER BASINS R. D. Forsythe[1] and C. R. Blackwelder[1], Dept. Geography and Earth Sciences, University of North Carolina at Charlotte, Charlotte, NC 28205, rdforsyt@email.uncc.edu.

Introduction: This contribution continues to explore a model first proposed by Forsythe and Zimbleman, 1995 [1] and expanded upon in the work of Forsythe and Blackwelder, 1998 [2]. The model views the ancient southern highlands of Mars as having formed under a climatic and hydrologic regime akin to semi-arid and arid lands on Earth. Within this regime a groundwater table existed within the upper regolith, sufficiently shallow to be easily intercepted by impact basins a few kilometers in diameter. These depressions, when isolated from regional surface drainage networks, represent closed-drainage watersheds. Where positioned along outflow systems, the crater basins formed lakes, within which fluvial and lacustrine evidence exists for baselevel-controlled hydrology/geomorphology (e.g. terraces[1]). The case for closed drainage crater basins is essentially a case for evaporite basins, and was further explored in detail in Forsythe and Blackwelder, 1998 [2], wherein approximately 140 evaporite basins were identified by locating craters with inflow, but no surface water outflow, channels. Baselevel indicators, stream channel hydraulics, and nominal assumptions regarding hydrogeologic properties for Martian regolith were used in this study to constrain a MODFLOW simulation of a generic Martian Noachian evaporite basin. This simulation yielded evaporation rates of approximately 10-20 cm/yr and precipitation rates of 10-20 mm/yr. Here we explore the geologic implications of the early work and attempt to build a more evolutionary scheme for crater basin evolution.

Hydrogeologic and Geologic Implications for the Martian Highlands: The evaporite basins of the Atacama Desert of Chile and those of the Great Basin in the United States form reasonable analogs to build a foundation of the stratigraphic, morphologic, and hydrologic processes that interact in the geologic evolution of closed-drainage basins. In the Atacama desert these processes are controlled by climatic variables of precipitation, evaporation, regional groundwater systematics, wind action, as well as tectonic and volcanic processes[3]. Depending on the balance of precipitation and surface water inputs, evaporation rates, and groundwater levels, closed crater basins will be one of two depositional types: clastic basins, or crystal-type evaporite basins. Clastic playa basins are sufficiently elevated above the water table to remain ground water recharge areas, and thus tend to leach, not precipitate, salts over the balance of seasonal fluctuations.

The discharge/evaporite basin model suggests that closed basins will infill with salts in a relatively short period of time. If regional groundwater under the Highlands has even a few % of dissolved minerals it will take, at most, only 1-2 million years for the 10 to 100 times the basin volume to exchange in water, and leave behind a thick salt (carbonates, sulfates and chlorites) deposit[2]. The salts will eventually build up to, and even rise above the water table; until the capillary forces and atmospheric ventilation can no longer exchange water efficiently from the water table. This depth from a practical perspective is likely in the range of a few meters.

Within the groundwater discharge model the flat basin center floor is viewed as the restored regional water table at the end of the basin's life as a groundwater discharge system. With this in mind, one can view the floors of the various basins throughout the Martian Highlands as snapshots of ground water levels in the few million years following the impact event. Compound impact basins such as those of Figure 1, and closely nested basins, document a decline of the Highlands' water table that was protracted and evolutionary rather than abrupt and catastrophic.

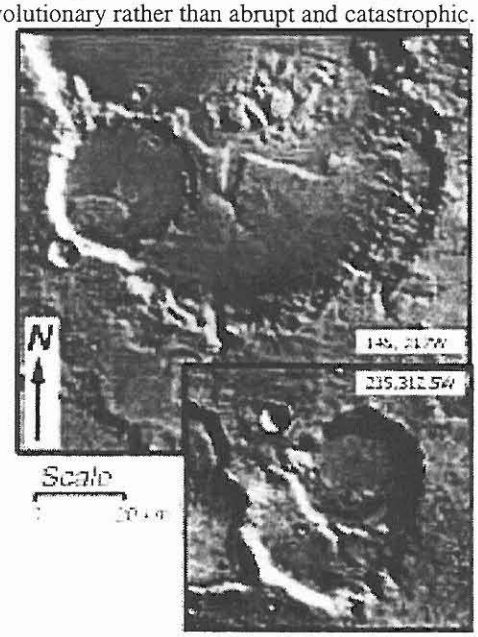

Figure 1. Two examples of compound closed drainage crater basins with lowered baselevels in the younger superimposed basin(s) [3].

The more evolutionary geologic implications from this model is that the basins will each undergo a similar series of evolutionary stages as the groundwater system is first perturbed and then relaxed during the cycle that the basin acts as a groundwater pump.

Here, we use the White Rock crater basin (7.8S, 334.75W) as an example. In figure 2, a stratigraphic section is proposed for the basin. All units are exposed, with exception of the postulated impact breccia and a lacustine unit. The basin history starts with an impact event that breaches the regional water table, and is quickly following first by deposition of the impact breccia and then inundated by groundwater flooding. This phase is somewhat akin to the early drawdown phase in a pumping test, where disequilibrium dominates with rapidly changing flow paths and potentiometric surfaces. Since groundwater flooding outpaces any possible depositional processes this leads to the formation of a lake, and one would expect that all crater impacts breaching the existing Martian water table by more than a few 10's of meters would produce a lake. Following the impact and lake phase, we expect to enter the main evaporite basin phase; this can be characterized as one having a local quasi-equilibrium groundwater flow regime, with discharges balanced by regional recharge. It is this dynamic equilibrium that was model with MODFLOW and suggested a longevity of a few 100,000 to perhaps a million years[2]. This model is life-limited by the exchange rate and regional concentration of salts in the Martian groundwater. Sooner or later, salts choke off the evaporation system, and shut down the discharge pump. This ends the evaporite stage of the basin, and it evolves to a stage akin to one of the 'recharge' playas of the Great Basin, where any precipitation will infiltrate the previous salt deposit and start to etch and dissolve the earlier deposited salts. In the case of the White Rock basin this stage was interrupted by deposition of the strata forming White Rock. The most likely hypothesis, currently, is that this is of volcanic origin (ignimbrite or ash).

As the Martian atmosphere continues to desiccate, the recharge-playa stage will be followed by a final stage (which continues today) under which wind continues to erode and deposit friable materials within and along the edges of these basins. In the case of White Rock, young fluidized debris flows are seen along the south edge of the basin, which suggest localized volatile reservoirs have persisted in perched locations within the upper regolith.

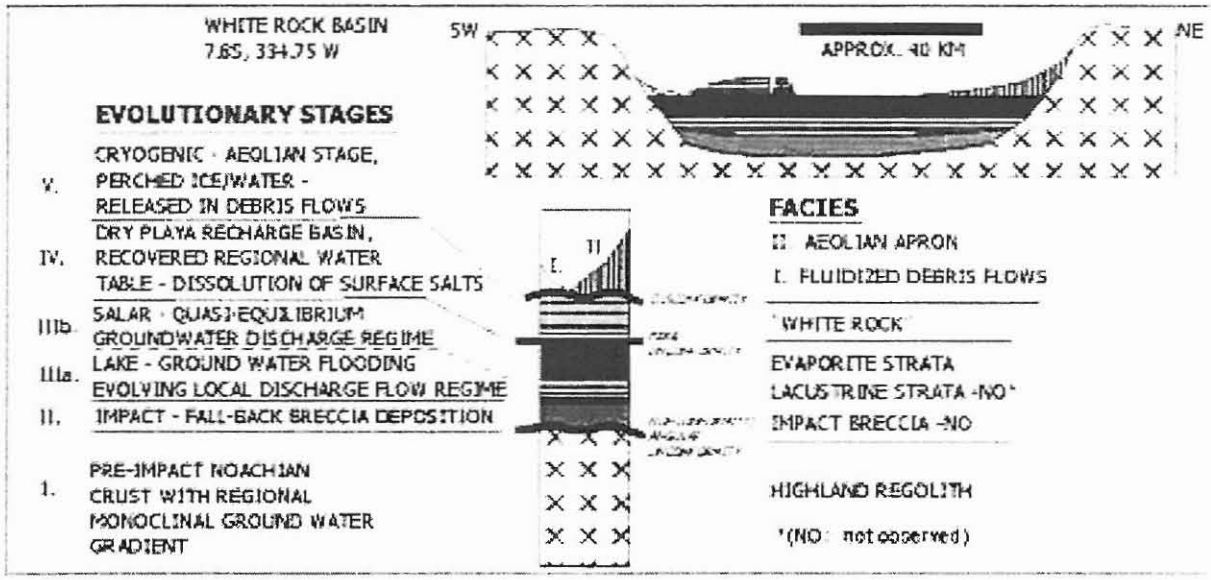

Figure 2. Evolutionary model for Noachian-Hesperian crater basins using 'White Rock' basin as an example.

References: [1] Forsythe, R. D. and Zimbleman J. R., (1995) *JGR, 100,* 5553-3363. [2] [1] Forsythe, R. D. and Balckwelder, C. R., (1998) *JGR, 103, 31,421-31,431* [3] Stoertz, G.E., and Ericksen, G. E., *USGS Prof.Paper 811, 65.*

EXPLORING THE MARTIAN HIGHLANDS USING A ROVER-DEPLOYED GROUND PENETRATING RADAR. J. A. Grant[1] , A. E. Schutz[2], and B. A. Campbell[1], [1]Smithsonian Institution, Center for Earth and Planetary Studies, MRC 315, Washington, DC 20560, grantj@nasm.si.edu, [2]Geophysical Survey Systems, Inc., 13 Klein Drive, North Salem, NH, 01950.

Introduction: The Martian highlands record a long and often complex history of geologic activity that has shaped the planet over time. Results of geologic mapping (e.g., 1-3) and new data from the Mars Global Surveyor spacecraft (e.g., 4, 5) reveal layered surfaces created by multiple processes that are often mantled by eolian deposits. Knowledge of the near-surface stratigraphy as it relates to evolution of surface morphology will provide critical context for interpreting rover/lander remote sensing data and for defining the geologic setting of a highland lander.

Rover-deployed ground penetrating radar (GPR) can directly measure the range and character of *in situ* radar properties [6-7], thereby helping to constrain near-surface geology and structure. As is the case for most remote sensing instruments, a GPR may not detect water unambiguously on Mars. Nevertheless, any local, near-surface occurrence of liquid water will lead to large, easily detected dielectric contrasts. Moreover, definition of stratigraphy and setting will help in evaluating the history of aqueous activity and where any water might occur and be accessible.

GPR data can also be used to infer the degree of any post-depositional pedogenic alteration or weathering, thereby enabling assessment of pristine versus secondary morphology. Most importantly perhaps, GPR can provide critical context for other rover and orbital instruments/data sets. Hence, rover-deployment of a GPR deployment should enable 3-D mapping of local stratigraphy and could guide subsurface sampling.

Development of an Impulse GPR for Mars: In recognition of the potential for constraining near-surface stratigraphy and structure, development of a miniaturized impulse GPR is well underway. Efforts are focused on design and testing of a prototype transducer array in parallel with fabrication of a low power, mass, and volume control unit. The operational depth of 10-20 meters is geared towards definition of stratigraphy, subsurface block distribution, and structure at the decimeter to meter scale needed for establishing geologic setting. Likely interface requirements influence target mass, power, and volume limits of 0.5 kg, 3W (peak), and 3400 cc, respectively.

GPR Transducers: Transducer development is driven in part by the assumption that most Martian surfaces will be dry, possess dielectric values generally between 3-10, and have corresponding loss tangents of ~0.01 +/- 0.005 [*e.g.*, 8, 9]. These expected environmental conditions together with a desire to produce an easily modified "generic" array (*e.g.*, for optimizing performance by changing antenna fan width to alter the center operating frequency) have yielded both high frequency bistatic (Fig. 1) and low frequency monostatic "rat-tail" transducer components.

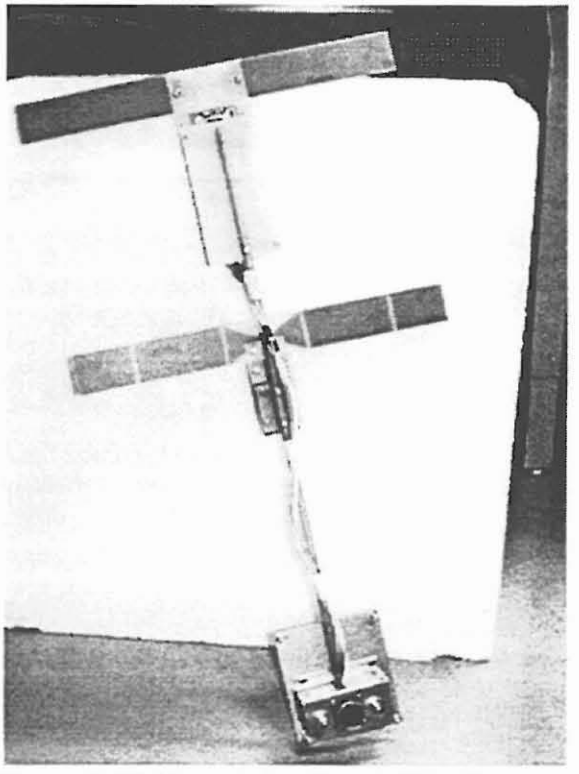

Figure 1. Field-tested breadboard high frequency bistatic transducer. Note table leg for scale.

Transducer deployment will likely occur above the ground (so as not to present a possible hazard to rover mobility) using a retractable bar with components mounted at the outboard end (see Fig. 1), thereby enabling good separation from the rover. Each of the transducers consists of a high-speed sample hold circuit that can incorporate a rf amplifier on its front end. It is unlikely that the risk of electrostatic charging will require significant design modifications because above ground deployment of the bistatic transducer precludes the need for isolation from the rover. Similarly, using the rover as part of the antenna could mitigate any unexpected problems associated with the low frequency component.

Sample output from the high frequency antenna component is displayed in Figure 2. The bistatic nature

of the high frequency antenna minimizes the "clear time" required and the antenna operates at 1.68 ns/cycle at a center frequency of 600 MHz. Construction involved standard parts and 38 cm-long resistively loaded dipoles mounted on a dielectric rod at a height of 15 cm above the ground. Operation of the antenna permits distinguishing radar reflections corresponding to stratigraphy to depths of ~15 meters.

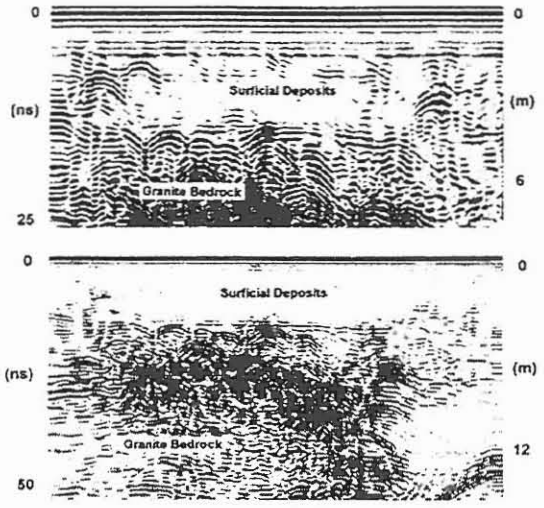

Figure 2. Sample data from high frequency bistatic transducer component shown in Figure 1. Data was collected in test-bed with stratigraphy consisting of sand fill overlying unconsolidated *in situ* sediments and granitic bedrock.

A prototype of a low frequency "rat-tail" antenna has also been tested and enabled distinguishing reflections up to 15 m below the surface. Initial operation of the "rat-tail" required use of bistatically configured, 40 cm long, resistivity loaded monopoles as antennas (center frequency 100 MHz).

GPR Control Unit: Design and construction of a complete "breadboard" impulse GPR control unit involves consolidation of electronics, function, and memory onto a single board in order to minimize mass and volume. The resultant prototype rover-deployable GPR is a major stride towards achieving stated system mass, power, and performance requirements. The system will operate at a range of up to 1000 nanoseconds and the data rate for simultaneous operation of both transducers is ~0.3 MB/day or less (assumes 50 m/day rover traverse). Because many rover components (including the wheels) will be metallic, and because electrostatic charging by dust may be important, the GPR will need to be in metal box and grounded to the rover frame.

Terrestrial Analogs for Mars: As an important step towards defining the potential of a rover-deployed GPR on Mars, data were collected at the site of the 2001 "blind" FIDO rover trials. Data were collected using a 400 MHz transducer under less than optimal conditions (highly conductive soils were wet due to recent rains). Nevertheless, data confirm the ability to constrain the geologic setting and provide context for interpreting data from other instruments. The GPR data

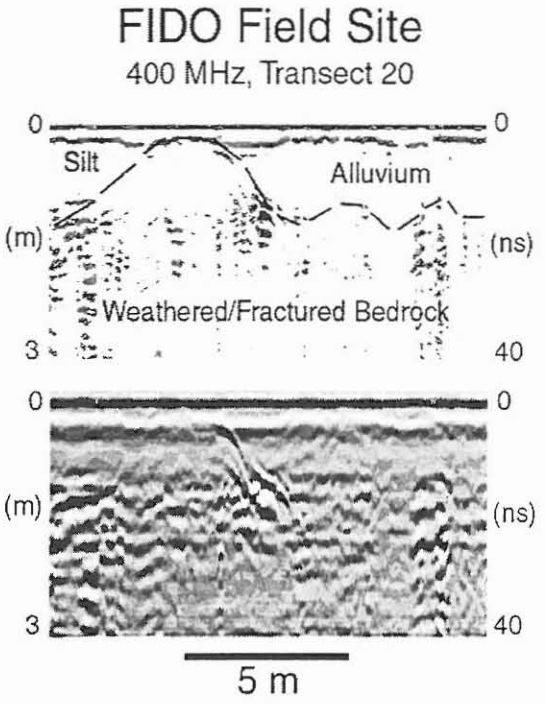

Figure 3. Sample 400 MHz GPR data from the 2001 FIDO field-test site. See text for discussion.

reveal (Fig. 3) that the blocky surface of the site is created by a stone pavement overlying a block-free horizon of eolian silt rather than bedrock. Moreover, data indicate underlying weathered bedrock extends laterally into a wash beneath a thin veneer of alluvium. These results highlight how interpretation of setting might be in error or how samples/measurements may be mistargeted without knowledge of shallow stratigraphy. Work funded by NASA PIDDP Grant NAG5-9658.

References: [1] Greeley, R. and Guest, J.E., 1987, USGS Map I-1802-B. [2] Scott, D.H. and Tanaka, K.L., 1985, USGS Map I-1802-A. [3] Tanaka, K.L., et al., 1992, p. 383-423, in Kieffer, H.H., et al. (eds.), Mars, U of A Press, Tucson, AZ. [4] Malin, M. C., et al., 1998, Science, 279, 1681. [5] Malin, M.C., and Edgett, K.S., 2000, Science, 290, 1927. [6] Olhoeft, G.R. (1998) *Proc. GPR'98*, Univ. Kansas, Lawrence, KS, 387. [7] Grant, J.A., et al. (2000) *LPSC XXXI*, LPI, Houston, TX. [8] Campbell et al. (1997) *JGR 102*, 19,307. [9] Plaut, J. J. (1998) *Deep Water Sounding on Mars Workshop,* NASA Ames, Mountain View, CA.

THE FERRAR DOLERITE: AN ANTARCTIC ANALOG FOR MARTIAN BASALTIC LITHOLOGIES AND WEATHERING PROCESSES. R. P.. Harvey[1] [1]Dept. of Geological Sciences, Case Western Reserve University, Cleveland OH 44106-7216 (rph@po.cwru.edu).

Introduction: The Ferrar Dolerite is one of the most prominent rocks of East Antarctica, forming well-exposed cliffs along the length of the Transantarctic Mountains. The Ferrar serves as an excellent analog for martian igneous lithologies on a number of scales, from planetary (global concepts of its origin) to the outcrop and hand specimen (cm-scale weathering features) to the microscopic (thin-section scale petrologic similarities to martian meteorites).

Planetary scale: The Ferrar dolerite is a shallow intrusive exposed on a scale seldom seen among terrestrial igneous rocks. Together with its contemporaneous extrusive counterpart in Antarctica (the Kirkpatrick Basalt) and coeval lithologies of Australia (the Tasmanian and Victoria dolerites) and South Africa (the Karoo dolerites and basalts) they represent a significant event in planetary history and one of the largest effusive events. The event in question is the breakup of Gondwanaland in the early to mid-Jurassic, contemporaneous with Ferrar intrusion approximately 177 Ma [1,2].

While not all localities offer supporting evidence, most authors suggest that the association between the Ferrar and the disassembly of Gondwanaland is not coincidental. The tectonic extension and rifting associated with the breakup of Gondwanaland (and Pangea before it) is typically considered a response to significant mantle upwelling beneath a singularly large and insulating continental mass [1, 3, 4]. Similar plumes are almost ubiquitously cited as the driving force behind large volume Martian magmatism, with the production of large volumes of mantle-derived magma at localized sites beneath thick immobile crust [e.g., 5]. The Ferrar may or may not be a good analogy in this regard; some isotopic studies of suggest an origin from very "fertile" mantle, while others prefer a mantle strongly influenced by assimilation of subducted crust [e.g., 6].

Outcrop Scale: The Ferrar is extremely well exposed in spite of its occurrence on the Earth's only ice-covered continent. Because it is stratigraphically young and one of the most resistant rocks within the heavily glaciated Transantarctics, at most localities it is exposed as cliffs, often several hundred meters high (Fig. 1) . The sills that make up the Ferrar therefore typically show very complete cross-sections of varying thickness and intrude among the older (Devonian-Triassic) sedimentary sequences of the Beacon Supergroup. Often these sills assimilate large lenses of the intruded sequences. Feeder dikes are rarely exposed, and in most localities (but not all) emplacement of the Ferrar appears to have been a single event contiguous across the Transantarctics. The sills are commonly differentiated, showing significant compositional and crystal settling features. Sills also show significant grain size variation from interior to exterior and around included lenses of sedimentary formations. Thick exposures of the Ferrar typically show columnar jointing and outcrop surfaces commonly show a pattern of strong exfoliation around the joints, creating rounded surfaces with developing adjacent regolith (Fig. 2). Although cross sections of the martian crust are typically not as well exposed as the Ferrar, studies of outcrop slopes and stability in Valles Marineris suggest

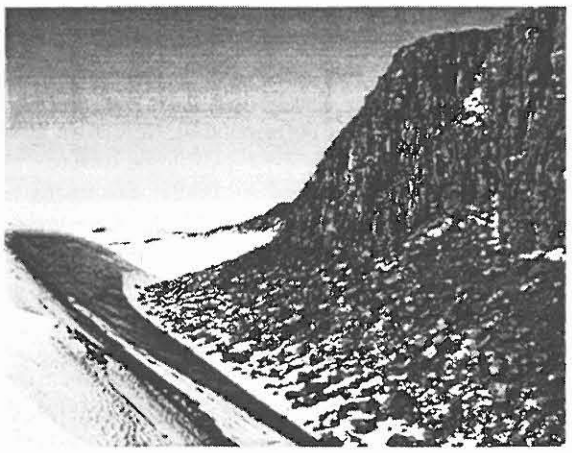

Figure 1, Typical occurrence of the Ferrar Dloerite as the major cliff-forming unit of the Transantarctic Moutains.

Figure 2. Typical weathering on exposed Ferrar surfaces.

the behavior of the Ferrar is analogous to that of massive martian volcanics [7, 8].

Hand Specimen Scale: Fresh Ferrar dolerite is a gray-green color because of the abundant mafic mineral content; upon weathering the Ferrar becomes a rich reddish-brown. In sawn or broken section coarse-grained interior Ferrar strongly resembles both the basaltic and lherzolitic shergottites, exhibiting cm-scale dark and light patches corresponding to relative abundance of pyroxene or feldspar petrologic texture. As is seen on the outcrop scale, smaller specimens are often rounded by exfoliation. However, finer-grained specimens exhibit a variety of classic desert habits including ventifaction, salt encrustations, desert varnish development and cavernous weathering [9, 10] (Fig. 3). Ferrar dolerite cobbles found in moraines or scree slopes are typically angular while cobbles found resting on ice are severely rounded, suggesting that the balance between chemical and mechanical weathering varies significantly between local sites.

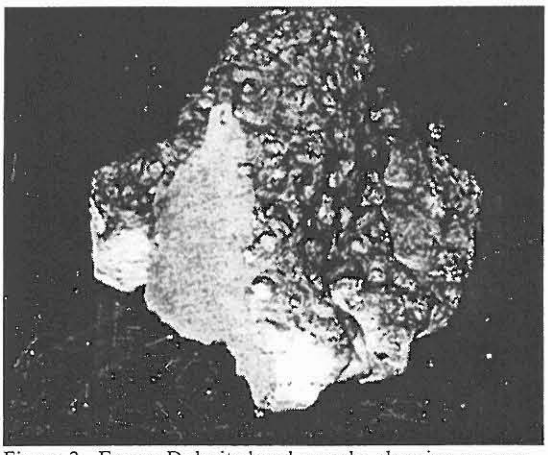

Figure 3. Ferrrar Dolerite hand sample, showing cavernous weathering on exterior while dense fracture-free interior remains unaltered. Specimen is approximately 22

The variety of weathering features exhibited by the Ferrar strongly resemble those seen in images returned by the Mars Pathfinder lander mission [11]. By analogy they show that the textural features observed at the Pathfinder landing site have plausible origins as the product of desert weathering of rocks of basaltic composition.

Thin-section Scale: the Ferrar dolerite bears broad geochemical and mineralogical similarities to Martian igneous lithologies. The Ferrar is an intrusive gabbroic rock containing two pyroxenes (both ortho- and clino-, with a third pyroxene commonly present in exsolution), two feldspars (plagioclase and alkaline) and a significant vol. percent of Fe and Ti oxides. Texturally the rock resembles the coarser basaltic shergottites in terms of mode, average grain size and a general cumulate appearance. Often pyroxene and feldspar grains are elongated and zoned in a manner similar to that seen in the coarser shergottites. Weathered examples of the Ferrar exhibit brown iron-staining of the mafic minerals as well as dissolution of feldspars and pyroxenes, and development of minor amounts of secondary quartz, clays and other poorly crystalline phases. A brown surface varnish deposit, a cryptocrystalline amalgam of silica and iron oxide, often protects the interior of specimens below. The Kirkpatrick basalt has been less extensively studied and is identical in terms of bulk chemistry and mineralogy but with a much finer texture, producing a much more resistant rock. It also can commonly be found in a vesicular texture with zeolites filling the vesicles, and both rocks commonly exhibit significant salt deposits in highly weathered specimens.

Summary The small amount of study completed so far suggests that the Ferrar dolerite (and Kirkpatrick basalt) is an excellent terrestrial analog for the basaltic martian meteorites in many ways. Currently we are in the process of testing this analogy in more detail, which requires study of the Ferrar with the extraordinary and exhaustive focus commonly turned toward Martian meteorites. Like the Munro Township basalts commonly used as an analogy to the nakhlites, the Ferrar should provide new insight into the origins of an important group of martian meteorites. This time, however, the rocks are unmetamorphosed, younger, and well-exposed, making it easier to explore not only petrologic similarities but also petrogenetic similarities. This should in turn provide new insight into the evolution of the martian crust and the distinctions between geological processes on Mars and Earth.

References: [1] Encarnacion et al, (1996) *GSA Abstracts w/ Programs* **28**, 162. [2] Heimann et al., (1994) *Earth Planet. Sci. Letters* **121**, 19-41. [3] Dalziel et al. (1987) in *Continental Extension Tectonics, Special Publication 28, Geol. Soc. London.* 433-441 [4] Kyle et al. (1981) in *Gondwana Five*, A.A. Balkama, Rotterdam 283-287 [5]Wilson L. and Head J.W. (2000) *LPS XXXI* , #1371. [6] Fleming et al., (1995) *Contr. Min. Petrol.* **121**, 217-236. [7] Caruso and Schultz (2001) *LPS XXXII* , #1745. [8] Lucchitta B. K. et al., (1992) in *Mars*, University of Arizona Press, 453-492. [9] Claridge and Campbell (1984) *NZ J. Geol. Geophys.* **27**, 537-545. [10]Conca and Astor (1987) *Geology* **15**, 151-154. [11]Mars Pathfinder Rover Team (1997) *Science* **278**, 1765-1768.

THE ENIGMATIC ARABIA TERRA, MARS. B. M. Hynek and R. J. Phillips, Department of Earth and Planetary Sciences and McDonnell Center for the Space Sciences, Washington University (One Brookings Drive, St. Louis, MO 63130 hynek@levee.wustl.edu).

Introduction: High-resolution altimetry and gravity data from Mars Global Surveyor (MGS) shed new light on the already perplexing province of Arabia Terra (Fig. 1)(0°-45°N, -25°E eastward across the prime meridian to 40°E). Traditionally, this region has been considered a part of the ancient highlands that cover the southern part of Mars that are thought to represent the final stages of heavy bombardment, over 3.7 G.A. [1]. However, recent results from MGS reveal that Arabia Terra has several unique properties, indicating that it may have a history considerably different than the rest of the uplands.

Perplexities of Arabia Terra: Arabia Terra is slightly larger in area than the European continent and is primarily comprised of degraded cratered terrain. This region has several attributes that distinguish it from the rest of the martian highlands. One major discrepancy is the paucity of valley networks in Arabia Terra as first noted by Carr [2] (Fig. 1a). Valley networks are generally believed to be fluvial in origin and occur on almost all Noachian-age surfaces except Arabia Terra. Extensive Noachian volcanism from the Tharsis igneous complex may be responsible for an early, thick atmosphere that led to dissection of the surface by fluvial erosion [3].

The global dichotomy separates the southern heavily cratered martian uplands from the low-lying, lightly cratered, smooth plains to the north. Typical elevations for the highlands, excluding the Argyre and Hellas impact basins, range between 0 and 3 km above the martian datum [4]. Conversely, Arabia Terra has an average elevation of –1.5 km, roughly 3 km below typical highland terrain.

The cratered uplands exhibit a dense crater population of all diameters including most of the large craters found on the planet. However, Frey et al. [5] have found topographic evidence for a buried population of craters in the northern plains comparable to the southern highlands. Plotted on Figure 1a are craters with diameters larger than 160 km diameter. These features are generally uniformly distributed across the southern highlands, excluding regions of post-Noachian resurfacing. Although there are large craters on the boundaries of Arabia Terra, much of the region of low elevation contains no craters of this magnitude (Fig. 1a).

Zuber et al. recently mapped the subsurface of Mars using MGS topography and gravity data and noted that Arabia Terra has a crustal thickness less than most highland terrain (Fig. 1b) [6]. In fact, the estimated value of ~35 km is similar to the thinner crustal province of the northern plains.

Multiple Working Hypotheses: We attempt to compile the proposed hypotheses (both pre- and post- MGS) regarding geographic portions of Arabia Terra that may yield insight into this unique region of Mars. Erosion, deposition, and exhumation have all been invoked to explain the surface features of Arabia Terra. Hynek and Phillips [7] argued that late Noachian fluvial erosion might be responsible for the unique morphology of Arabia Terra. Moore [8] hypothesized that a thick mantling eolian or volcanic deposit could explain the subdued nature of the craters in northeastern Arabia Terra. Edgett and Parker [9] proposed that western Arabia was underwater at some point early in martian history and attribute its appearance to marine erosion and deposition. Table 1 tests the compatibility of these hypotheses with the anomalous observations described above. While eolian or volcanic deposition can explain some features of Arabia Terra, these processes would not result in an unusually low elevation, thinner crust, or lack of large craters. The marine hypothesis requires an ocean covering the northern plains and greater than 4 km deep to submerge western Arabia and thus seems unlikely, but cannot be ruled out. We conclude that erosion, not deposition, is most consistent with the lack of valley networks, relatively low elevation and thin crust, and the lack of large craters. It remains unclear whether this region is exposed basement of the northern plains that has been uplifted or if it belongs to the highland province and has undergone extraordinary denudation and peneplanation.

Figure 1. Images illustrating the perplexities of Arabia Terra (noted AT) including a lack of valley networks, relatively thin crust, and mixed composition. MOLA shaded relief image shown in (a) with global valley network locations (black lines) and craters > 160 km in diameter (white dots). Note the low elevation and paucity of valley networks and large craters of Arabia Terra. (b) represents crustal thickness map modified from [6] with approximate global dichotomy boundary superposed. Crustal thickness of Arabia Terra is much closer to the northern lowlands than the cratered uplands.

References: [1] Hartmann W.K. and Neukum G., *Space Sci. Rev.* (in press); [2] Carr M.H., (1995) *JGR*, 100, 7479-7507; [3] Phillips R.J., et al., (2000) *Science*, 291, 2587-2591; [4] Smith D.E., et al., (1999) *Science*, 284, 1495-1503; [5] Frey H., et al., (2001) *LPS XXXII*, abs. no. 1680; [6] Zuber M.T., et al., (2000) *Science*, 287, 1788-1793; [7] Hynek B.M. and Phillips R.J., (2001) *Geology*, 29, 407-410; [8] Moore, J.M., (1990) *JGR*, 95, 14,279-14,289; [9] Edgett K.S. and Parker, T.J., (1997) *GRL*, 24, 2897-2900.

Table 1

Proposed Hypothesis	Compatibility of Observations with Hypotheses			
	Lack of Valley Networks	**Low elevation**	**Thin crust**	**Few large craters**
Late Noachian erosion and peneplanation of surface (likely fluvial in origin) [7]	YES. Intense erosion and peneplanation could remove valley networks, as evident south of Arabia Terra.	YES. Likely a kilometer of cratered uplands removed and carried to the northern plains.	POSSIBLY. Surface peneplanation may have caused crust to thin in response to removal of overburden.	POSSIBLY. Erosion could remove the early, larger craters with small craters forming during the later stages and after denudation.
Exposed basement of the northern plains [6]	POSSIBLY. The present surface may not have been exposed during the period of valley formation.	YES. Elevations are similar to the adjacent northern plains.	YES. Crustal thickness comparable to that of the northern plains.	POSSIBLY. Erosion may have removed the craters.
Thick mantling deposits of eolian or volcanic in origin [8]	YES. A mantling deposit could bury pre-existing valley networks.	NO. A mantling deposit would result in a higher, not lower elevation.	NO. Loading would create a thicker, not thinner crust.	NO. Small craters, would be buried or subdued before the large craters.
Submarine erosion and deposition [9]	YES. Marine erosion could remove networks or prevent them from forming.	UNLIKELY. Erosion could lower the elevation, but requires an ocean > 4 km to submerge region, given current topography.	YES. Marine erosion could result in a thinning of the crust due to removal of overburden.	POSSIBLY. Early, large craters could have been eroded subaqueously.

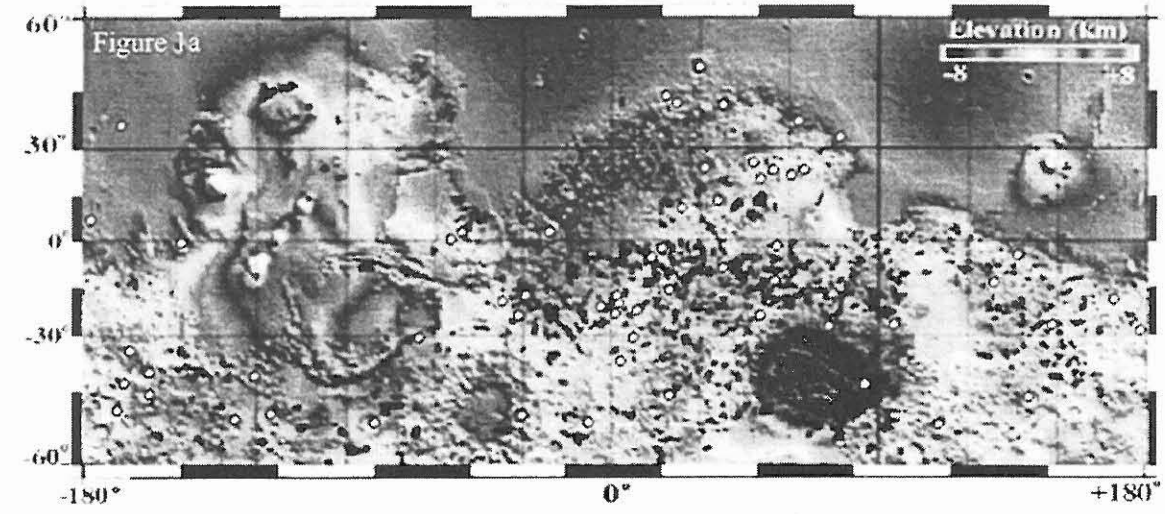

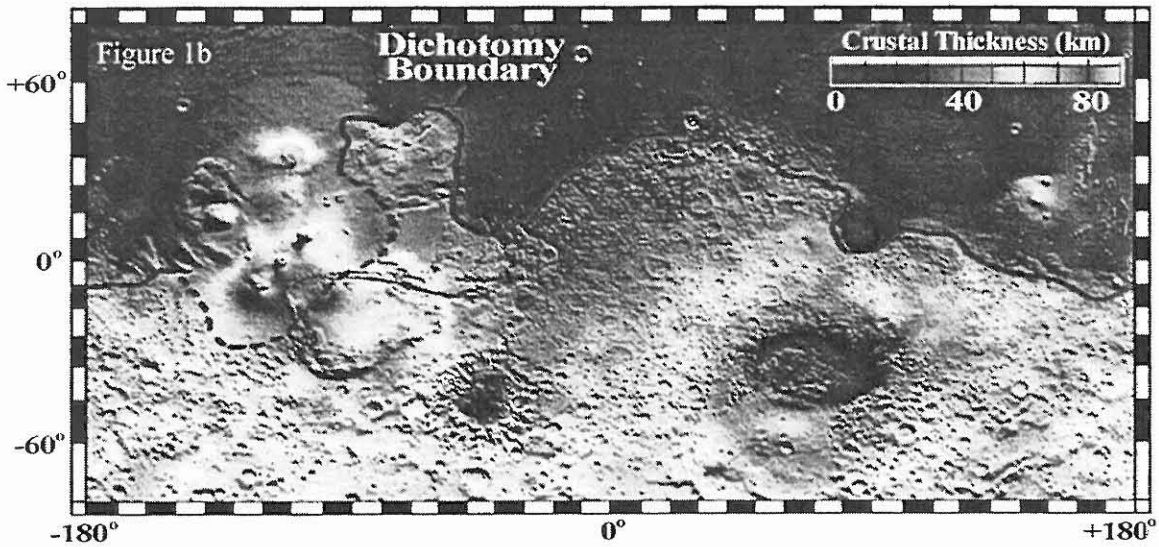

DRAINAGE BASIN INTEGRATION IN THE MARTIAN HIGHLANDS. R. P. Irwin III[1, 2] and R. A. Craddock[2], [1]Department of Environmental Sciences, Clark Hall, University of Virginia, Charlottesville VA 22903, Irwinr@nasm.si.edu. [2]Center for Earth and Planetary Studies, National Air and Space Museum, Smithsonian Institution, 4th St. and Independence Ave. SW, Washington DC 20560-0315, craddock@nasm.si.edu.

Introduction: Martian ancient valley networks commonly have short valley lengths compared to their terrestrial counterparts [1], which suggests that the martian landscape has poorly integrated drainage or that the valley networks are poorly developed within their catchments. Superposition relationships and crater counts hold that valley network development occurred contemporaneously with highland crater degradation [2]. MOLA topographic data [3,4] and stereo photography [4] have been used to delimit drainage basins on the quadrangle and larger map scales. Here we discuss the effect of cratering on valley network development and the response of the networks to disruption by impacts.

Drainage basin origin: Mapping in Terra Cimmeria [3] indicates that highland impact craters superimpose and were later modified by individual drainage networks. In many cases, drainage divides connect and follow the rims of large impact craters, which suggests that these craters played a strong role in defining the extant drainage basins (Fig. 1 in [3]). Degraded crater morphology depends on the age of the crater and, in some cases, on the crater's location within the drainage basin. Large craters that formed on pre-existing drainage divides (ridges that are high and wide relative to the superimposed crater) were degraded primarily by superimposed networks, while craters that formed on thalwegs in the catchment were more susceptible to breaching and infilling by the valley they intersect (Figs. 1, 2). The crater rim of this latter type is often breached in a single location (Fig. 1). When an extant drainage basin was impacted, the crater either shifted the drainage divide, increased the height of the divide, dammed the valley, or shifted the valley course depending on the location and size of the impact. Craters greater than about 15 km in diameter tended to divert valleys, while smaller degraded craters appeared more susceptible to breaching and infilling. Ejecta deposits of the largest (~100 km) craters appeared to dam catchments where the crater rim did not intersect the catchment thalweg. Further analysis of the global MOLA dataset will refine these diameters and fundamental observations on the planetary scale.

Slope and basin floor units: Qualitatively, it appears that valley networks are deeply primarily where there is a steep regional gradient, or where some reduction in downstream base level has increased the stream gradient in an otherwise near-level catchment. Nearly flat, dissected intercrater plains exhibit smaller drainage basins with poor valley development and shorter valley lengths. Smooth intercrater plains units developed in the floors of closed drainage basins (Fig. 2). These units can have little or no consistent slope, but more commonly there is a lower gradient toward some location near the center of the basin floor. Further research will constrain the slopes common to deeply dissected terrain and intercrater smooth plains units.

Drainage basin integration: Stream piracy commonly occurs on the Earth when one stream receives more water than a neighbor, and its rate of headward growth or downcutting increases, further increasing the size of its contributing watershed. On Mars, the process is assumed to have operated similarly. Where an obstruction to flow (crater rim or ejecta) was rapidly emplaced, ponding or deposition up-valley of the rim eventually breached the divide. These valleys then experienced a sudden reduction in base level and a deeply-incised "bedrock valley" developed upstream of the crater (Fig. 1). More commonly an impact crater would be smaller then the catchment it superimposed, and the valley would be diverted without breaching the crater (Fig. 2). Impact craters occurring on flat plains eventually degraded to the "cookie cutter" morphology, where a widened rimless depression is not breached by valleys. This difference suggests that sediment deposition around a crater, or superposition on a regional gradient, are important factors in determining whether a crater will be breached. At advanced stages of degradation ("ghost craters"), even large craters and impact basins become fully integrated with surrounding drainage networks [6].

Closed drainage basins commonly developed in the interiors of impact craters, where the level of the basin floor is lower than the elevation of the surrounding topography. Interior slope gullies commonly reached the crater floor without development of a terrace or delta, which suggests that interior sediment was well distributed. These crater floors would develop in circumstances where no net directional preference existed for the incoming sediment, and standing water was ephemeral or not present. Closed basins also occurred on surrounding intercrater plains, especially where a low divide was emplaced by an impact structure. These plains exhibited poor valley incision and network development. Evaporite deposits have not been noted to date in basin interiors. This suggests that the basin floors were well-drained and did not contain

long-lived standing water, that ubiquitous mantling of basin floors has taken place, or that the influx of sediment was greater than the influx of chemical precipitates. The former and latter explanations are consistent with thermal emission results for Terra Cimmeria [6].

In several locations, these elevated closed catchments appeared to control the headward growth of theater-headed valleys. In these cases, headward growth of valleys in lower drainage basins favors the direction of the more elevated basin, eventually resulting in integration of the elevated basin with the lower one. These basins are commonly connected by a deeply-incised valley.

Figure 1. MDIM2 and contour map of part of Terra Cimmeria. The 92-km crater at top-center has been breached by a pre-existing valley network. Small craters are breached by valleys, while >15 km craters and those atop older drainage divides are not breached.

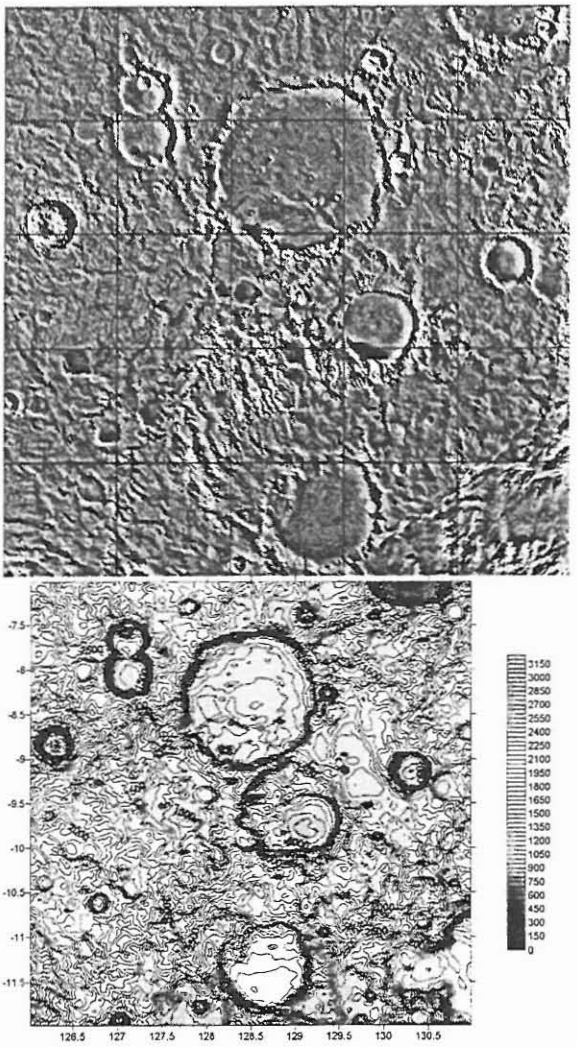

References: [1] Carr M. H. (1996) Water on Mars, pp. 75-76. [2] Craddock R. A. and Maxwell T. A. (1993) *JGR, 98,* 3453–3468. [3] Irwin R. P. and Howard A. D. (2001) *LPSC XXXII,* Abstract #1377. [4] Banerdt W. B. and Vidal A. (2001) *LPSC XXXII,* Abstract #1488. [5] Grant J. A. (2000) *Geology, 28,* 223-226. [6] Christensen P. R. et al. (2000) *JGR, 98,* 9609–9621.

Figure 2. MDIM2 and contour map of a similar 5° x 5° scene near the southern margin of Isidis Basin, where there is a higher population of preserved craters. A 40-km crater just right of center receives a broad valley network, which may have continued unhindered to the UR corner of the scene prior to emplacement of the crater. Valleys are diverted by craters of ~15 km in diameter. Smooth intercrater plains have developed in depressions with no outlet.

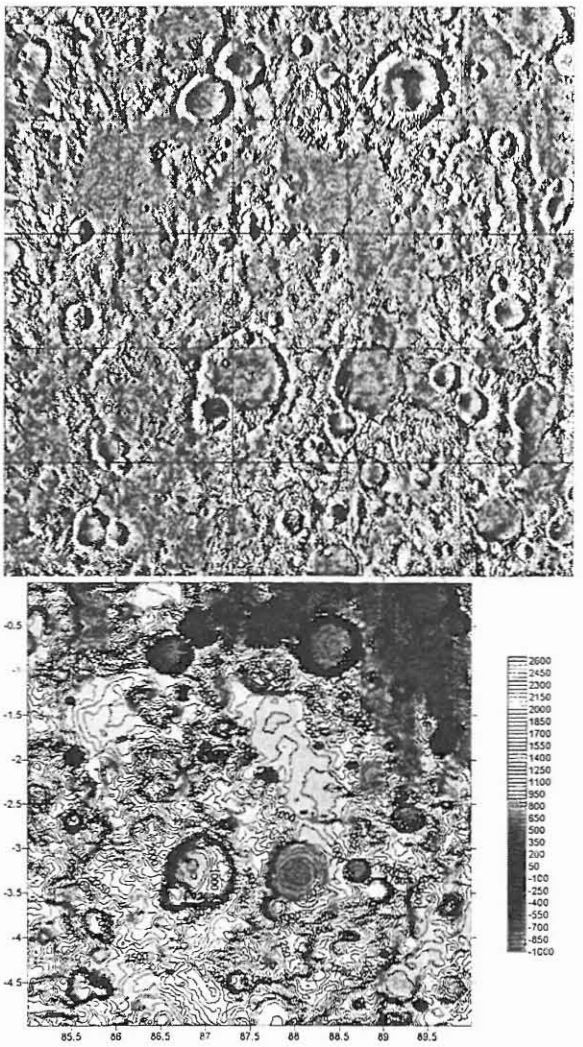

DOUBLE CRATERS AND CRATER MODIFICATION. A. Kereszturi (Department of Physical Geography, Eötvös Loránd University, H-1083 Budapest, Ludovika tér 2., Hungary (E-mail: irodaweb@irodaweb.hu))

Introduction: Connected double craters can be devided into two groups: 1. the two crater formed by the simultan impact of two bodies, 2. one crater postdates the other. In the first cases we can find nearly straight wall between the two craters (or no wall at the small craters), in the second cases the younger crater rim postdates the older crater. On Mars we can find several great double craters without straright walls or postdating rims. In this cases some process eroded away the straight wall or the rim part where the two craters connected. The presence of the erosion/depositon process is suggested by the smooth sedimentary infill too. Because the surface erosion processes greatly varied during the evolution of Mars [1, 2, 3], we can expect different ratio for the erosion of connected double craters in different times. Based on their diameter distribution it is possible to analyze this tendency.

Theoretical assumptions: We were looking for connected craters with smooth sedimentary infill (formed by deposition process) and without walls or rims between the craters. Where we can't find these walls and rims we can suspect that some kind of erosion destroyed it. (It is possible that a simultan impact doesn't create straight wall between the two craters, but this effect is present probably in the smaller craters only.) From theoretic point of view the dissecting wall destroying process can be: 1. ancient erosion process in the Noachian, 2. relative recent process related to subsurface ice, and fretted terrain [4]. If we analyse the latitudinal and size distribution of these craters it will be possible to decide wich processes worked in the craters.

Working method: Based on the Viking's images [5] we analyzed the craters with diameter greater than 1 km between 0°-50°S latitude and 0°-8°E longitude. The cause of the choosed 1 km limit is to give a representative distribution, in spite the variable resolution of the Viking's images. The diameter was measured by Surfer and Excel programs, the errors of the measurements are below 20%.

Results: In the surveyed area we find 1911 single craters, and only 36 connected craters (it means 16 pairs). There are some examples on Fig 1. for the connected craters. General characterestics: they have smooth sedimentary infill, no signs of the ancient crater wall, and the outer rim does not rise above the surrounding terrain. (In Fig. 1. The last double crater (bottom right) seems to be relatively young with rampart surrounding it. It is hard to analyze the connection of the two craters because of the limit of resolution.) If we compare their size distribution it is visible that there are no excess of smaller craters (see Fig 2.: A – distribution all of the craters, B – distribution of the single, C – the double craters).

Discussion: We devided the processes can make smooth crater infill into two groups: 1. old, nearly Noachian aged erosion process and 2. relative recent processes like terrain softening [6, 7], thermocarst [8] and fretted terrain making processes. (There may be other kind of processes too but based on the up to date knowledge we can take into account only these processes.) At the 2. group the erosion processes appear to have latitudinal distribution. Our sample (36 double craters) is small for a latitudinal statistic, but no latitudinal concentration is obvious jet. The small number of small double craters suggest that the wall destroying process is size dependent, or the process was active in the past, and we can see it only at the greater craters today, which were not totally distroyed by other erosion process during the evolution of Mars. Even in this case we can not rule out that recent erosion process working on them too.

Future work: Based on this analysis we can find that it is a possible method to analyse crater modification and its relation to diameter and/or age with double craters. In the future we would like to spread the analysis for all of the globe based on the Viking's images, survey for smaller double craters in the MGS's images and present morphological analysis of the floor of great double craters with MGS's images.

References: [1.] Cabrol N. A. (2000) LPSC XXX. #1022, [2] Baker V. R. et al. (2000) LPSC XXXI. #1863, [3] Carr M. H. (1999) 5th International Conference on Mars #6030, [4] Carr M. H. (1981) The surface of Mars, Yale University Press, [5] Planetary Data System, [6] Jankowski D. G., Squyres S. W. (1992) Icarus 100/26-39. [7] Squyres S. W., Carr M. H. (1986) Science 231/249-252, [8] Corstard F.M. (1995) Icarus 114/93-112.

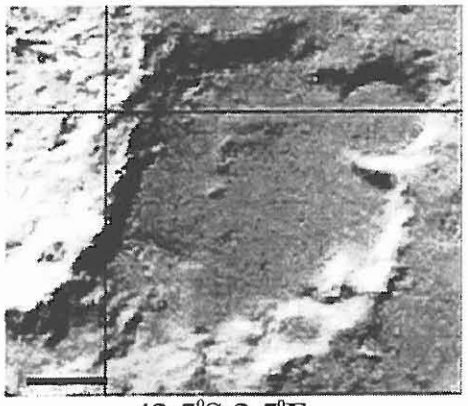

43.5°S 3.5°E

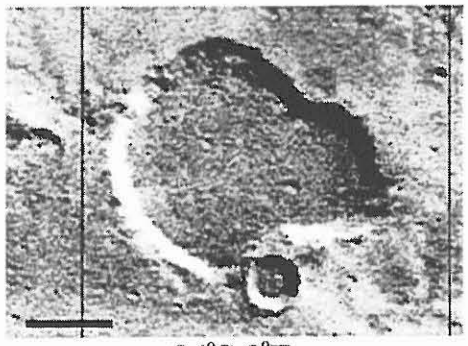

34°S 2°E

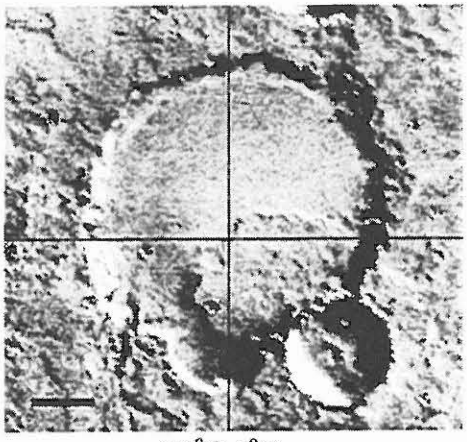

21°S 1°E

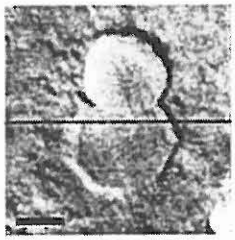

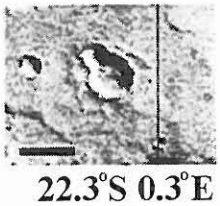

22.3°S 0.3°E

4°S 1°E

Fig. 1.

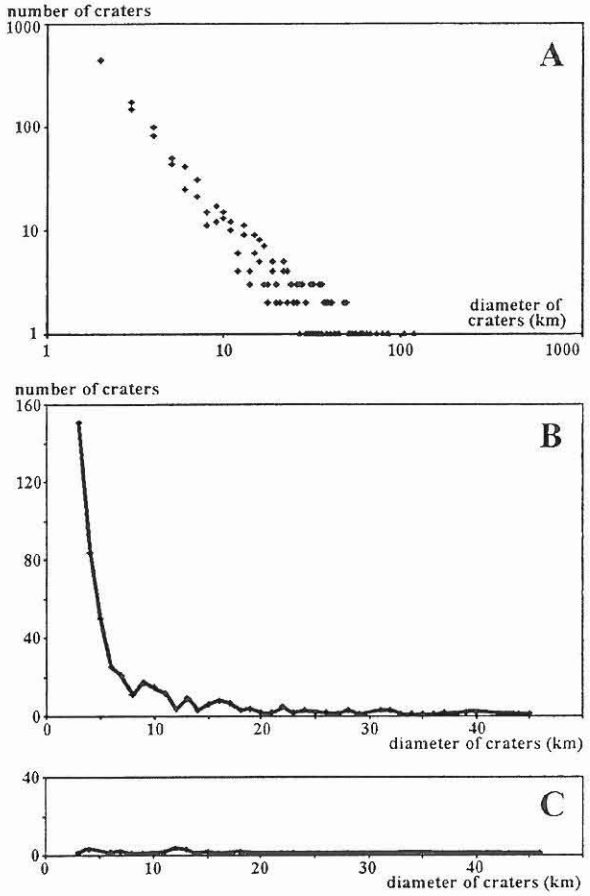

Fig. 2.

DETECTING MINERALS ON MARS USING TES, THEMIS, and Mini-TES. L. E. Kirkland[1], K. C. Herr[2], J. W. Salisbury[3], E. R. Keim[2], P. M. Adams[2], and J. A. Hackwell[2]. [1]Lunar and Planetary Institute, kirkland@lpi.usra.edu; [2]The Aerospace Corporation, El Segundo, CA; [3]Johns Hopkins University, *retired.*

Introduction: There has been no definitive infrared spectral evidence for carbonates on Mars, and this result affects early Mars "dry" vs. "wet" hypotheses. The near-term search for minerals is being conducted by the 1996 Thermal Emission Spectrometer (TES), the 2001 9-band radiometer THEMIS, and the 2003 lander Mini-TES. Christensen et al. [1,2] conclude that TES has recorded the signature of surface silicates and hematite. However, TES has not detected definitive signatures of minerals such as carbonates and sulfates, although they are predicted to be present, and TES was expected to be able to detect them [3]. Current explanations for the puzzling lack of carbonate detections include that they were never there; are buried [4]; altered by UV radiation [5]; occur exclusively in small deposits (exposed over less than one-tenth of the TES ~3 km x 5 km field of view) [6,7]; or are rough and weathered, and so exhibit low spectral contrast [8,9].

If Mars had a denser atmosphere in its past and liquid water on its surface, then large deposits of carbonates likely formed [10]. Thus the lack of carbonate detections affects interpretations of Mars' geologic and climatic history, even though its cause is poorly understood. It may also affect landing site selections.

Interpretations of TES spectra typically use laboratory spectra of smooth, fresh mineral surfaces [11] (e.g. Fig. 1 limestone). However, spectra of fresh mineral surfaces are frequently a poor match to spectra measured of rough and weathered surfaces (e.g. Fig. 1 calcrete and hot spring carbonate). For TES, THEMIS, and Mini-TES to attain their predicted mineral detection limits, minerals must be present under specific conditions: well-crystalline, uncoated, smooth-surfaced at several scales, and low atmospheric downwelling radiance contribution [8,9]. These issues raise the question of whether non-silicate minerals are rare on Mars, or whether smooth, uncoated deposits of well-crystalline minerals are rare. These caveats should be considered when using a lack of mineral detections to interpret the geologic and climatic history of Mars.

Lab spectra. The TES team spectral library contains measurements of crushed, sieved (710–1000 μ), washed samples [11]. If a spectrum exhibits a strong band that is not observed in TES spectra, then it is concluded that the mineral is not present at the ~10% level [1,2]. In order for this method to produce accurate interpretations, fresh and weathered surfaces must exhibit the same band depth; materials with the same composition must always weather to produce the same surface roughness, regardless of the internal microstructure; and there must be no other effects that reduce the spectral contrast, including volume scattering, reflected downwelling radiance, and cavity effects caused by surface roughness [8,9].

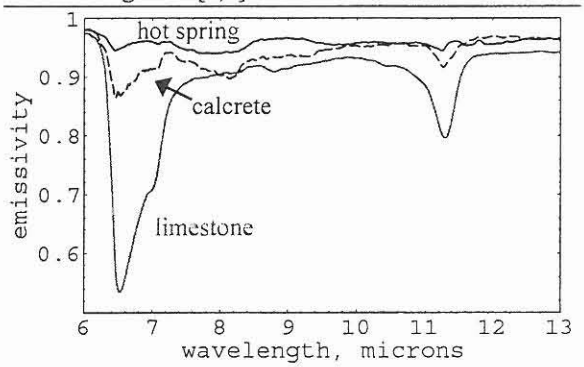

Figure 1: Spectral contrast variations. These carbonate hand samples are from the Mormon Mesa, Nevada (limestone, calcrete) [9] and New Mexico (hot spring). Spectra are converted using emissivity = 1 - hemispherical reflectance.

In general, the ability to detect a mineral is directly proportional to the depth and width of the spectral bands, and the instrument's sensitivity and sampling interval (Fig. 2) [8,9]. TES interpretations are based on contrasts such as exhibited by the Fig. 1 limestone. The calcrete and hot spring deposit samples would be much less detectable, perhaps undetectable. This is not currently considered in TES interpretations or predictions of THEMIS and Mini-TES detection limits.

Remote sensing data. Almost all airborne terrestrial thermal infrared studies have focused on multichannel radiometer (multi-spectral) data sets, typically with 4–10 bands. Good reviews are presented by [12,13], and two common instruments are TIMS and MASTER [14]. TIMS has 6 bands in the ~8–12 μm region, and TIMS studies formed the remote sensing foundation for TES interpretations [3, p.7725].

Instruments that measure with less than ~10 bands lack the spectral detail to provide a direct, diagnostic signature of most minerals and rocks, except quartz and some silicates [15]. However, under some conditions materials with narrow or weak features may be statistically differentiated from surrounding regions based on differences that are not uniquely diagnostic, and then the targets are subsequently identified using ground truth [e.g. 15-19]. Thus for non-silicates, TIMS studies typically use statistical techniques to define spectral type regions, which are then identified using ground truth. This "TIMS+ground-truth"-style approach is used to map terrestrial mineralogy.

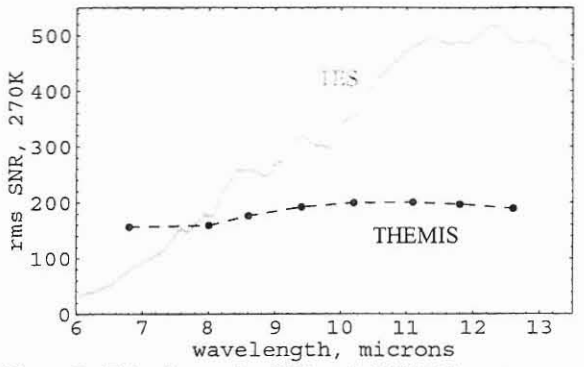

Figure 2. This shows the TES and THEMIS root mean square signal-to-noise ratio (SNR) for a 270K blackbody [8,9]. Higher numbers represent greater sensitivity. THEMIS' SNR was calculated for peak SNR=200. Mini-TES is predicted to have similar signal-to-noise ratio and spectral sampling as TES. SEBASS SNR is ~2500 at 10 μm.

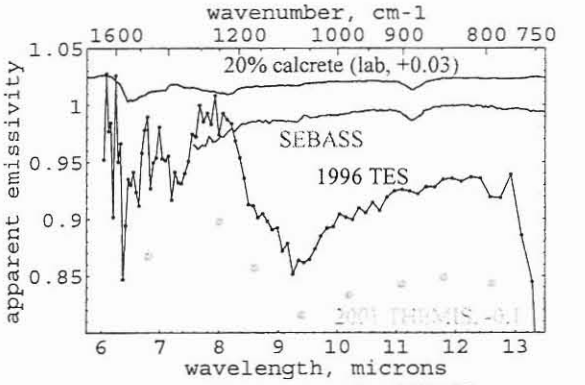

Figure 3: Representative spectra. The THEMIS spectrum is simulated from the TES spectrum (#57023856). The SEBASS spectrum was measured of a region with near 100% calcrete coverage. The lab calcrete spectrum is scaled to approximately match the SEBASS spectral contrast.

Since TIMS studies showed a multi-spectral instrument cannot identify most minerals without ground-truth, TES and Mini-TES were designed as hyperspectral instruments. TES typically measures 143 bands over ~5.7–50 μm. It was planned for TES to identify the minerals present, and then THEMIS would map the identified minerals at higher spatial resolution. Mini-TES (~5–29 μm, 160 bands, [20]) would measure from a lander.

However, given the heavy reliance on ground truth for the "TIMS+ground-truth" studies, they leave an important, essentially unstudied remote sensing question: How do thermal-infrared hyperspectral signatures measured from an airborne or satellite platform compare to laboratory signatures typically used to interpret the data sets? Since (until recently) no airborne instrument existed that measures with a sensitivity broadly comparable to laboratory spectra, this question remained untested. However, TES, THEMIS, and Mini-TES are field instruments, so interpretations of these data sets are only as good as our understanding of the spectral behavior of field materials measured in the field environment.

Hyperspectral field data. We used unique, very high signal-to-noise ratio, hyperspectral data measured by the airborne SEBASS (7.6–13.5 μm, 128 channels) [9]. A literature search found no peer-reviewed studies that made extensive use of airborne thermal infrared imaging spectrometer (hyperspectral) data [8]. Thus SEBASS provides the unprecedented capability to move hyperspectral testing for TES interpretations from the laboratory into the field environment; to examine weathering effects over a much broader range of samples than is possible with laboratory samples alone; and to characterize effects not commonly reproduced in the laboratory environment. We also measured *in situ* spectra using field spectrometers (6.7–14.3 μm), and laboratory spectra (2.5–200 μm) of field samples collected with the *in situ* upper surface marked for comparison to the field data [9].

Results. Fig. 3 shows a SEBASS spectrum measured of a region with near 100% coverage by indurated calcite (calcrete), and a calcrete laboratory spectrum scaled to approximate the band contrast observed by SEBASS [9]. The calcrete exhibits greatly reduced spectral contrast relative to spectra currently used for TES interpretations [e.g. Fig. 1 limestone], mainly from a cavity effect caused by roughness present on several scales [8,9].

These spectra demonstrate that massive materials can have significantly lower spectral contrast than laboratory spectra that are currently used to interpret TES data. As a result, a lack of detections in TES, THEMIS, and Mini-TES data must be approached with caution when using the result as an input to geologic and climatic studies.

References: [1] Christensen P. et al. (2000a) *JGR 105*, 9632. [2] Christensen P. et al. (2000b) *JGR 105*, 9609. [3] Christensen P. et al. (1992) *JGR 97*, 7719. [4] McKay C. and Nedell S. (1988), *Icarus 73*, 142. [5] Mukhin L. et al. (1996) *Nature 379*, 141. [6] Kerridge J. (1997) LPI Tech. Rep. 97-01, 15. [7] Farmer J. and Des Marais D. (1999) *JGR 104*, 26,977. [8] Kirkland L. et al. (2001a) *Appl. Optics 40:27*. www.lpi.usra.edu/science/kirkland. [9] Kirkland L. et al. (2001b) *SPIE Vol. 4495*, www.lpi.usra.edu/science/kirkland. [10] Pollack J. et al. (1987) *Icarus 71*, 203. [11] Christensen P. et al. (2000c) *JGR 105*, 9735. [12] Kahle A. et al. (1993) Ch.5 in *Remote Geochemical Analysis: Elemental and Mineralogical Composition*. [13] Hook S. et al. (1999), *Remote Sensing for the Earth Sciences, 3rd ed. Vol. 3*, 59. [14] Hook S. et al. (2001) *Rem. Sens. Env. 76*, 93. [15] Crowley J. and Hook S. (1996) *JGR 101*, 643, 1996. [16] Kahle A. and Rowan L. (1980) *Geology 8*, 234. [17] Gillespie A. et al. (1984) *GRL 11*, 1153. [18] Gillespie A. et al. (1986) *Rem. Sens. Env. 20*, 209. [19] Gillespie A. (1992) *Rem. Sens. Env. 42*, 137. [20] Puschell J. (2001) *pers. comm.*

THE COMPOSITION OF THE MARTIAN HIGHLANDS AS A FACTOR OF THEIR EFFECTIVE UPLIFTING, DESTRUCTION AND PRODUCTION OF VOLUMINOUS DEBRIS. G.G. Kochemasov, IGEM of the Russian Academy of Sciences, 35 Staromonetny, Moscow 109017, Russia. kochem@igem.ru

As was predicted before "Pathfinder" launch [1,2,3,4] the composition of the martian highlands is principally different from that of the martian lowlands (earlier the majority of scientists believed that both crusts are basaltic: altered and fresh). The wave planetology precludes similar compositions (similar densities) for uplifted and subsided blocks of a rotating celestial body (Theorem 4,[5]). The higher global relief range, the higher density range of mean lithologies of raised and fallen planetary blocks. At Venus it is the range between magnesian and alkali basalts, at Earth between tholeiites and andesites (the mean composition of continents), at Mars between Fe-basalts and rocks of granitic, syenitic, albititic affinities [1,2]. The new discoveries at Mars support this natural requirement. Fractionated Si, Al, K-rich rocks occur in the contact between lowlands and highlands (something similar to the intermediate andesites between basaltic oceans and light –not dense continents at Earth). The MGS gravity data indicate that the thick highland crust is much less dense than the thin lowland crust. The high chlorine content in the martian rocks and soils (0.3-0.6 weight %) is a geochemical indicator of acid and more probably alkaline igneous compositions of highlands. In terrestrial rocks such Cl contents as 0.2-2.5 % can be found in nepheline and sodalite syenites of Lovozero massif (Kola peninsula), in sodalite-bearing lavas in Latium (Italy), in France, at Mount Suswe (Kenya) [6]. Chlorine contents in intermediate and basic terrestrial rocks are much lower (0.005-0.01 weight %).

It is interesting that typical etched appearance of martian fragments may indicate at markedly different hardnesses of composing them minerals. All Cl-bearing minerals and feldspathoids (halite, sodalite, nepheline) are softer than feldspars and colour minerals of rock matrix. The preferable erosion of soft minerals by weathering agents such as sandy winds and fragment friction can produce Cl-rich fines covering the entire martian surface.

One important consequence of intrusion in the continental crust of magmatic bodies of smaller densities than surrounding media is their constant drive to arise or to occupy space with larger planetary radius (Theorem 4, [4]). The best terrestrial example of this tendency is probably two Palaeozoic nepheline syenite massifs at Kola peninsula: Khibiny (~ 1500 sq.km) and Lovozero (625 sq. km) –two ring complexes of 40 and 25 km in diameter. Two mountain massifs, reaching heights of 1191 and 1120 meters, protrude the thoroughly smoothed low Precambrian plane of the peninsula. They have sharp and steep contacts with surrounding Pcm migmatites and gneisses. In a sense, they can be compared to the annular Olympus Mons having sharp high scarps. "Dense" background in the contact between lowlands and highlands surrounding this huge but not dense body pushes it up. There are no such scarps around other three large volcanoes on Tharsis bulge which is purely continental "not dense" formation.

Raised bodies, occupying space with larger planetary radius and thus larger areas, tend to expand and fall apart. That is why such mountain massifs are intensively broken by radial and tangential (arc-like) faults, rifts and grabens. They are subjected to fracturing by various fractional dimensions (see, for example, Lunar Planum on Tharsis and chaotic terrains). Large amount of debris of various dimensions is formed, this is facilitated by contrast densities of constituent minerals and by soft easily breakable minerals. On the martian highland surface craters produced by impacts and degassing are typically highly eroded; radial cracks on rims,

debris flows of various scales, lobate features, landslides occur everywhere. Smaller craters disappear, fretted and chaotic terrains are formed. Sticking out mountain relics (flat and sharp topped) disintigrate by splitting off slopes. Subsurface ice (if it exists) plays a certain role, but collapses, intersecting vallies, dry debris flows can be formed as a mere consequence of uplifting. Some "pedestal craters" can be uplifting masses of smaller densities.

Wet conditions (because of subsurface ice, atmospheric fogs, temporary flows) facilitate chlorine leaching and formed chemically aggressive medium alters rocks, oxidizes iron (rusty appearance of Mars). Chlorine in aluminosilicate acid rocks is usually accompanied by fluorine which is also very aggressive substance, and Cl content increases along with fluorine. Chlorine enriches AL, Na, Ca, Mg, F –rich and relatively Si-poor rocks [7]. So, high Cl may be an indication of lithologies akin syenites – rocks rich in AL, Na and poor in Si. Chlorine favours sodium rocks more than potassium ones. From the other hand, uranium is geochemically more bound to sodium, and thorium is closer to potassium. May it be an indication that the highland rocks are more Na-rich than K-rich? Gamma-spectrometer of "Mars-5" determined over highlands U ($1.0\pm0.5\cdot10^{-4}$ weight %) and Th ($2.4\pm0.5\cdot10^{-4}$). For terrestrial standards U is closer to intermediate-acid rocks ($3.5\cdot10^{-4}$ for acid), Th is closer to basic rocks ($3\cdot10^{-4}$). Soon the Odyssey orbiter will clarify this question. But due to Pathfinder we already know how much potassium there is in the contact highland-lowland zone and this is a good bench-mark.

The martian cratered highlands, composed of "not dense" relative to basalts igneous material, due to tendency of uplifting and hence intensive destruction produce huge amount of detrital material obliterating small craters, smoothing crater rims, giving landslides and lobes, dry (and wet?) debris flows and layered deposits .

References:

[1] Kochemasov G.G. (1995) Possibility of highly contrasting rock types at martian highland/lowland contact //In: Golombek M.P., Edgett K.S., and Rice J.W.Jr., eds. Mars Pathfinder Landing Site Workshop II: Characteristics of the Ares Vallis Region and Field Trips to the Channeled Scabland, Washington. LPI Tech. Rpt. 95-01, Pt.1, Lunar and Planetary Inst., Houston, 63 pp.

[2] Kochemasov G.G. (1997) How regular is planetary tectonics: martian test // Annales Geophysicae, Suppl.III to Vol. 15, Pt. III, 767.

[3] Kochemasov G.G. (1998) Felsic continents of Mars // Annales Geophysicae, Suppl.III to Vol. 16, Pt. III, C1027.

[4] Kochemasov G.G. (1999) On a successful prediction of martian crust fractionation based on comparative wave planetology // The Fifth International Conference on Mars, July 18-23, 1999, Pasadena, California, Abstr. # 6034, (CD-ROM).

[5] Kochemasov G.G. (1999) Theorems of wave planetary tectonics // Geophysical Research Abstracts, V.1, #3, 700.

[6] Kochemasov G.G. (2001) High chlorine content in martian rocks and soils as an indication of acid highland lithologies // In: Eleventh Annual V.M. Goldschmidt Conference, Abstr. #3070, Lunar and Planetary Inst., Houston (CD-ROM).

[7] Webster J.D. (1997) Exsolution of magmatic volatile phases from Cl-enriched mineralizing granitic magmas and implications for ore metal transport // Geochimica et Cosmochimica Acta, V.61, #5, 1017-1029.

SNOOPY: STUDENT NANOEXPERIMENTS FOR OUTREACH AND OBSERVATIONAL PLANETARY INQUIRY. K. R. Kuhlman,[1] M. H. Hecht,[1] D. E. Brinza,[1] J. E. Feldman,[1] S. D. Fuerstenau,[1] L. Friedman,[2] L. Kelly,[2] J. Oslick,[2] K. Polk,[2] L. E. Möller,[2] K. Trowbridge,[2] J. Sherman,[2] A. Marshall,[2] A. L. Diaz,[2] C. Lewis,[3] C. Gyulai,[3] G. Powell,[3] T. Meloy,[4] P. Smith,[5] [1]Jet Propulsion Laboratory, California Institute of Technology, 4800 Oak Grove Dr., Pasadena, CA 91109, [2]The Planetary Society, Pasadena, CA 91106, [3]Visionary Products, Inc., 11814 South Election Drive, Suite 200, Draper, UT 84020, [4]West Virginia Univ., Morgantown, WV 26506, [5]The Univ. of Arizona, Tucson, AZ 85721.

Introduction: As scientists and engineers primarily employed by the public, we have a responsibility to "communicate the results of our research so that the average American could understand that NASA is an investment in our future..."[1]. Not only are we employed by the public, but they are also the source of future generations of scientists and engineers. Teachers typically don't have the time or expertise to research recent advances in space science and reduce them to a form that students can absorb. Teachers are also often intimidated by both the subject and the researchers themselves. Therefore, the burden falls on us -- the space scientists and engineers of the world -- to communicate our findings in ways both teachers and students can understand. **S**tudent **N**anoexperiments for **O**utreach and **O**bservational **P**lanetary Inquir**Y** (SNOOPY) provides just such an opportunity to directly involve our customers in planetary science missions.

The Mars Environmental Compatibility Assessment (MECA) Student Nanoexperiments: The MECA Student Nanoexperiment Project was a partnership between MECA, The Planetary Society (TPS) and Visionary Products, Inc. (VPI). The MECA instrument suite, developed at the Jet Propulsion Laboratory (JPL), was scheduled for launch aboard the canceled Mars Surveyor Lander 2001. The MECA Patch Plate was designed to expose various materials to the Martian environment and be observable by the Robotic Arm Camera (RAC). Students 18 years of age and younger were invited to propose experiments that were consistent with MECA's Mission: to help us better understand how humans will be able to live on Mars.

Each nanoexperiment was required to fit into single MECA Patch Plate (Figure 1) hole, 1 cm in diameter and 1 cm deep, have a mass of 3 g or less, require no power, and require only a single image by the RAC. The students were asked to submit both a short proposal and a prototype of their experiment.

While most entries came from the United States, several were received from Canada, Australia, Brazil, Israel, Japan and the United Kingdom. Two finalists and an alternate were selected based on scientific merit, feasibility and relevance to MECA's mission. Chosen for flight were "Angle of Repose of Martian Dust," proposed by Lucas Möller of Moscow, Idaho and "Contradistinctive Copper," proposed by Jessica Sherman and Kelly Trowbridge of Lansing, New York (Figure 1). These experiments addressed the behavior of windblown Martian dust on surfaces and the oxidation of different textures of a possible building material, respectively. An alternate nanoexperiment was derived from similar proposals by Adam Marshall of Chapel Hill, North Carolina and Andre Luis Diaz of São Paulo, Brazil, who each proposed to observe the behavior of spacesuit materials in the Martian environment (Figure 2).

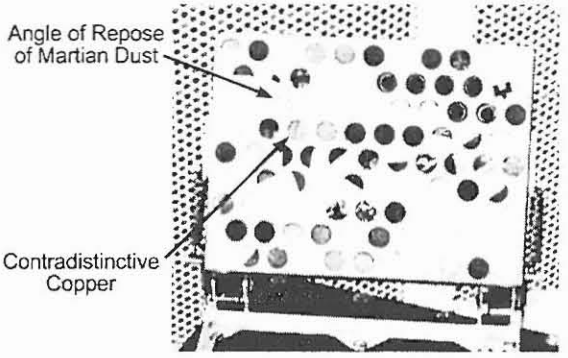

Figure 1. Nanoexperiments in the MECA Patch Plate.

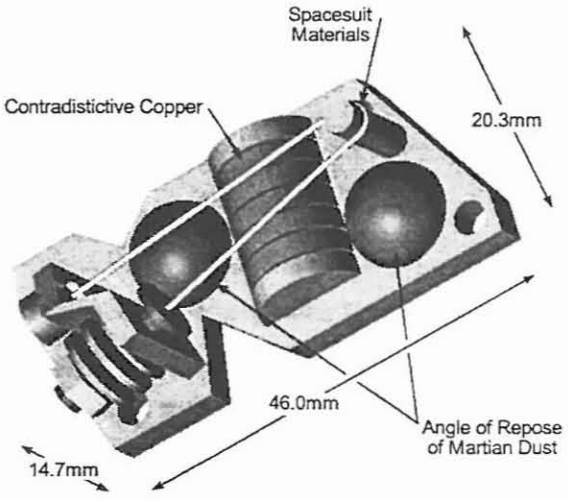

Figure 2. The SNOOPY payload.

An important goal of this project was publication of the students' work and results in the scientific literature. One student, Lucas Möller presented the results of his Angle of Repose nanoexperiment using JSC Lu-

nar-1 [2] and JSC Mars-1 [3] simulants at the 32nd Lunar and Planetary Science Conference [4].

SNOOPY – Payload Integrated E/PO: The nanoexperiments, now called SNOOPY, have been redesigned with a generic lander interface (Figure 2). The new design allows for uncertainty in the final resting angle of the lander and alleviates imaging problems due to uncertain lighting conditions. We took this opportunity to add the third nanoexperiment, which has been simplified to a single fiber of Kevlar® under tension. The creep of the fiber is measured as a function of time and environmental conditions.

The SNOOPY team plans to produce curricula describing how students and teachers can reproduce the nanoexperiments and perform their own calibration experiments. Should SNOOPY eventually fly, the data returned will be released to students and teachers as soon as it is released to the SNOOPY team. In the interim, the students will publish their calibration results in the scientific literature.

The Future: The education and public outreach goals of SNOOPY are twofold: 1) to provide opportunities for students to participate in planetary science missions and 2) to involve students worldwide in the science return and interpretation on a real-time basis. The first of these goals has been realized even though the original mission has been canceled. The second goal can be partially realized even if SNOOPY does not complete its mission. The Planetary Society and JPL plan to develop curriculum units that allow teachers and students to replicate the calibration experiments of the "student principal investigators" and to compare their results with the official calibrations. Should SNOOPY eventually fly, the images returned will be released on the World Wide Web as soon as they are made available to the investigators. Students around the world will be able to see and interpret the results and compare them to their own calibrations and to the behavior of their local materials. An online forum will allow the discussion of results.

Lessons Learned: The SNOOPY project demonstrates the value a non-profit organization like The Planetary Society can add to planetary missions. In pursuit of their goal to disseminate knowledge about space exploration, TPS is able to cooperate with the space agencies of the world, translate scientific information into everyday language and reach into classrooms worldwide. By working with small engineering firms like VPI, hardware could be developed quickly and cheaply, without many of the constraints found in government programs.

References: [1] Goldin D. (1999) Testimony before the Committee on Science, U.S. House of Representatives, April 28, 1999. [2] McKay D. S., et al. (1993) *LPSC XXIV*, 963-964. [3] Allen C. C. et al. (1997) *LPSC XXVII,* 27-28. [4] Möller L. (2001) *LPSC XXXII,* Abstract #1470.

Acknowledgements: The research described in this paper was carried out at the Jet Propulsion Laboratory, California Institute of Technology, under a contract with the National Aeronautics and Space Administration.

AUSTRALIAN RED DUNE SAND: A POTENTIAL MARTIAN REGOLITH ANALOG.

K. R. Kuhlman[1], J. Marshall[2], N. D. Evans[3], and A. Luttge[4] (1) Jet Propulsion Laboratory, MS 302-231, Pasadena, CA, 91109; kkuhlman@jpl.nasa.gov, (2) SETI Institute, NASA Ames, Moffett Field, CA, (3) Oak Ridge National Laboratory, Oak Ridge, TN, (4) Rice University, Houston, TX.

Introduction: To demonstrate the potential scientific and technical merits of *in situ* microscopy on Mars, we analyzed a possible Martian regolith analog -- an aeolian red dune sand from the central Australian desert (near Mt. Olga) [1]. This sand was chosen for its ubiquitous read coating and the desert environment in which is it found. Grains of this sand were analyzed using a variety of microanalytical techniques. A database of detailed studies of such terrestrial analogs would assist the study of geological and astrobiological specimens in future missions to Mars.

Potential instrument concepts for in situ deployment on Mars include local electrode atom probe nanoanalysis (LEAP), vertical scanning white light interferometry (VSWLI), scanning electron microscopies, energy dispersive x-ray microanalysis (EDX), atomic force microscopy (AFM) and X-ray diffraction (XRD). While *in situ* deployment of these techniques is many years away, ground-based studies using these analytical techniques extend our understanding of the data obtained from instruments to be flown in the near future.

Pseudoconfocal microscopy: Optical microscopy will be one of the first techniques used to observe Martian dust. However, optical microscopy suffers from narrow depths of field at high magnifications. Pseudoconfocal microscopy is a technique that takes advantage of this lack of depth of field to produce "in focus" optical images, such as shown in Figure 1. This image was produced using a stack of 32 images taken at a magnification of 100X and a depth of field of approximately 14 micrometers. The images were then deconvolved and combined using the Extended Focal Imaging (EFI) module in the analySIS® 3.1 software package from Soft Imaging System Corporation [4]. The image illustrates the ubiquity and non-uniformity of the red-orange coating on every grain.

Vertical scanning white light interferometry (VSWLI): A potential flight technique, VSWLI provides about 0.5 to 1.5 micrometer lateral resolution and vertical resolution on the order of two nanometers for surface features up to 100 microns high [2]. This technique complements the atomic force microscope (AFM) by providing a bridge between optical microscopy and the high-resolution measurement of surface morphology by the AFM. The three-dimensional image in Figure 2 illustrates the capabilities of this technique. This image also shows the difference in surface texture of one of the coated grains. Note the smooth texture on the left of the image and the rough texture on the right. This may indicate the difference between an abraded surface (left) and a surface that is coated (right). Pitting due to chemical weathering is also visible and quantifiable using VSWLI.

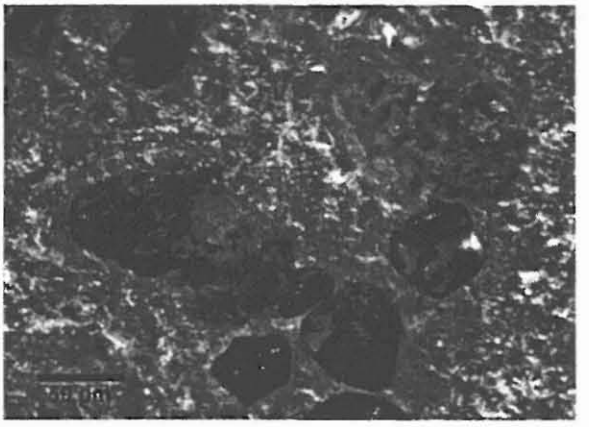

Figure 1: Pseudoconfocal optical image of red aeolian sand produced using a stack of 32 images. Magnification = 100 X. Background is frosted glass.

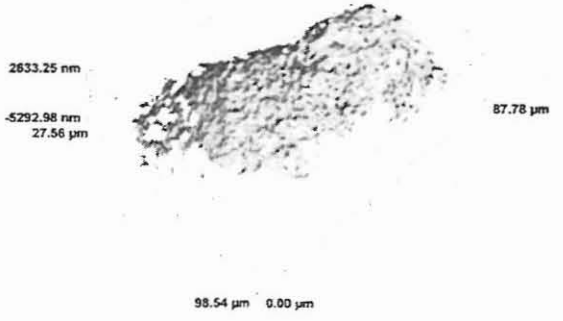

Figure 2: Vertical scanning white light interferometry (VSWLI) reconstruction of the surface of a coated grain.

Scanning electron microscopy (SEM): One of the analytical techniques that is often taken for granted on Earth, but extremely difficult to implement *in situ*, is SEM. When combined with an energy dispersive X-ray spectrometer (EDX), SEM can reveal surface morphology and chemical composition on the scale of micrometers. This technique is very important for understanding the deposition of these surface coatings and modification by chemical and aeolian processing (Figure 3). Surface weathering and the nature of the underlying particle can also be ascertained. Energy dispersive mapping of a cross-section shows that the

coating (on the right of the back-scattered electron image in Figure 4) contains both iron and aluminum (Figure 5). This coating is likely an aluminum-rich sol-gel that originates from clays in the region. The clays may have been dissolved by water during brief periods of precipitation, and percolated through the sand leaving evaporites in the crevices of the particles. The EDX spectra also indicate the presence of O, K, P, Ca, Ti, Cr, Ni, Zn, Cu and Au.

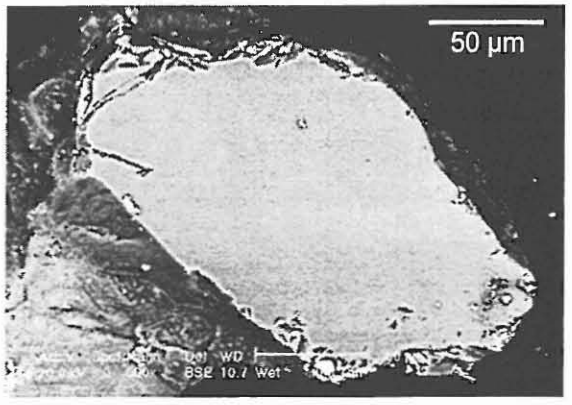

Figure 3: Backscattered electron image of the cross section of a grain showing fractures and cracking at the edges from aeolian transport.

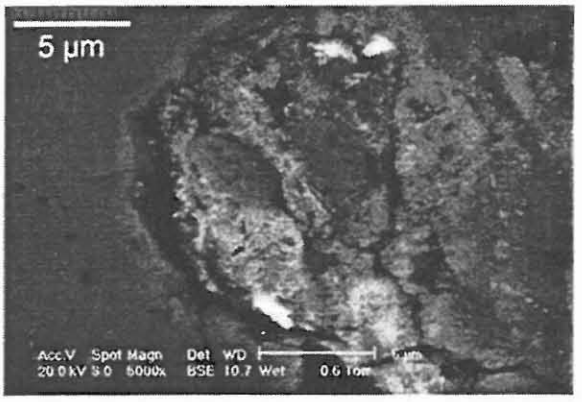

Figure 4: Backscattered electron image of cross section showing texture of the coating. The polished cross-section of the quartz particle is on the left. Note the bright "grains" within the film that appear in the Fe image in Figure 5.

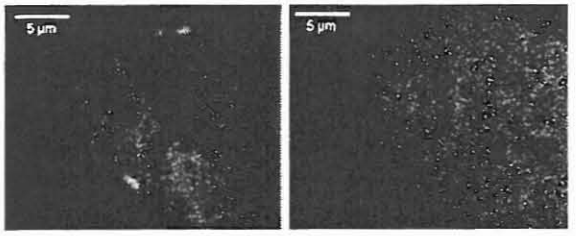

Figure 5: Iron (left) and aluminum (right) EDX maps of cross section in Figure 4. Note that the iron and aluminum coat the outer surface of the grain.

Transmission electron microscopy (TEM): Preliminary TEM of a cross-section of a particle of the red sand shows that the film is not uniform (Figure 6). In fact, the film appears to be composed of tiny crystalline grains within a non-crystalline matrix. These nanocrystals have a distinctively hexagonal shape (Figure 6), strongly indicating hematite. A very small amount of hematite nanocrystals could easily be responsible for the intense red color of the sand.

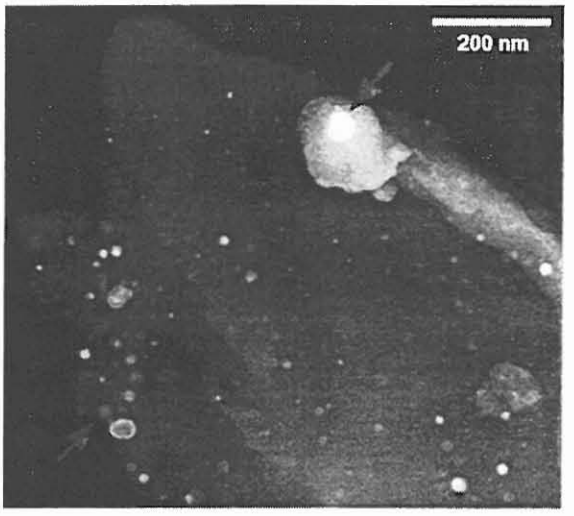

Figure 6: High-resolution TEM image of coating on a grain of Australian red sand. Note the hexagonal shape of the indicated nanocrystals.

Conclusions: Using this variety of techniques to examine the aeolian sample provided a robust set of data that enabled conclusions to be drawn about the origin of the red coating and environmental conditions in general. Our conclusions correlated well with what was actually known about the provenance of the sample and with reports of similar red sands in the literature. Studies of terrestrial analogs will further our understanding of the processes occurring on Mars. Work will continue with TEM, LEAP, AFM and XRD. Results provide us with incentive to miniaturize analytical instruments for *in situ* deployment and field equipment for future human explorers of extreme environments.

References: [1] Collected by Carol Breed, USGS, 1980, [2] Luttge, A. et al. (1999) *American Journal of Science*, **299**(7-9) 652-678, [3] http://www.soft-imaging.com/. [4] Kuhlman, K. R., R. L. Martens, T. F. Kelly, N. D. Evans and M. K. Miller (2001) "Field Ion Microscopy and Three-Dimensional Atom Probe Analysis of Metamorphic Magnetite Crystals," *Ultramicroscopy*, In Press.

Acknowledgements: Research at JPL and SETI was sponsored by NASA. Research at the ORNL SHaRE User Facility was sponsored by U.S. DOE, under contract DE-AC05-00OR22725 with UT-Battelle, LLC, and through the SHaRE Program under contract DE-AC05-76OR00033 with Oak Ridge Associated Universities.

VENTIFACT FORMATION IN THE MOJAVE DESERT: FIELD ANALOGS FOR MARTIAN PROCESSES. **J.E. Laity**[1], **N.T. Bridges**[2] and **T.K. Boyle**[3], [1]Department of Geography, California State University, Northridge, CA 91330; julie.laity@csun.edu, [2]Jet Propulsion Laboratory, MS 183-501, 4800 Oak Grove Dr., Pasadena, CA 91109; nathan.bridges @jpl.nasa.gov,[3]Department of Geography, California State University Northridge, CA 91130; tim.boyle@csun.edu

Two field studies in the Mojave Desert, California, shed light on processes of ventifact formation. The field sites are located on a ridge at Little Cowhole Mountain, which lies approximately 12 km south of Baker, and on an unnamed ridge situated along the northern boundary of the Mojave River Sink (Rasor Road site). The rocks at Little Cowhole Mountain are a blue-grey marble/dolomite, whereas those at Rasor Road are Miocene volcanic rocks (basalt). At both sites the abrasive agent is a fine-grained aeolian sand which was probably derived largely from the Mojave River. There are minimal modern inputs of sand to either site: abrasion occurs as a result of unique climatic and topographic conditions which allow pre-existing sand to be recycled from one aspect of the ridge to the other. Climatic conditions are well suited for ventifact formation. Owing to the dry climate (marked by low average relative humidity, infrequent dew, and low annual rainfall), rates of chemical weathering are low. Where resurfacing of the rocks by sand abrasion proceeds at a rate greater than weathering, the ventifacts are considered "active." Active ventifacts are found atop and straddling the ridge crests, in the zone of maximum wind velocity and sediment supply. Inactive ventifacts occur where modern weathering processes exceed abrasion rates; principally on the basal two-thirds of the hillslope, where wind velocity and sediment supply are lower. At intermediate locations between the slope base and crest, ventifacts are either active or inactive, depending on local conditions. The presence of relict ventifacts at the study sites, as well as elsewhere in the eastern Mojave Desert, suggests that the conditions for ventifact formation must have been more intense and extensive in the past.

The experimental research at Little Cowhole Mountain spanned approximately five years, and considered abrasion, sediment supply, and climate. Artificial targets (balsa wood posts and 2m high painted poles) were positioned across the study site to monitor the degree and timing of abrasion. To assess wind energy, a weather station, along with 12 satellite anemometers, were deployed. Sand levels were measured during each site visit. As anticipated, topographic effects were important, and areas of wind acceleration (the ridge crest and a topographic saddle) showed maximum erosion, reflected both in the form of the ventifacts and the abrasion recorded on the emplaced targets. Abrasion was found to result both from moderate intensity, high-frequency winds and from high intensity, low-frequency events. Neither appeared to play a more important role in the overall erosion of the site.

Research at the Rasor Road site included direct observation of a strong wind event on March 6, 2000, when a large Pacific front moved into southern California. Significant saltation occurred at wind speeds of 8-10 m/s. In front of the storm (during the morning and early- to mid- afternoon period), winds were southeasterly, exceeding 8 m/s for 15 hours, and 14 m/s for 8 hours, with a maximum sustained wind speed of about 22.5 m/s. During this period, sand from the eastern slopes moved up the hill, uncovering some ventifacts and burying others, and creating a hilltop dune which moved westward across the ridge. Sand was sorted into linear parallel bands of particles many meters in

length (sand ribbons), and ramps and moats, similar to those observed on Mars, were formed around boulders which presented near vertical faces to the wind. Sand moved across the ridge crest in a cloud 2m or more in height, and was flung horizontally 30m or more to accumulate on the westward slope. The wind direction reversed to westerly after the front had passed (late afternoon and early evening), blowing at speeds of 8 to 13 m/s for four hours. The sediment was partially blown back to its original location. Despite the relatively long duration of the wind event, significant abrasion for each ventifact occurred for only a short period, owing to burial and shielding effects as the sand surface topography changed throughout the storm.

Together, the studies illustrate that the processes that interact to form ventifacts are highly complex, and must be studied at many scales. Small-scale effects, such as local topography, plant cover, or even the spatial distribution of boulders, strongly influence the formation of each individual ventifact. Mesoscale effects (hillslope form, total availability of sediment, seasonality of winds, etc.) determine the distribution of overall erosional energy and the location of active and relict forms.

Relict ventifact textures are preserved for long periods if conditions are sufficiently arid to limit weathering processes. Fossil ventifacts, with flutes and grooves larger than modern forms and a widespread distribution in the southern California deserts, were probably formed during the late Pleistocene, when sand supply from river flow was greater and wind velocities were higher than today. Such conditions are broadly comparable to the Noachian period on Mars.

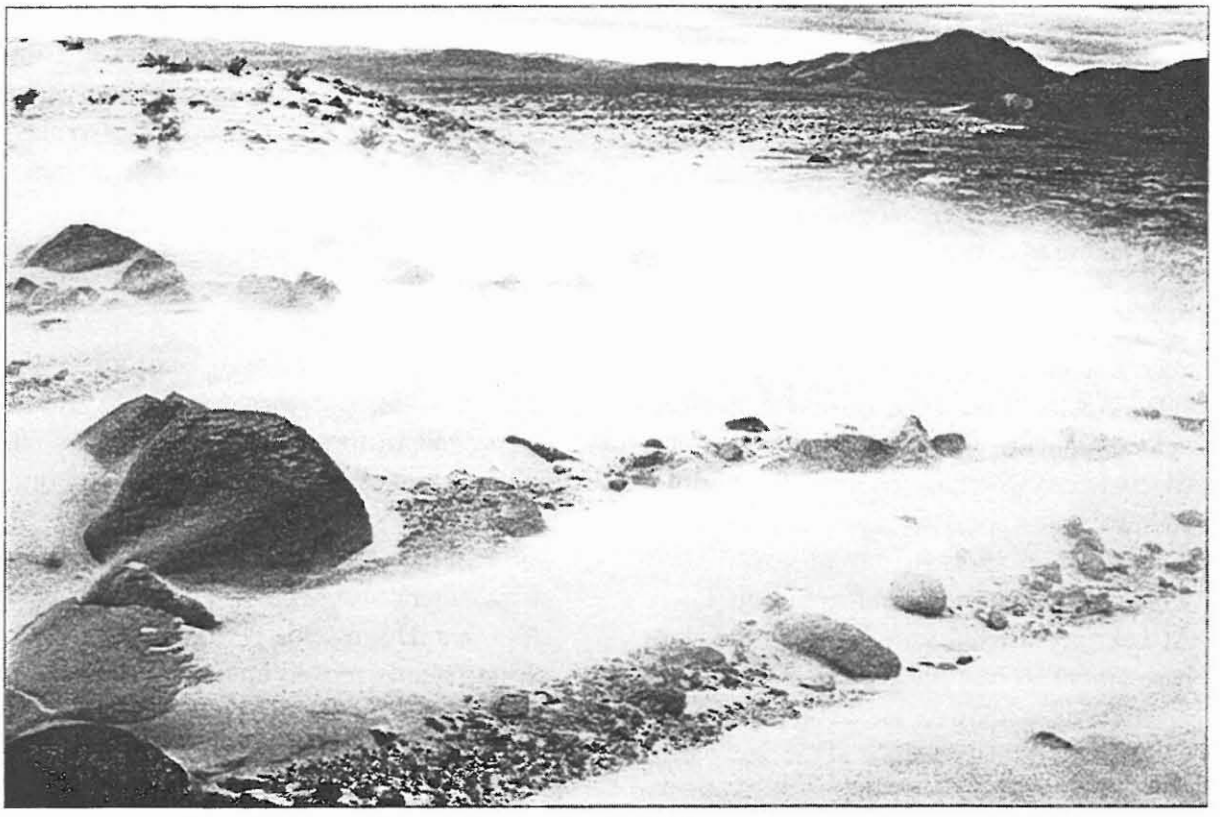

Figure 1: *High wind event at Rasor Road, March 2000.*

FLUVIAL DEGRADATION OF THE CIRCUM-HELLAS HIGHLANDS OF MARS. S. C. Mest[1] and D. A. Crown[1,2], [1]Department of Geology and Planetary Science, University of Pittsburgh, Pittsburgh, PA 15260, scmst25@pitt.edu, [2]Planetary Science Institute, 620 N. 6th Avenue, Tucson, AZ 85705, dcrown@pitt.edu.

Introduction: Geologic mapping and geomorphic analyses of Noachian- to Amazonian-aged terrains in the highlands east and north of Hellas basin have revealed the effects of volcanic, fluvial, aeolian, and mass wasting processes [1-7]. Mars Global Surveyor (MGS) and Viking Orbiter data sets are currently being used to qualitatively and quantitatively analyze highland evolution, particularly degradation resulting from fluvial processes. Fluvial features include small highland gullies, well-integrated valley networks, and extensive outflow channels systems. These features represent different types of fluvial activity, and their presence in units of different ages indicates fluvial activity spans a large portion of the region's history. It is necessary to characterize the features and units in which they occur in order to fully understand the nature of Martian fluvial activity and ultimately the history of Mars' climate. The results of these studies support the goal of NASA's Mars Exploration program by determining 1) locations for future landing sites, 2) areas in which water may be present in the subsurface, and 3) areas where life may have developed and its fossilized remnants may have been preserved.

Circum-Hellas Geologic Mapping: Geologic mapping at the 1:2M and 1:500K scales has been completed in the Promethei Terra region (27.5°-47.5°S, 245°-270°W) [3-6] and is currently in progress in the Noachis Terra region (15°-25°S, 270°-275°W) [7]. Examination of small-scale morphologic characteristics of highland surfaces as observed in high resolution Mars Orbiter Camera (MOC) images complements Viking Orbiter image-based mapping studies.

Geology of the Promethei Terra region. Heavily-cratered, Noachian-aged highland materials are the oldest deposits in the area [8,9]. These materials form rugged, mountainous terrains; some exposures are incised with small gullies [1,3-6]. Intermontane basin fill, Late Noachian to Early Hesperian in age, consists of sedimentary material eroded from highland massifs and deposited in adjacent low-lying areas. Many deposits contain well-integrated valley networks and channels [4-6]. The presence of intermontane basin fill provides evidence for a complex sequence of erosional and depositional events within the highlands.

A series of Late Noachian- to Early Amazonian-aged sedimentary plains units have been identified that embay highland terrains and record the effects of continued fluvial activity [3-7]. Dissected and channeled plains are characterized by smooth surfaces dissected by narrow, sinuous channels and low-relief scarps. The nature of dissected and channeled plains suggests large volumes of water flowed over their surfaces causing localized erosion and redistribution of sediments. Smooth plains material is interpreted to consist of materials deposited from overflow of Reull Vallis and/or deposited following erosion of the highlands by valley networks. In Viking Orbiter and MOC images smooth plains material contains pits or small-scale undulations resulting from scouring and/or aeolian processes.

Aeolian, mass wasting, and fluvial activity appear to have formed some of the youngest (Late Hesperian to Amazonian) deposits in the region including debris aprons and smooth, lineated, and pitted materials that fill craters [1,3-6]. Debris aprons are believed to consist of unconsolidated debris mass-wasted from highland massifs and bound by water and/or ice [1,10-15]. Most are found at the bases of massifs of ancient highland materials, but others occur along interior crater and vallis walls. Crater fill material is believed to have had a variety of sources including material eroded from interior crater walls by fluvial processes, lacustrine deposits, coalesced debris aprons, and aeolian deposits.

Geology of the Noachis Terra region. Highland terrains north of Hellas [7] record a different history than the eastern Hellas region. Heavily cratered highlands and intercrater plains exhibit surfaces that have been primarily degraded by fluvial processes. In particular, the northern part of the region contains an extensive dendritic valley network with many sinuous tributaries that dissect the plains and older crater ejecta blankets. The intercrater plains also contain numerous scarps believed to be erosional in nature and are most likely related to the fluvial activity that formed the valleys. Crater morphology varies throughout this area, especially among large (>25 km diameter) craters. Some craters have well-preserved rims and continuous ejecta blankets, whereas other craters have degraded or completely eroded rims or little to no ejecta blanket.

Circum-Hellas Fluvial Systems: The eastern Hellas region contains four large outflow channel systems - Reull, Dao, Niger, and Harmakhis Vallis (~1200, 230, 800, and 1500 km long, respectively) - believed to be mid- to Late Hesperian in age [1-6,16,17]. Their source areas consist of large steep-walled depressions formed by collapse of volatile-rich plains [1,3,4,16-18]. The source areas are connected to their main canyons by areas of collapsed plains, of which portions contain scour marks indicative of surface flow. The main canyons are steep-walled, flat-floored troughs with little sinuosity [1,3-6]. A large side canyon enters Reull Vallis from the south and exhibits at least two layers along its walls and may have been the location of late-stage outbursts of water [3-6]. The south-facing walls of Dao, Niger, and Harmakhis Valles display gullies believed to have formed by water that emerged from a layer below the canyon rims [17,19]. The valles cut into various highland and plains materials as they extend toward Hellas basin [1,9]; Dao and Harmakhis breach the basin rim and terminate on the basin floor. Vallis floor material consists of remnants of the collapsed plains, fluvial deposits, and contributions from wall collapse (1,3-6,17). The valles (as well as smaller adjacent channels) most likely formed by a combination of subsurface flow that caused the plains to collapse, and surface flow that eroded the plains [1,3-6,18].

Highland materials in the circum-Hellas region exhibit well-developed valley networks and channels, and the interior walls of large craters and the flanks of Hadriaca Patera are incised with gullies [1,3-6]. Small-scale valley networks, east of Hellas, are found in intermontane basin fill, and valley forms on steeper massifs occur as parallel gullies [5,6]. Within the fill, valley networks exhibit dendritic, parallel, or rectilinear patterns with well-developed tributary systems. Some valleys erode headward into surrounding highland materials, whereas other valleys have theater-headed terminations within intermontane fill deposits. The largest drainage systems consist of two or more basins connected by a single valley that appears to have breached its divide [5,6]. The Noachis Terra study area contains an extensive dendritic network of valleys that dissect heavily cratered materials [7]. Most valleys appear degraded, having rounded banks and are sometimes bisected by craters or partially buried by crater ejecta. Smaller networks just south of crater Millochau appear more pristine suggesting 1) different erosional properties of the dissected materials and/or 2) significant age differences in valley formation. The second option suggests fluvial erosion occurred over a long period of time to produce the extensive network of valleys and then became more localized to produce smaller networks near Millochau, as no pristine valleys are found as tributaries of the larger network. Highland valley networks could have formed by combinations of runoff and sapping processes. Faults and fractures within and underlying the eroded deposits could have also influenced the network patterns observed.

Several large craters (>25 km in diameter) in the study areas have degraded rims, parallel interior gullies that head near crater rims and terminate on crater floors, dissected or complete lack of ejecta blankets, and smooth floors [3-7]. The morphologies of the incised channels and the range of crater preservation suggest a combination of fluvial processes and mass wasting is responsible for erosion and degradation of circum-Hellas highland craters [19,20]. Crater Millochau (north of Hellas) and other large craters in the area contain smooth to partially eroded floor deposits and terraced knobs suggesting a lacustrine depositional environment [7]. Identification of other depositional sinks within this part of the highlands is important for understanding the degradational history of the highlands.

The flank materials of Hadriaca Patera also contain numerous valleys that radiate from the volcano's summit. Most of the valleys are trough-shaped, lack tributaries, and are theater-headed near the summit. V-shaped channels are observed in some valley interiors suggesting a contribution by surface runoff; however, their overall morphology indicates that sapping has modified the channels [1,21].

Circum-Hellas Hydrology: Drainage Basin and Valley Network Analyses: Mars Orbiter Laser Altimeter (MOLA) data are being used in conjunction with the ArcInfo Geographical Information System to quantitatively characterize the surface hydrology of these regions [22,23]. For valley networks identified in Promethei Terra, modeled drainage basins are irregular or circular in shape, due to the shapes of adjacent highland massifs and crater rims. Basin lengths range from 9 to 100 km, widths from 5 to 75 km, and areas range from 43 km^2 to 7400 km^2. Dissection varies with basin size; smaller basins are more densely dissected whereas larger basins usually contain more areas of undissected terrain. Drainage densities calculated for eastern Hellas drainage basins range from 0.037 to 0.09 km^{-1}. This is consistent with values for Margaritifer Sinus (0.03-0.07 km^{-1}) [24,25], higher than Martian global average values (0.001-0.01 km^{-1}) [26], but lower than terrestrial values (>2 km^{-1}) [27-31]. The MOLA DEM is being used to determine slope, aspect, flow direction, watershed, and flow accumulation.

Conclusions: Water has played a key role in shaping the highlands surrounding the Hellas basin. Fluvial features are preserved in materials ranging from Late Noachian to Amazonian in age. The presence of sedimentary deposits within and surrounding the highlands, as well as smooth to partially eroded interior crater deposits, indicates an extensive amount of post-Noachian resurfacing has occurred. The nature of most of these deposits suggests they are fluvial in origin, resulting from flood events, channel deposition, or within a lacustrine environment. By understanding the nature of the fluvial features in the circum-Hellas region, the properties of the materials in which they occur, and the geologic history of these terrains, we can begin to constrain past Martian climatic conditions.

References: [1] Crown, D.A. et al. (1992) *Icarus*, **100**, 1-25. [2] Tanaka, K.L. and G.J. Leonard (1995) *JGR*, **100**, 5407-5432. [3] Mest, S.C. (1998) M.S. Thesis, Univ. Pittsburgh. [4] Mest, S.C. and D.A. Crown (2001) Geology of the Reull Vallis region, Mars, *Icarus*, in press. [5] Mest, S.C. and D.A. Crown (2001) *USGS Geol. Invest. Ser. Map I-2730*, in press. [6] Mest, S.C. and D.A. Crown (2001) Geologic Map of MTM Quadrangles -45252 and -45257, *USGS*, in review. [7] Mest, S.C. and D.A. Crown (2001) Geologic Map of MTM Quadrangles -20272 and -25272, *USGS*, in preparation. [8] Scott, D.H. and K.L. Tanaka (1986) *U.S. Geol. Surv. Misc. Inv. Ser. Map I-1802A*. [9] Greeley, R. and J.E. Guest (1987) *U.S. Geol. Surv. Misc. Inv. Ser. Map I-1802B*. [10] Crown, D.A. and K.H. Stewart (1995) *LPS XXVI*, 301-302. [11] Stewart, K.H. and D.A. Crown (1997) *LPS XXVIII*, 1377-1378. [12] Squyres, S.W. and M.H. Carr (1986) *Science* **231**, 249-252. [13] Zimbelman, J.R. et al. (1989) *Proc. LPS 19th*, 397-407. [14] Pierce, T.L. (2001) M.S. Thesis, Univ. Pittsburgh. [15] Pierce, T.L. and D.A. Crown (2001) *LPS XXXII*, abstract 1419. [16] Price, K.H. (1998) *USGS Misc. Invest. Ser. Map I-2557*. [17] Crown, D.A. and S.C. Mest (2001) *LPS XXXII*, abstract 1344. [18] Squyres, S.W. et al. (1987) *Icarus*, **70**, 385-408. [19] Malin, M.C. and K.S. Edgett (2000) *Science* **288**, 2330-2335. [20] Craddock, R.A. and T.A. Maxwell (1993) *JGR*, **98**, 3453-3468. [20] Grant, J.A. and P.H. Schultz (1993) *JGR*, **98**, 11,025-11,042. [21] Gulick, V.C. and V.R. Baker (1990) *JGR*, **95**, 14325-14344. [22] Mest, S.C. et al. (2001) *LPS XXXII*, abstract 1419. [23] Mest, S.C. et al. (2001) *suppl. to EOS (Trans. AGU)*, abs. number P31A-05. [24] Grant, J.A. (1997) *LPSC XXVIII*, 451-452. [25] Grant, J.A. (1997) *LPSC XXIX*, abstract 1285. [26] Carr, M.H. (1996) *Water on Mars*: NY, Oxford Univ. Press. [27] Gregory, K.J. (1976) *Drainage networks and climate*, in Geomorphology and Climate, Wiley-Interscience, Chinchester, p. 289-315. [28] Gregory, K.J. and D.E. Walling (1973) Drainage Basin Form and Process, Halsted Press, NY. [29] Morisawa, M.E. (1962) *GSA Bull., 73*, 1025-1046. [30] Schumm, S.A. (1956) *GSA Bull., 67*, 597-646. [31] Smith, K.G. (1958) *GSA Bull., 69*, 975-1008.

REMOTE SENSING OF EVAPORITE MINERALS IN BADWATER BASIN, DEATH VALLEY, AT VARYING SPATIAL SCALES AND IN DIFFERENT SPECTRAL REGIONS. J. E. Moersch[1], J. Farmer[2], and A. Baldridge[2], [1]Department of Geological Sciences, University of Tennessee, 206 G.S. Building, Knoxville, TN 37996, jmoersch@utk.edu; [2]Geology Department, Arizona State University, Tempe, AZ 85287.

Introduction: A key concept behind the overall architecture of NASA's Mars Surveyor Program is that remote sensing observations made from orbit will be used to guide the selection of landing sites for subsequent missions to the surface. An important component of the orbital phase of this strategy is mineralogical mapping of the surface with infrared spectrometers and imaging systems. Currently, the Mars Global Surveyor Thermal Emission Spectrometer (TES) is spectrally mapping Mars in the 6-50 μm region at a spatial resolution of 3km [1]. Starting later this year, the Thermal Emission Imaging System (THEMIS) aboard the Mars 2001 Odyssey orbiter will image the entire surface of the planet in eight broad bands in the 6.5-14.5 μm region at a spatial resolution of 100m [2]. In 2003, ESA plans to launch the OMEGA instrument on Mars Express, which will map the planet in the visible and near infrared regions from an elliptical orbit at spatial resolutions of up to 100m [3]. Currently, NASA is selecting a visible and near-infrared mapping spectrometer for an orbiter that will launch in 2005. This instrument will likely map at a constant spatial resolution of at least 50m.

From an astrobiological perspective, the utility of these spectral datasets will be in locating potential paleohabitats for martian life, via the detection of minerals that form in the presence of liquid water[4]. Deposits of evaporite minerals in putative martian paleolake basins are a particularly attractive target to look for because of the areal extent of these features[5], the strong spectral features of these minerals[6], and the characteristic sequences in which they appear along the margin of a basin[7].

Despite considerable geomorphic evidence indicating the presence of ancient lake basins on Mars [e.g., 8], to date no evaporite deposits have been reported from the TES experiment. But is this to be expected, given the limited spatial resolution of TES data? Might we still hope to find such deposits in upcoming experiments? One way to address this question is to use existing datasets from terrestrial analog sites to attempt to determine spatial and spectral thresholds of detectability for these minerals in a natural setting.

Data: Death Valley, California, contains a well-studied series of playa deposits with a wide range of evaporite minerals [8]. Carbonates, sulfates, and halite deposits are found in the typical basinward sequence along the western margin of the Cottonball, Middle, and Badwater Basins within Death Valley. Previous studies of Badwater Basin in the visible/near-infrared (0.35 – 2.5 μm) region with AVIRIS data [9] and in the thermal infrared (8 – 12 μm) region with TIMS data [10] have demonstrated the utility of remote sensing techniques for mapping playa evaporite deposits on Earth.

The present work makes use of remote sensing data acquired over Badwater Basin by the MODIS/ASTER Airborne Simulator (MASTER) and the Airborne Visible-Infrared Imaging Spectrometer (AVIRIS). MASTER is a pushbroom imager that simultaneously acquires data in 50 channels from the visible to the thermal infrared (0.46 – 12.85 μm) at a spatial resolution of 5-15 m. Ten of the channels fall within the 7 – 13 μm region, making MASTER an outstanding analog for the upcoming THEMIS experiment at Mars. AVIRIS is also a pushbroom imager, and operates over 224 bands in the visible and near infrared at a spatial resolution of 20m, making it an excellent analog for ESA's OMEGA instrument and NASA's 2005 mapping spectrometer. Calibration of these datasets has been accomplished through atmospheric modeling/removal (MODTRAN for MASTER and ATREM for AVIRIS) and ground-truthing activities such as field spectroscopy and collection of samples for laboratory analysis [12].

Analysis and Discussion: The approach we have used to assess the effects of spatial resolution on the detectability of evaporates in the thermal infrared portion of the spectrum is as follows: standard hyper- and mulispectral processing techniques are applied to the MASTER Badwater Basin data in its native (5-15m) spatial resolution to extract pure spectral endmembers. These endmembers are given mineral identifications based on comparisons with mineral spectra from spectral libraries [e.g., 13]. The MASTER data are then mapped pixel by pixel in terms of the spectral endmember that best matches each pixel. Then we start over wtih the MASTER data de-resolved to lower spatial resolutions and repeat the process, to simulate observations by, for example, THEMIS (100m resolution) or TES (3km resolution).

The figure below shows the mineral classifications we have found for Badwater Basin in the thermal infrared at full (5-15m, on left), 100m (center), and 3km

(right) spatial resolution. At full resolution and 100m, evaporite minerals are seen on the west side of the basin in typical "bathtub rings" of carbonates (shown in medium brown) and sulfates (cyan and aquamarine) surrounding a playa composed predominantly of halite (blue). Note that the halite has not been detected directly because it has no significant absorptions in this spectral region (or in the vis/near-ir, for that matter). Rather, it is inferred here from its lack of spectral features and from prior knowledge from the field. The only significant difference between the mineral map made at full resolution versus the one at 100m is that no spectrally pure sulfates are found in the 100m data because "pure" sulfate areas are mixed with adjacent sulfate/silicate mixes. Pixels containing carbonates are mixed with silicates at all spatial resolutions. Their detectability in mixtures is enhanced by the relatively unambiguous carbonate ν_2 band at 11.2 μm.

The right panel in the figure reveals that 3 km is near the spatial threshold of detectability for carbonates in the Badwater Basin, and it is beyond the limit for sulfates. Likewise, 3km is insufficient to resolve the diagnostic "bathtub ring" morphology of the evaporite deposits in Badwater Basin. Halite in the basin is areally extensive enough to be mappable at 3km, but without significant spectral features, it is questionable whether it would be identified as such without prior knowledge.

What are the implications of these results for the detection of evaporites on Mars? It may mean that the reason TES has failed to detect evaporates on Mars is simply because it lacks the necessary spatial resolution. However, a number of cautions must be applied when making such inferences. 1) Badwater Basin is the only terrestrial analog we have studied at varying spatial resolutions so far, 2) TES has a much higher spectral resolution than MASTER, which may mean it is better able to discriminate spectral components, 3) the martian atmopsheric window is somewhat wider that the Earth's, making additional spectral bands (some noticeably deeper) available for the detection of key minerals, 4) it is possible that martian evaporite deposits, if they exist, are simply of a different spatial scale than those found in Badwater Basin.

We are presently extending our work at Badwater Basin into the visible and near-infrared with AVIRIS data. Additionally, we are beginning to examine other terrestrial basins using visible/near-ir/thermal-ir observations from the Advanced Spaceborne Thermal Emission and Reflection Radiometer (ASTER) instrument, now orbiting Earth on the first EOS satellite.

References: [1] Christensen, P.R., et al. (1992), *JGR, 97,* 7719-7734, [2] Christensen, P.R., et al (1999), *LPI Cont.. 991,* 28-29, [3] ESA website sci.esa.int., [4] Farmer, J., and D. Des Marais (1999), *JGR, 104,* 26977-26995, [5] Goldspiel, J. and S. W. Squyres (1991), *Icarus, 89,* 392-410, [6] Lane, M., and P. R. Christensen (1997), *JGR, 102,* 28581-25592, [7] Eugster, H.P., and L.A. Hardie (1978), *Lakes: Chemistry, Geology, and Physics,* Springer-Verlag, 237-293, [8] Cabrol, N., and E. Grin (1999), *Icarus, 142,* 160-172, [9] Hunt, C.B., et al. (1966), *U.S. Geol. Surv. Prof. Pap., 494-B,* [10] Crowley, J.K, *(1993), Remote Sens. Environ., 44,* 337-356, [11] Crowley, J.K., and S. J. Hook (1996), *JGR, 101,* 643-660, [12] Baldridge, A., et al. (2001), *Geol. Soc. Am. annual meeting, in press.*, [13] Christensen, P.R., et al. (2000), *JGR, 105,* 9735-9738.

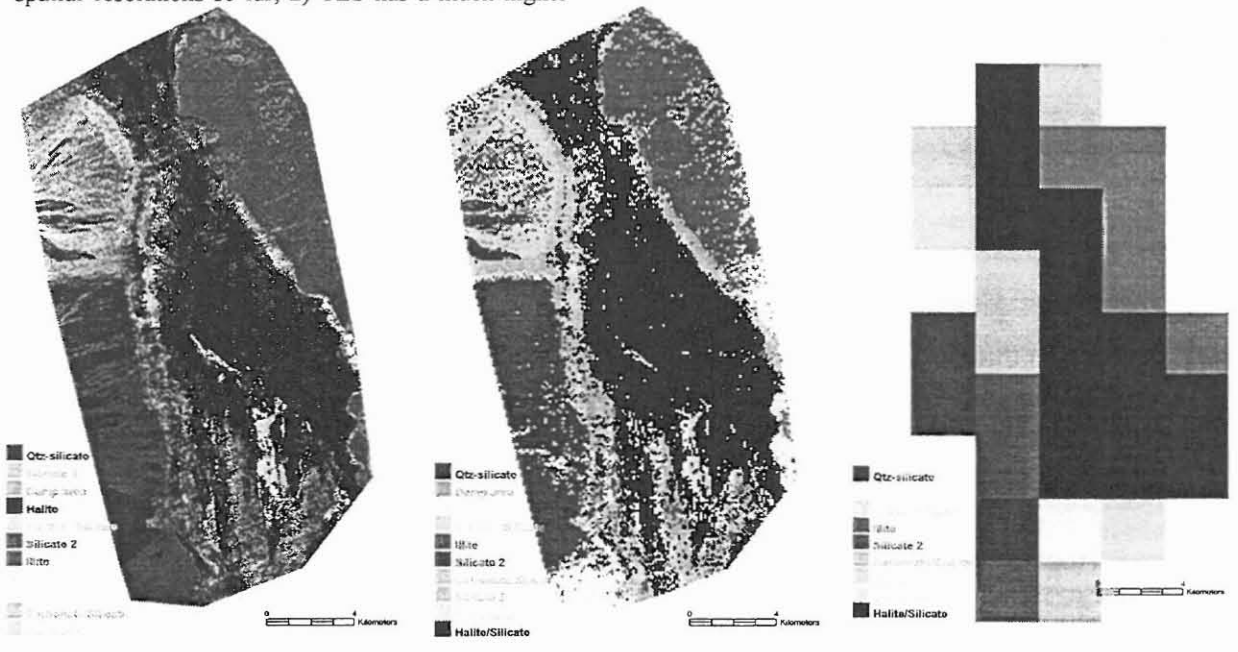

SURFICIAL STUDIES OF MARS USING COSMOGENIC NUCLIDES. K. Nishiizumi, Space Sciences Laboratory, University of California, Berkeley, CA 94720-7450 (kuni@ssl.berkely.edu).

Introduction: Cosmogenic nuclides (CNs) are produced by cosmic-ray nuclear interactions with target nuclei in rocks, soils, ice, and the atmosphere. Cosmogenic nuclides have been widely used for investigation of solar system matter for several decades [1]. Stable nuclides, such as ^{3}He, ^{21}Ne, and ^{38}Ar, are built up over time as the surface is exposed to cosmic rays. The concentrations of cosmogenic radionuclides, such as ^{10}Be, ^{26}Al, and ^{14}C also build up with exposure time but reach saturation values after several half-lives.

Especially since the development of accelerator mass spectrometry (AMS), CNs in terrestrial samples have been routinely used for geomorphic studies such as glaciation, surface erosion, and tectonics, and studies of atmospheric and ocean circulation [2]. Cosmogenic nuclides on Mars will be able to answer questions of exposure ages, erosion rates, tectonic events, and deposition rates of sediments and/or volatiles. The concentrations of cosmogenic stable nuclides give the integrated exposure time of the rock/mineral, and the activities of radionuclides give recent records for times back as long as a few half-lives.

Cosmogenic Nuclides on Mars: Unlike on the Earth, cosmic rays readily reach the Martian surface because of the planet's thin (~15 g/cm^2) atmosphere and very weak magnetic field. The CN production rates and profiles in the Martian surface are similar to those on the Moon, even after taking into account the average Martian atmospheric depth of 15 g/cm^2 [3]. The production rates of various CNs on Mars can be calculated using the Los Alamos High Energy Transport (LAHET) Code System (LCS) that has been well tested using a database of CN observations in lunar, meteoritic, and terrestrial samples. Because the production rates on Mars are 3 orders of magnitude higher than those on the Earth's surface, at levels similar to those in meteorites and lunar samples, many CNs can be measured in Martian surface features.

Although production rates of nuclides on the Martian surface are similar to those in extraterrestrial materials, the applications of CNs on Mars are similar to terrestrial applications [*e. g.* 4]. The terrestrial applications of CNs have included erosion and exposure histories of landforms (glaciation, floods, landslides, and faults), ages of impact craters, deposition or ablation rates of soils and icecaps, and ages of young volcanic eruptions. Steady state erosion of bedrock surfaces may give information on long-term erosion rates of the Martian surface. The histories of aeolian dust and layered terrains near the poles can also be studied. The use of multiple CNs is required to constrain exposure histories of Martian surface samples.

Some CNs of particular promise for unraveling the histories of Martian surfaces during the last 10^7 years are listed in Table 1 along with their half-lives and the major target elements from which production occurs. These are mostly the same CNs often used to study other extraterrestrial materials. The (^{53}Mn)-^{10}Be-^{26}Al-^{21}Ne combination is very good for solving complex histories of terrestrial surface morphologies as well as histories of meteorites. However, given the present detection methods and limits these important CNs can only be measured in returned samples.

The radionuclide ^{14}C made in the Martian atmosphere has been proposed to study the nature of atmosphere-regolith interactions [5]. However, the Martian atmosphere is so thin that production of ^{14}C from soil nitrogen could be a serious complication [6]. Some CNs made in the Martian atmosphere could be deposited on the surface, as is the case for terrestrial cosmogenic nuclides.

Table 1. Cosmogenic nuclides made on Mars.

Nuclide	Half-life (yr)	Major targets
^{129}I	1.57×10^7	Te, Ba, La
^{53}Mn	3.7×10^6	Fe
^{10}Be	1.5×10^6	O, Mg, Si, C
^{26}Al	7.05×10^5	Si, Al, Mg
^{36}Cl	3.01×10^5	K, Ca, Fe, Cl
^{81}Kr	2.3×10^5	Sr, Y, Zr
^{41}Ca	1.04×10^5	Fe, Ca
^{59}Ni	7.6×10^4	Fe, Ni
^{14}C	5,730	O
^{60}Co	5.27	Co
^{22}Na	2.61	Mg, Si
^{54}Mn	0.855	Fe
^{3}He	stable	O, Mg, Si, Fe
$^{20\text{-}22}$Ne	stable	Mg, Si
$^{36, 38}$Ar	stable	Ca, Fe
^{150}Sm	stable	^{149}Sm
^{158}Gd	stable	^{157}Gd

Issues Addressed by Measurements of Cosmogenic Nuclides: Some examples are *1) Absolute exposure age determination of surface materials and impact craters.* Based on results for meteorites and lunar samples, we anticipate that Martian surface materials have been exposed to cosmic rays for only a small fraction of the age of the solar system. Ejection by an impact is one mechanism (volcanism and surface erosion or ablation are others) for excavating deep-lying material, and thereby starting the cosmic-ray clock. The exposure ages of impact ejecta thus provide an absolute determination of a crater's age. The ages of South Ray and North Ray Craters on the Moon [*e. g.* 7] and of Meteor Crater on Earth [*e. g.* 8], for example, have been determined in this way. Analogous information for a Martian crater would provide a crucial, absolute calibration point for relative terrain ages obtained by crater counting.

2) Erosion rates. Micrometeorite milling erodes lunar samples at rates of about 1 mm/Myr [9]. Wind blown dust particles also erode surface features. Erosion rates on Mars are not well constrained. The erosion rate falls naturally out of modeling calculations, where it appears as a necessary parameter in the deconvolution of CN depth profiles and activity ratios.

3) Regolith gardening. The rate of gardening (overturn and mixing by meteorite impact) in a regolith can be inferred by comparing the depth profiles of CNs in short cores [10]. Deeper-scale gardening processes can be deduced by comparing the depth profiles of CNs that are produced by thermal neutron capture but have different half-lives. Good candidates for such measurement are radioactive ^{41}Ca, ^{60}Co, and stable ^{156,158}Gd and ^{150}Sm [*e. g.* 11].

4) Ice cap evolution. Ratios and concentrations of two or more CNs with different half-lives measured in rock fragments in the ice cap will provide ice accumulation or sublimation rates [12].

Sampling Requirements for Sample Return: Although masses needed for measurement vary for most of the nuclides listed in Table 1, in meteorites and near-surface lunar samples they seldom exceed 10 mg and can be as small as 1 mg. If a larger sample is available, measurements of both stable and radioactive CNs could be made for samples taken from depths of up to ~3 m depending on the details of the irradiation. At greater depths, the production of CNs is likely to have been too small to measure. ^{129}I is a special case requiring more material.

The irradiation of the samples during the return trip to Earth raises additional complications [13]. Large solar particle events and galactic cosmic ray (GCR) particles could produce short-lived radionuclides such as ^{22}Na, ^{54}Mn, and ^{60}Co at levels comparable to those present at the time of sample collection. As massive shielding of the return capsule is not feasible, and would increase rates for GCR-induced reactions, some means for monitoring the production of CNs should be included in the design of the mission.

Detection of Cosmogenic Radionuclides on the Surface of Mars: Because the production rates of CNs on Mars are high, the activities of some cosmogenic radionuclides can be detected by an instrument on the surface of Mars. An excellent candidate is ^{26}Al, but other nuclides, such as ^{22}Na, ^{54}Mn, ^{60}Co, as well as the naturally occurring ^{40}K and the U-Th decay chains can be measured.

However, the high cosmic-ray intensity on the Martian surface increases detector background levels. This requires either massive shielding for detectors or coincidence and/or anti-coincidence counting systems. However, massive shielding is not practical on the surface of Mars except by putting detector systems into deep cores or tunnels. The γ-γ coincidence method is a good technique for the detection of several important radionuclides. The coincidence can be obtained with two γ-ray detectors in order to reduce background levels.

^{22}Na-^{26}Al-^{21}Ne pair: These three nuclides are produced in similar nuclear reactions. The ratio and activities of ^{22}Na and ^{26}Al will tell us recent sample geometry and history. ^{22}Na can give the sample's geometry during the last 5 years and a prediction for the ^{26}Al and ^{21}Ne production rates at that location. ^{26}Al and *in-situ* ^{21}Ne [14] can be used to determine the exposure time and erosion rate at the location or average shielding depth and the gardening rate of regolith samples [15].

A good detector system for Martian surface γ-ray measurements could be made using CdZnTe room-temperature solid-state detectors [16]. While the energy resolution is not as good as Ge detector, it is good enough (about 2%) for use in a coincidence system and would be lighter and more compact.

Conclusion: The measurement of multiple CNs is required to understand surficial histories of Mars. The high CN production rates on Mars allow us to use multiple nuclides as in studies of terrestrial samples, meteorites, and lunar samples. Although sample return is extremely important for such studies, we feel that *in-situ* γ-ray measurements of CNs on Mars during future missions can provide valuable information about the history of the Martian surface.

Acknowledgement: This work was supported by NASA and DOE grants.

References: [1] Reedy R.C. *et al.* (1983) *Annu. Rev. Nucl. Part. Sci. 33*, 505-537. [2] Tuniz C. *et al.* (1998) *Accelerator Mass Spectrometry* pp. 371. [3] Masarik J. and Reedy R.C. (1995) *LPS. XXVI*, 901-902. [4] Nishiizumi K. *et al.* (1993) *ESPL 18*, 407-425. [5] Jakosky B.M. *et al.* (1996) *JGR 101*, 2247-2252. [6] Masarik J. and Reedy R.C. (1997) *LPS XXVIII*, 881-882. [7] Marti K. *et al.* (1973) *Proc. Lunar Sci. Conf. 4th*, 2037-2048. [8] Nishiizumi K. *et al.* (1991) *GCA 55*, 2699-2703. [9] Kohl C.P. *et al.* (1978) *Proc. Lunar Planet. Sci. Conf. 9th*, 2299-2310. [10] Langevin Y. *et al.* (1982) *JGR. 87*, 6681-6691. [11] Russ G.P., III *et al.* (1972) *EPSL 15*, 172-186. [12] Nishiizumi K. *et al.* (1996) *Trans. Am. Geophys. Union 77*, F48. [13] Gooding J.L. (1990) *NASA Technical Memorandum Series NASA-TM-4148*, 242. [14] Swindle T.D. (2000) *Concepts and Approaches for Mars Exploratioin LPI Contribution No.1062*, 294-295. [15] Nishiizumi K. and Reedy R.C. (2000) *Concepts and Approaches for Mars Exploratioin LPI Contribution No.1062*, 240-241. [16] Moss C.E. *et al.* (2000) *LPS XXXI*, CD-ROM.

POSSIBLE FORMATION PROCESSES FOR MARTIAN CRYSTALLINE HEMATITE.

E. D. NOREEN[1&2], M. G. CHAPMAN[2], and K. L. TANAKA[2], [1]ericnoreen@yahoo.com; [2]USGS, 2255 N. Gemini Dr, Flagstaff, AZ 86001-1600.

Introduction: The Thermal Emission Spectrometer (TES) on the Mars Global Surveyor (MGS) has detected large concentrations of bulk crystalline hematite within the western equatorial region of Mars [1,2]. The hematite represents a unique and enigmatic spectral signature of surface rock distinct from basalt or basaltic andesite. Analysis of the spectral data also suggests that the hematite grains are axis-oriented [3]. This discovery of large concentrations of hematite is interesting because on Earth, production of iron oxides at this scale would require large quantities of liquid water, a known requirement for life. While no one hypothesis as to how the hematite formed has been excluded at this time, examination of the morphology of the deposits may favor a hydrothermal origin.

Location of Deposits: All of the bulk crystalline hematite signatures found so far are confined to a limited geographic area within the western equatorial region. The hematite is restricted to a ~1200 km band trending N80°E from Valles Marineris (VM), to Aram Chaos, and terminating at the largest deposit within Sinus Meridiani (SM). The deposit in SM is centered near 2°S latitude between 0 and 5°W longitude covering an area >175,000 km^2 [1]. Within Aram Chaos, a heavily modified crater, lies the next largest accumulation of hematite [1] covering an area ~5000 km^2. The interior of central VM contains several deposits 25-800 km^2.

The hematite signatures have been found on several different geologic units. In SM the hematite is confined to unit *sm* [4], a smooth, layered friable surface variously interpreted as eolian/volcanic deposits [5], paleopolar deposits, and wind eroded sedimentary deposits [4].

At a larger scale within central VM the hematite is confined to a single mapped unit, *Airs*, interpreted to be eolian deposits or airfall tuff [6]. High-resolution Mars Orbital Camera (MOC) images show that the hematite in central VM occurs within a unit similar in appearance to the hematite area in SM.

Discussion of Possible Formation Processes: Using the spectral, geologic/geomorphic and topographic relationships, we are able to develop some constraints on the possible formation processes of the hematite. The bulk crystalline hematite occurs in limited areas within the equator suggesting that this hematite formed through a process not ubiquitous to the whole planet. Spectral evidence indicates that the grains are >=10 microns [1] and axis oriented [3] limiting the formational processes to those that can produce the preferred growth and size.

All of the hematite areas show some evidence of near-surface water activity in nearby fluvial, groundwater, or lacustrine features. South of unit *sm* there are extensive ancient channels within *hc*, a heavily cratered unit, that terminate at the contact of the units [4,7]. Directly northeast of unit *sm* in an adjacent unit, there is a 1-km-diameter feature seen in MOC image M0401289, which shows a 'bullseye' pattern perhaps suggesting lacustrine evaporative deposits within a pre-existing crater, a thermokarst collapse, or possibly a pseudocrater. Aram Chaos contains chaotic terrain, possibly caused by near-surface water activity. VM is the source area for many of the massive outflow channels in the region--the chasmata-sourced channels may have been produced in catastrophic floods caused by shallow level magmatic activity melting ponded ice [8].

Mars Orbital Laser Altimeter (MOLA) data has revealed that the occurrences of hematite exist in a variety of topographic terrains. Within unit *sm* it occurs on a gentle slope downtrending to the northwest; in the eastern area of *sm* a high concentration is on a local topographic high. In Aram Chaos it occurs on the floor of the eroded crater between small mesas. In VM and the remaining areas it occurs on relatively gentle slopes and troughs. It then becomes apparent that rugged topography, found in Aram Chaos and VM, limits the exposure of the hematite deposits when compared to the expansive deposit in Sinus Meridiani, which occurs on broad, gentle topography. It is unknown whether topography is a controlling factor in the formation process or if the deposits are simply eroded more easily in gentle topography.

Non-aqueous Formation Processes. There are several formation processes that do not require the presence of water. Crystalline hematite can form as a surface coating on individual grains or the surface of a rock [1]. The axis oriented nature of the spectra require that surface or grains be aligned, as in a winnowed or polished eolian surfaces; this hypothesis is inconsistent with the signatures being limited to one region on Mars. Also, most terrestrial forms of hematite surface coatings occur as red hematite, which is not consistent with the TES data.

Large specular grains of hematite can also form within intrusions with a high oxygen fugacity [9], which could produce an alignment of hematite grains through laminar flow. However, the Martian occur-

rences are not topographically consistent with large-scale intrusions.

The hematite could also occur as the oxidation of Magnetite-rich lavas [1], a hypothesis supported by a basaltic spectral association. While there is a lack of evidence for lava flows within Sinus Meridiani, the geomorphology of all occurrences are consistent with basaltic ash deposits, which may have been oxidized. If these units are ash deposits, primary hematite could also form within the cooling unit of an ignimbrite [9].

Sedimentary Aqueous Formation Process. On Earth, the majority of iron deposits have been interpreted to form through precipitation from iron-rich fluids. The most well known deposits are banded iron formations (BIFs), which are alternating layers of silica-rich and iron-rich bands. The iron bands form through precipitation from iron-rich water upwelling from an anoxic depth to shallow oxygenated waters [9]. Terrestrial formation of BIFs produces large quantities of quartz and chert [9], which are not seen in the TES data. In addition, a requirement for this process is a large body of water. While Valles and Aram Chaos may have had large lakes within them at some time in the past, the tilted topography of Sinus Meridiani makes deposition of unit *sm* in surface water bodies unlikely if the hematite is geologically recent. SM is gently dipping to the northwest with no large basins existing within the hematite unit sm; on the contrary, there are localized topographic highs in areas of highest hematite concentration.

Leaching of soils can produce an enrichment in iron oxides in the form of red nanophase hematite, which could then be metamorphosed into gray crystalline hematite by burial [9]. This theory is unlikely due to extremely high amounts of rainfall required as well as the depth of burial necessary to convert red hematite to gray and the subsequent removal of the overburden, which is not reflected in topography of SM. If a suitable thickness of overburden had been removed from *sm* to expose the hematite, *sm* should not have similar elevations to the surrounding heavily cratered terrain. The range in topography from *sm* and the directly adjacent Noachian terrain (~ 4 Ga) is less than 500 meters.

Hydrothermal Formation. The specular hematite could likely have formed through the precipitation from iron-rich hydrothermal fluids: VM contains numerous possible volcanic vents, fissure lava flows, and possible ash deposits [8,10]. Within SM, the hematite unit appears consistent with ignimbrite deposits, based on localized layering and mantling of topography, and numerous mounds that can be interpreted as fumarolic [7]. All occurrences of the hematite show indications of near-surface or surface water activity. Due to these associations, a hydrothermal enrichment in iron oxides is our favored hypothesis.

Individual hydrothermal deposits can occur as strongly discordant veins and breccias to massive concordant bodies. Massive concordant bodies can occur along permeable horizons such as poorly welded tuffs [11] consistent with the interpretation that the hematite units are volcanic ash deposits.

The fumerolic features within Sinus Meridiani could have formed through fluids escaping through vertical tubes by hydrothermal means, as well as through the exhalations of a cooling ignimbrite.

Future Work: Later this year the Mars Odyssey will arrive in orbit around Mars and soon begin sending back data from the Thermal Emission Imaging System (THEMIS). This instrument has a much better spatial resolution than TES, 100 meters compared to 3 km, and may be able to determine if there is any aqueous mineralization associated with the hematite signatures.

Within the hematite area in SM there are several locations suitable as landing sites for the 2003 Mars Exploration Rover (MER). Given the generally bland mineralogic landscape of Mars seen in the TES data [12], the concentrated crystalline hematite locales are the only known areas in which we confidently expect to find rock and mineral types dissimilar to that of the Viking and Pathfinder landing sites [7]. Currently, three out ten of the high priority sites for the 2003 MER mission lie within the SM hematite concentration indicating the intense interest in this locale.

References: [1] Christensen, P.R. et al. (2000) *JGR.***105**, 9623-9642. [2] Noreen, E. et. al. (2000) Mars Tharsis Workshop, [3] Lane, M. D. et. al., (2000) *LPSC XXXI.* [4] Edgett, K.S., and Parker, T.J., (1997) *GRL 24*, 2897-2900. [5] Scott, D. H., and Tanaka, K.L. (1986) *USGS Map I-1802-A.* [6] Lucchitta, B.K. (1999) *USGS Map I-2568*, [7] Chapman M. G. (1999) 2nd Mars Surveyor 2001 Landing Site Workshop. [8] Chapman M. G. and Tanaka, K.L. (2001) *JGR 105*, 10087-10100 [9] Sidder, G.B. (1991). *Geology of N. America. Geol. Soc. Of Amer.* v. P-2. 63-86. [10] Lucchitta, B.K. (1990) Icarus. **86**. 476-509. [11] Hauck, S.A. (1990) *U.S. Geol. Sur. Bull.* 1932, p.4-39. [12] Christensen, P.R. et al. (1998) Science. 279. 1692-1698.

ACCESSING MARTIAN FLUVIAL AND LACUSTRINE SEDIMENTS BY LANDING IN HOLDEN CRATER, MARGARITIFER SINUS. T. J. Parker[1] and J. A. Grant[2], [1]Jet Propulsion Laboratory, California Institute of Technology, Mail Stop 183-501, 4800 Oak Grove Dr., Pasadena, CA 91109, timothy.j.parker@jpl.nasa.gov, [2]Center for Earth and Planetary Studies, National Air and Space Museum, MRC 315, Smithsonian Institution, Washington, DC 20560, grantj@nasm.si.edu.

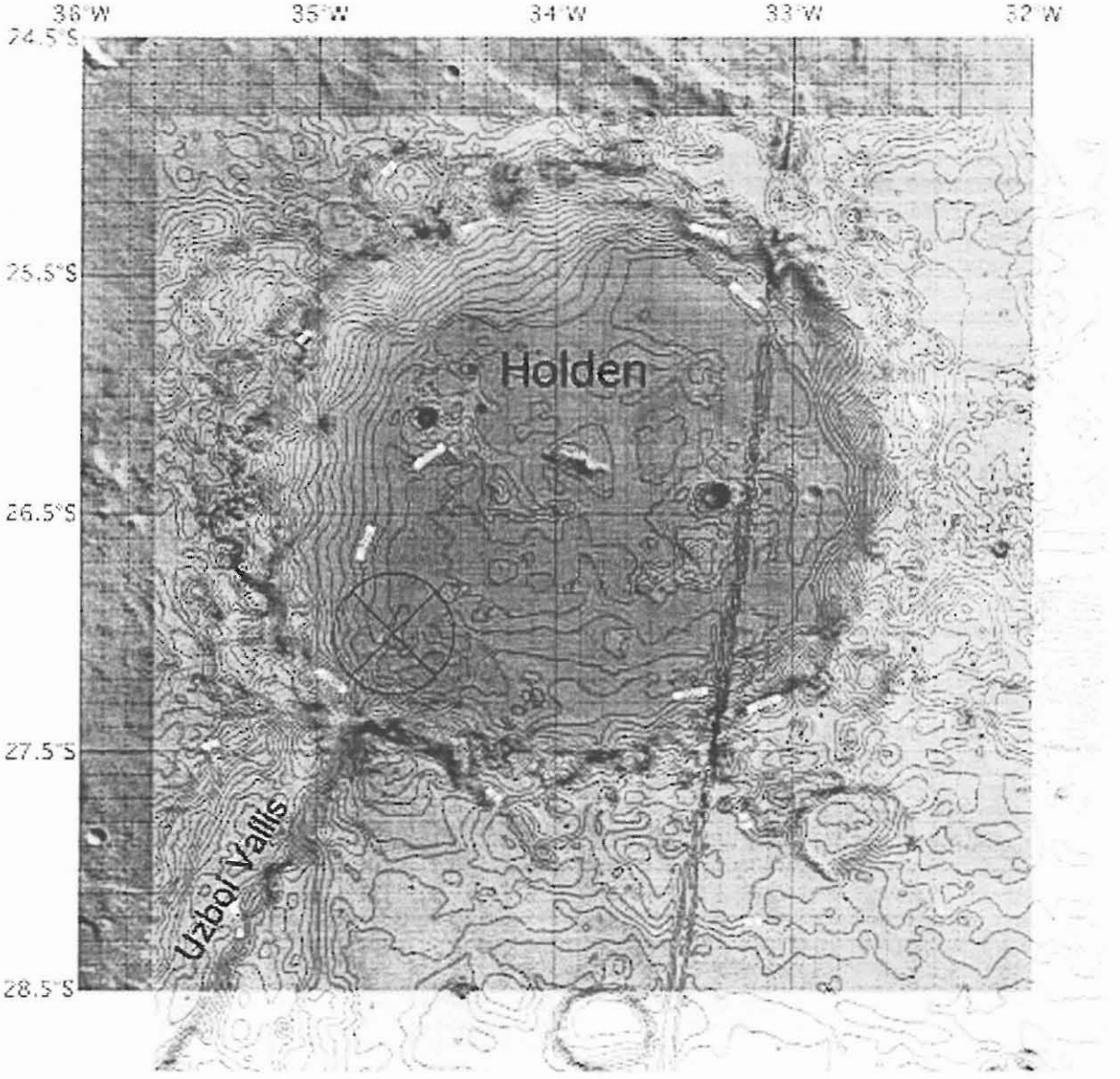

Figure 1: Holden Crater and vicinity. MDIM-1 with MOLA topography overlain (diagonal "groove" is due to an uncorrected orbit profile). 30km circle at southwest crater floor is proposed sample landing site. Coordinate grid in MDIM-1 Areographic. Contour interval 100 meters.

Introduction: Rover missions to the surface of Mars after MER 2003, are likely to be centered around focused geologic field mapping. One objective with high priority in selecting landing sites for these missions will be to characterize the nature, spatial distribution, internal structure, composition, and depositional history of exposed sedimentary layered deposits by visiting a number of distributed outcrops identified previously (and with a high degree of certainty) from orbit .

These deposits may contain prebiotic material, even fossil organisms, but their primary value will be to enable an assessment of the planet's climate at the time they were emplaced. High resolution imaging

from a mobile rover will enable the detailed study of these deposits over a wide area, their internal structure and mineralogy at distributed localities, and could resolve biologically-derived structures (such as stromatolite-like textures) if they are present. With the addition of a spectrometer, it should be possible to ascertain the presence of carbonates, sulfates, organics, water (liquid, frost, and bound water), as well as a variety of silicate minerals in the context of the collected imagery. Such a mission approach is directly relevant to future exploration of Mars, because it provides the geologic context comparable to what a field geologist visiting a site for the first time would acquire.

Rover missions after MER will likely have much better targeting and hazard avoidance landing systems, enabling access to planimetrically-challenged sites of high scientific interest. These vehicles will also likely have greater mobility than MER, capable of driving greater distances in a shorter amount of time. Many scientists and mission planners have realized the need to design a rover who's mobility can be comparable to the dimensions of its 3-sigma landing error ellipse.

Why Holden? Holden Crater is one of dozens of large craters on Mars that exhibit layered deposits, presumed to be ancient lake sediments, on their floors. It is one of several of these that has a prominent channel breaching its rim, further supporting the lake origin of the deposits in its interior. Though many of these craters were known to contain layered material since the Mariner 9 Orbiter mission, the MGS MOC camera has revealed these deposits in much greater detail than was possible before [1]. A number of investigators have noted that Holden formed on a large channel system that appears to have flowed from the north rim of Argyre Basin to Chryse Planitia during the late Noachian, based on Viking Orbiter and Russian Orbiter images [e.g., 2]. Further, Parker [3] recognized that Holden subsequently received flow from Nirgal Vallis during the Hesperian, which had ponded for a time in Uzboi Vallis until breaching Holden's southwest rim. MOC images of the breach and the crater floor have corroborated this interpretation with the revelation of finely layered (several meters scale) relatively bright material and large ripple-like bedforms oriented with respect to channel flow from this breach (fig. 1). These features are comparable in scale to large debris fans in the Puddle and Tule Valleys within the Bonneville basin of Utah. These valleys, initially isolated from the rest of the lake, were filled catastrophically when the lake level rose to the height of the lowest pass separating them from the lake [4,5]. An outcrop of the smaller of these fans is shown in Figure 3.

Holden was chosen over other putative crater lake sites as offering the greatest chance for community consensus regarding its origin for the following reasons: 1) Most proposed Martian highland crater lakes are not associated with in-flowing channels, so the lake origin of the interior deposits is not straightforward. 2) Many craters with in-flowing channels do not exhibit exposed layers in MOC images, so it is uncertain whether layers will be identified with higher resolution orbiter images or ground panoramas. (Gusev Crater is an often-cited example) 3) In some craters with in-flowing channels and exposed layers, the layers are clearly not directly associated with the channels. Gale crater (a potential MER A landing site) is an example of this. It's layered deposit is more than 3 km higher than the lowest point along the crater's rim (and is even higher relative to the in-flowing channel), so it cannot be from discharge through the channel into the crater, casting doubt on its lacustrine origin.

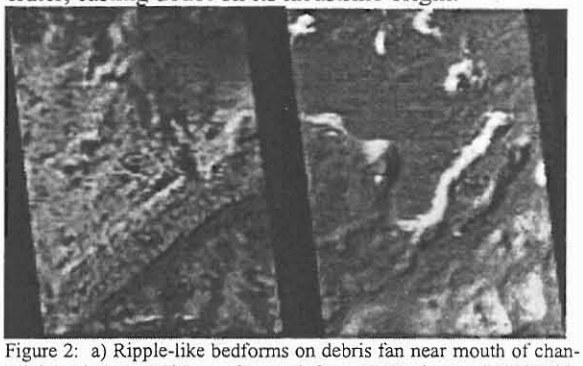

Figure 2: a) Ripple-like bedforms on debris fan near mouth of channel breach into Holden. Cropped from MOC image M0202300. Map projected image width = 2.82 km. b) Exposures of layered deposits on southern floor of Holden. Base of southern crater wall at bottom of scene. Cropped from MOC image M0302733. Map projected image width = 2.87 km. NASA/JPL/MSSS.

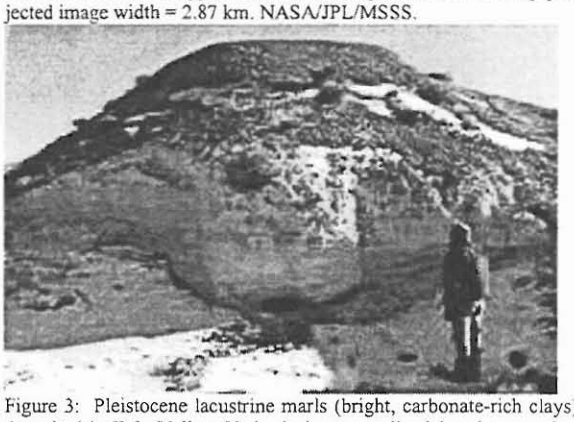

Figure 3: Pleistocene lacustrine marls (bright, carbonate-rich clays) deposited in Tule Valley, Utah, during an earlier lake phase predating Lake Bonneville. Note angular unconformity between lower and upper halves of marl exposure. Darker material overlying marls is poorly sorted, cross bedded gravels of a debris fan that formed on top of the older marls when Lake Bonneville overtopped the divide separating Tule Valley from the lake (Sand Pass). Tule Valley was dry just prior to this event. This feature is similar in appearance (though smaller in scale) to the unconformable overlap of the Holden debris fan over the bright layered material.

References: [1] Malin, M. C., and Edgett K. S. (2000) *Science, 290,* 1927-1937, [2] Pieri, D. C. (1980) NASA TM 81979, 160p. [3] Parker, T. J. (1985) MS Thesis, 165p. [4] Sack, D. (1990) Utah Geol. Min. Surv. Map 124, 26p. [5] Sack, D. (1997) Brigham Young U. Geol. Studies 42, II, 355-356.

HIGH LATITUDE TERRESTRIAL LACUSTRINE AND FLUVIAL FIELD ANALOGS FOR THE MARTIAN HIGHLANDS. J. W. Rice, Jr., Department of Geological Sciences, Arizona State University, P.O. Box 871404, Tempe, AZ 85287-1404, jrice@asu.edu.

Value of fieldwork: "Study nature not books" was the overriding philosophy of Louis Agassiz, the first geologist to formulate and advance the theory of Ice Ages. His work was primarily based on his field observations. J. Harlan Bretz also followed this philosophy in determining that catastrophic floods formed the Channeled Scabland in Washington state. It is with this philosophy in mind that Mars analog field investigations are being conducted in regions on earth that approximate Martian climatic, geologic, and geomorphic conditions. High latitude field investigations conducted in Iceland, the ice-free regions of Antarctica and the High Arctic are a very useful aid and tool to understanding certain Martian geological processes and landforms. These regions will also be used one day to train astronauts in preparation for manned missions to Mars within the next 15–20 years. Analog field studies do have limitations after all they are conducted on earth. However, a catastrophic flood, for example on either Mars or earth (Iceland), will leave behind similar landforms and deposits (Figs. 1&2). The value of conducting field investigations in terrestrial geologic studies is obvious and unquestioned despite advancements in remote sensing capabilities. Planetary geologic studies are conducted in a 'reverse format' compared to terrestrial geologic studies. These differences can be summarized by the following: terrestrial geologic studies go from local to global explanations and planetary geologic studies go from global to local explanations. Therefore, in order to understand Mars we should first attempt to understand our own terrestrial backyard. This is not as easy as it appears take the Channeled Scabland; although everyone now agrees that catastrophic floods formed this landscape, there is no agreement on the quantity and magnitude of these floods. This landscape was formed only about 13,000 years ago and is easily accessible for field studies. It is interesting to conjecture that some processes and landforms on Mars may be distinctly and uniquely Martian. Nevertheless, the value of fieldwork in deciphering Martian geologic processes will be crucial to the planning and operations of any future surface missions to Mars.

Icelandic jökulhlaups as analogs for Martian outflow channel deposits and landforms: The Dao and Harmakhis Valles outflow channel complex is located near the flanks of the highland volcano, Hadriaca Patera. Dao and Harmakhis Valles flow southwest and dissect the Hellas rim before debouching and ponding in this basin. These channels are thought to be mid to late Hesperian and have large collapse depressions as their source, these depressions formed by the collapse of volatile rich materials [1-3]. The proximity of these two outflow channels to a large volcano suggest a possible mechanism for the initiation of the catastrophic floods. In this paper I propose to use Icelandic jökulhlaups (catastrophic outburst floods) as models to aid in understanding the geomorphology and sedimentation processes of these outflow channels. The most voluminous and catastrophic floods known to occur on Earth in historic times are the Icelandic jökulhlaups. The largest jökulhlaups in Iceland can have peak discharges on the order of 10^6 m^3/s and depths of 60-70 m. Jökulhlaups are caused by the abrupt drainage of ice dammed lakes or subglacial volcanic eruptions. The probable causes of Martian floods are massive releases of subsurface water/ice due to possible subsurface volcanic activity. These mechanisms are very similar to the release of jökulhlaups in Iceland. For Mars the water/ice reservoirs are located in the subsurface and are released by the build up of hydrostatic pressure or volcanism; Icelandic jökulhlaups are very similar except the water/ice reservoirs are located on the surface. However, these surface reservoirs are similar to the Martian subsurface reservoirs in that they are isolated, massive and discrete bodies. One important aspect of jökulhlaups is that they can be studied in the field as they occur. This is important because modern day floods provide a much better control on the process-form relationships than for paleo-floods where processes, have to be inferred from the sedimentary record. Another important aspect of jökulhlaups is that channel systems begin as point sources, at glacier termini or lacustrine breakout points, where flow is then directed along one or two primary incised channels until is emerges as unconfined outwash. This is analogous to Martian outflow channels, which also begin at point sources (chaotic terrain and box canyons), and then flows unconfined into a basin region. This relationship can be seen quite well in the Dao and Harmakhis Valles region. Recent field work (2000 and 2001) conducted along the Jökulsa a Fjöllum jökulhlaup complex in the north central highlands of Iceland has confirmed the passage of more than one large flood (10^5 to 10^6 m^3/s) and identified both erosional and depositional landforms analogous to Martian outflow channels. Erosional landforms include streamlined hills, extensive washed/stripped lava flows, and cataracts. Depositional landforms consist of pendant bars, boulder bars, imbricated boulder trains, transverse ribs, and giant current ripples. Morphometric data were also collected on several flood deposited boulder fields (size, form, shape) with individual boulders up to 12.7 m diameter.

Antarctic ice covered lakes as analogs for Martian bodies of water: The ice free regions of the Antarctic are the best Mars analogs on earth. The reason for this is that Antarctica is the coldest, driest, and windiest place on earth. Therefore, I will use the perennial ice covered lakes of Antarctica as my model for past standing bodies of water on Mars. I believe that the following field observations should be kept in mind when addressing this issue. Field investigations conducted in the Bunger Hills of eastern Antarctica reveal that classic coastal features such as wave cut terraces, spits, and bars are either absent or less well developed. Ice dominated coasts are low energy environments as

compared to coasts which are wave dominated, storm environments. The presence of ice off a coast prevents the formation of waves and limits the fetch distance. Ice in the coastal zone and on the beach absorbs wave energy and reduces the effectiveness of any wave action that does occur. However, ice impingement upon the coasts, due to thermal expansion of ice or wind driven slabs of ice, does create unique landforms. Boulder barricades and sediment ridges and mounds are seen along polar beaches. Ice rafted rock fragments and erratics are also often found on these coasts.

Conclusions: This work provides an enhanced knowledge of unconfined catastrophic flood processes and how to identify deposits of different flood types (hyperconcentrated, debris flow, water rich, or ice-choked). The combined Icelandic/Antarctic field work and Martian geologic/geomorphic analysis will be used to test the jökulhlaup hypothesis as an analog to explain Martian outflow channel deposits and landforms and to increase the predictive accuracy of surface characteristics of fluvially emplaced sediments from orbit. This will be important in the assessment of future landing sites associated with major discharges of water and sediment.

References: [1] Crown, D.A. et al. (1992) Icarus, 100, 1-25. [2] Price, K.H., (1998) USGS Misc. Invest. Ser. Map I-2557. [3] Crown, D.A. and S.C.Mest (2001) LPS XXXII, abstract 1344.

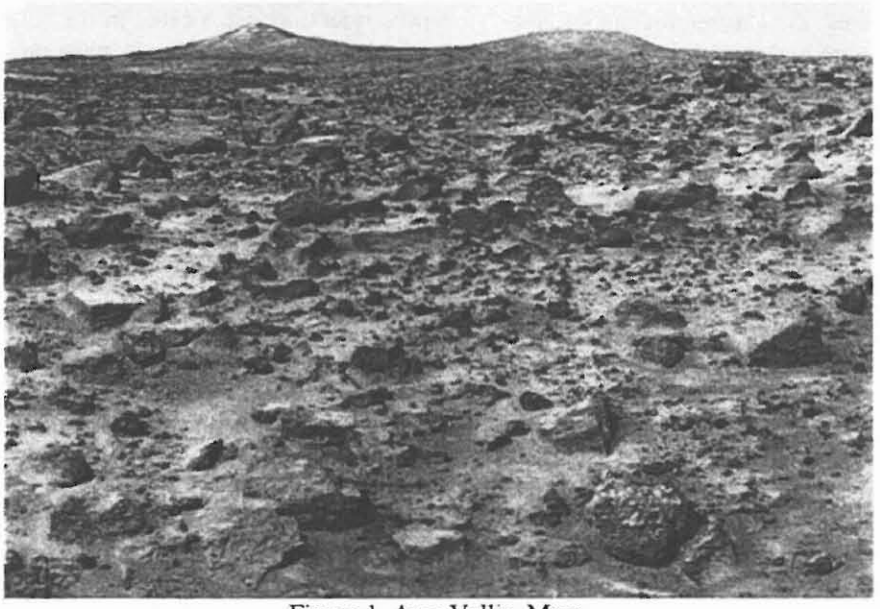

Figure 1. Ares Vallis, Mars.

Figure 2. Jökulsa a Fjöllum, Iceland.

AEOLIAN AND PLUVIAL FEATURES IN THE EASTERN MOJAVE DESERT AS POTENTIAL ANALOGS FOR FEATURES ON MARS. J. R. Zimbelman, CEPS/NASM MRC 315, Smithsonian Institution, Washington, DC 20560-0315; jrz@nasm.si.edu.

Introduction. The semi-arid environment of the eastern Mojave Desert has allowed aeolian processes to play a significant role in the Pleistocene and Holocene history of the region. This abstract summarizes some of the observations derived from over twenty years of field work in the eastern Mojave Desert and surroundings, focusing on aeolian features that should be analogs to features seen in MOC images of Mars.

Sand Paths. Accumulations of sand have been described in many parts of the Mojave Desert. The advent of spacecraft imaging provided a regional perspective that led to the hypothesis that the sand congregated along discreet paths of transport [1]. Field studies confirmed the presence of both sand dunes (active and stabilized) and sand sheets along the two paths identified from orbital photography, one that follows the Bagdad, Bristol, Cadiz, and Danby playas to the Colorado River (Bristol Trough path) and a parallel but more southerly path between the Emerson, Dale, Palen, and Ford playas to the Colorado River (Clark's Pass path) [1]. A third sand accumulation east of the Colorado River, on the Cactus and La Posa Plains near Parker, Arizona, was initially thought to be related to the Mojave sand paths [1], but recent chemistry results confirm that the Arizona sands are derived from mature Colorado River sediments rather than the immature near-source sands throughout the Mojave [2]. While the source of the Arizona sands is distinct from the Mojave deposits, they are very similar to a large accumulation of sand at the Algadones Dunes further down the river [3], illustrating the enormous importance of fluvial transport, even within a desert, in transporting sand-sized particles that subsequently are redistributed by aeolian processes. The stabilized transverse dunes near Parker (Fig. 1) are essentially identical to stabilized dunes found throughout the sand paths in the Mojave. Differential Global Positioning System (DGPS) surveying provides cm-scale topographic data for the stabilized dunes (Fig. 2), which should prove valuable for making quantitative comparisons with similar-scale features on Mars (see below). The majority of the sand along the transport paths is found in broad sand sheets rather than dunes, although where the prevailing winds pile sand against the windward side of hills or mountains, substantial sand ramps are built up, such as the enormous dissected sand ramp at Soldier Mountain, which accumulated in the last 7 to 25 thousand years, based on luminescence dating [5].

Figure 1. Oblique view of stabilized transverse dunes west of Parker, Arizona. JRZ, 2/1/97.

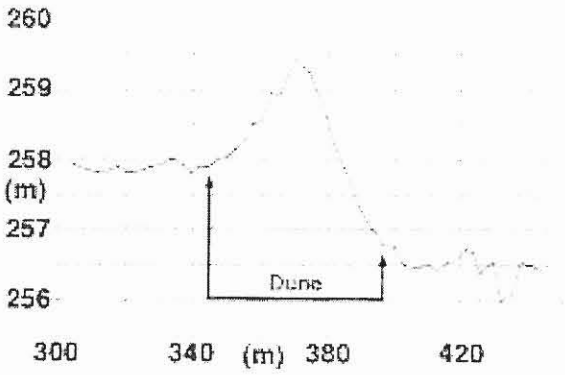

Figure 2. Portion of DGPS survey of a stabilized transverse dune near Parker, Arizona. Dune is ~1.5 m high over a width of ~50 m. Precision of measurements are ~2 cm horizontal and ~4 cm vertical.

Paleolakes. The playas along the Mojave sand transport paths indicate that pluvial processes have been intermixed with the aeolian processes. The pluvial episodes in the eastern Mojave likely corresponded to global climatic variations in the Pleistocene-Holocene [e.g., 5, 6], and may have enhanced local sand supplies that subsequently merged into the current transport pathways. Most Mojave playas do not have preserved shorelines at present (they are likely buried beneath the enormous alluvial fans associated with virtually all mountains), but around the Palen playa are patches of gypsum-rich lacustrine deposits that indicate an extensive body of water was present during the last high stand. The Mojave lacustrine materials may be good analogs for possible pluvial or fluvial deposits inferred to be within craters in the Martian highlands [e.g., 7-9], and may also be good places to test concepts of searching for past life in such environments.

Post-MOC Mars. The amazing MOC images show a wealth of new detail about the Martian surface and environment [e.g., 10]. The nearly ubiquitous evidence for aeolian deposition and/or erosion reveals a very dynamic history for all Martian sediments [11, 12]. Extensive remobilization of Martian surface materials was hinted at from the highest resolution Viking images [e.g., 13], but the substantial areal distribution and exquisite detail of the MOC images leaves no room for doubt about the role of wind, water, and maybe even ice in working on Martian surface materials. Dunes are very abundant in MOC images [12], but the smallest dune-like features (Fig. 3) might tell us

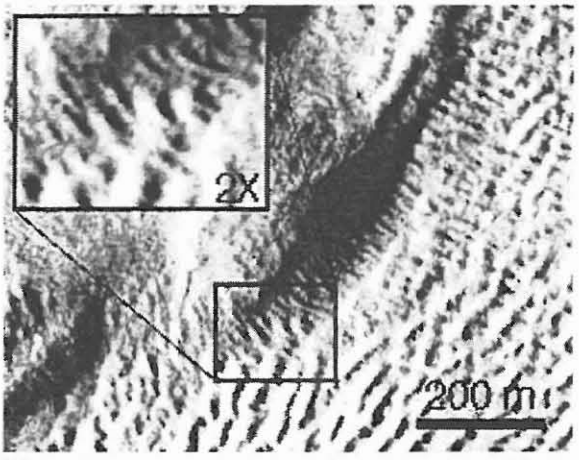

Figure 3. Dunes (lower right) and/or ripples (center) in the Acheron Fossae region. 2X enlargement in inset. MOC image SP2-50206, 5.6 m/p, solar inc. 85.4° (which limits dune height to < 1.5 m, similar to the Mojave dunes as in Fig. 2). Image from NASA/JPL/MSSS.

important information about the role of saltation and surface creep in aeolian transport on Mars. At least some of the small dunes on Mars have not been active during the twenty years between Viking and MGS [14], raising questions about the conditions under which many aeolian features were active on Mars. Dark sand within Nili Patera, in the Syrtis Major low albedo region, accumulated into massive dunes that represent significant regional sand transport (Fig. 4), at a scale substantially different from the small dunes discussed above. Increased image resolution may not be the best way to address the questions raised by the Martian features [15]; instead, we need to focus on identifying the scale most relevant for the various processes inferred to be responsible for the landforms.

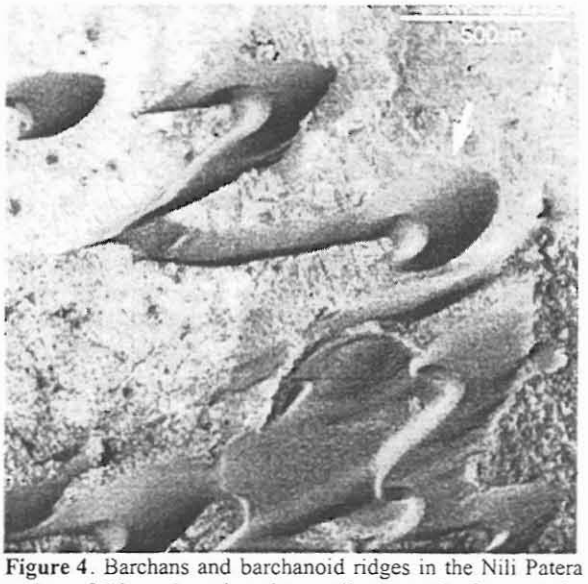

Figure 4. Barchans and barchanoid ridges in the Nili Patera region of Mars. Asuming the small crescentic faces to the SW are slip faces for individual dunes, then the largest barchan (arrow) is ~70 m tall, with a total volume of ~2.3 million cubic meters. MOC image FHA-00451, 5.9 m/p. Image from NASA/JPL/MSSS.

REFERENCES: [1] J.R. Zimbelman et al., in Desert Aeolian Processes (V. Tchakerian, Ed.), pp. 101-129, Chapman and Hall, 1995. [2] J.R. Zimbelman and S.H. Williams, accepted for publication in GSA Bull. [3] Muhs et al., in Desert Aeolian Processes (V. Tchakerian, Ed.), pp. 37-74, Chapman and Hall, 1995. [4] http://www.nasm.si.edu/ceps/research (web site describing Mojave research). [5] H.M. Rendell and N.L. Sheffer, Geomorph., 17, 187-197, 1996. [6] V.P. Tchakerian, Phy. Geogr., 12, 347-369, 1991. [7] S.H. Williams and J.R. Zimbelman, Geology, 22, 107-110, 1994. [8] R.D. Forsythe and J.R. Zimbelman, JGR, 100(E3), 5553-5563, 1995. [9] N.A. Cabrol and E.A. Grin, Icarus, 149, 291-328, 2001. [10] M.C. Malin and K.S. Edgett, Science, 288, 2330-2335, 2000, and 290, 1927-1937, 2000. [11] M.C. Malin et al., Science, 279, 1681-1685, 1998. [12] K.S. Edgett and M.C. Malin, JGR, 105(E1), 1623-1650, 2000. [13] J.R. Zimbelman, Icarus, 71, 257-267, 1987. [14] J.R. Zimbelman, GRL, 27(7), 1069-1072, 2000. [15] J.R. Zimbelman, Geomorph., 37, 179-199, 2001.